Suppression of Vibratory Stresses in Mechanical Structures due to Dynamic Loading

Author

Sabeeh Hussan Raza
2007-NUST-MsPhD-Mech-11

Supervisor

Dr. Muhammad Afzaal Malik

DEPARTMENT OF MECHANICAL ENGINEERING
COLLEGE OF ELECTRICAL & MECHANICAL ENGINEERING
NATIONAL UNIVERSITY OF SCIENCES AND TECHNOLOGY
ISLAMABAD

June, 2009

Suppression of Vibratory Stresses in Mechanical Structures due to Dynamic Loading

Author

Sabeeh Hussan Raza

2007-NUST-MsPhD-Mech-11

A thesis submitted in partial fulfillment of the requirements for the degree of

M.Sc. Mechanical Engineering

Thesis Supervisor:

Dr. Muhammad Afzaal Malik

Thesis Supervisor Signature: _____

DEPARTMENT OF MECHANICAL ENGINEERING

COLLEGE OF ELECTRICAL & MECHANICAL ENGINEERING

NATIONAL UNIVERSITY OF SCIENCES AND TECHNOLOGY, ISLAMABAD

June, 2009

DECLARATION

I certify that research work titled "*Suppression of Vibratory Stresses in Mechanical Structures due to Dynamic Loading*" is my own work. The work has not been presented elsewhere for assessment. Where material has been used from other sources it has been properly acknowledged / referred.

Signature of Student

Sabeeh Hussan Raza

2007-NUST-MsPhD-Mech11

ACKNOWLEDGEMENTS

All praise to Allah almighty, the most beneficent and merciful.

I would like to thank my supervisor, Dr. M. Afzaal Malik, for his guidance, encouragement and assistance throughout my thesis. He was always willing to help and discuss about the thesis progress proposing new ideas.

I would also like to thank Dr. Wasim Akram Tarar who was helping me with his expertise in Altair Hypermesh, Patran and Nastran software programs. I appreciate his patience and his guidance for the whole thesis. I would like to thank Lt. Col. Dr. Syed Waheed Ul Haq and Mr. Raja Amir Azeem for being on my thesis committee.

Finally, I would like to express my gratitude to all the individuals who have rendered valuable assistance to my study.

Dedicated to my parents, brother and sister who have always supported and encouraged me. It is only because of their prayers that enable me to accomplish my job effectively.

ABSTRACT

Rotor assemblies particularly those used in flight vehicle turbines typically contain aerodynamically shaped blades, or airfoils, which operate at high speeds and in hostile environments. As a result, the rotor blades are subjected to steady and vibratory loads which generate significant internal and external stresses. These vibratory stresses are the main cause of failure in aerospace/mechanical structures and machine components. Failure occurs due to these vibratory stresses in gas turbine engines and rotating machinery components while operating at resonant frequency. To prevent blade failure, the excited resonant response needs to be attenuated to an acceptable level. Several approaches have been adopted to suppress blade vibration by providing additional damping through blade dampers. A magnetomechanical coating is used as a very effective method for damping of these stresses. Vibratory stress damping in components like turbine blades through magnetomechanical coating is already established in the literature.

The objective of this research is to explore the feasibility of using a magnetomechanical surface coating material for increasing the high-frequency damping of turbine blades. This research involves formulation of a parametric expression for determining the optimum value of coating layer for a given geometry of a beams, curved plate and turbine blade under dynamic loading conditions. Finite element method (FEM) is used for modeling, simulation and analysis of the parametric model. Beam theory is applied as a mathematical model for obtaining the mode shapes for the beam. A finite element analysis procedure is performed to acquire the matrix of data and the data is correlated with beam theory model for initial verification. The data is further evaluated to form the required model for calculating thickness of coating for a beam, curved plate and turbine blade. The resulting parametric expression is verified through comparison with already published experimental data available in literature. This research has a wide ranging application in the areas of gas turbine engines and rotating machinery components.

Keywords: Rotor blades, vibratory stresses, magnetomechanical surface coating, FEM

TABLE OF CONTENTS

LIST OF FIGURES

LIST OF TABLES

Nomenclature

σ_i	average internal stress
σ	vibratory stress
σ_{loc}	local internal stress
σ_{cr}	critical stress on the saturation point
r	$= \frac{\sigma_i}{\sigma} \equiv \frac{\varepsilon_i}{\varepsilon}$
μ	coated beam loss factor
μ_c	coating material loss factor
μ_q	uncoated beam loss factor
E	coated beam Young's modulus of elasticity
E_c	coating material Young's modulus of elasticity
E_q	uncoated beam Young's modulus of elasticity
I	coated beam moment of inertia
I_q	uncoated beam moment of inertia
h	thickness of the coating layer
l	length of the beam
$2t$	thickness of the beam
b	width of the beam

$K\lambda_m$ Magnetic parameters

ΔU_p Coating Material energy Dissipation density

t thickness of coating in inches

y yield stress in Ksi

Chapter 1. Introduction

Many load carrying structural systems, such as Aircraft structures, being extremely flexible, are prone to distortion under load. These loads are mostly caused by aerodynamic forces, which themselves depend on the geometry of the structure and the orientation of the various structure components to the surrounding airflow. The resultant structural distortion causes the changes in aerodynamic load leading to further distortion [1]. The interaction of aerodynamic and elastic forces is known as aeroelasticity.

Flight Vehicles undergo tremendous loading which results in phenomenon such as buckling, flutter, fatigue, creep etc. These loads are a threat to vehicle safety and inefficiency factors which eventually lead to failure. Nowadays in aeronautics concerns are made for the improvement of prediction methods that are involved in the design of aircraft and rotorcraft. Future aircraft types are designed for at least the same goals, but structure with higher fatigue life; higher damage tolerance capability and higher corrosion resistance are required to minimize the maintenance costs and to comply with the requirements of the operator and the enhanced airworthiness regulations [1].

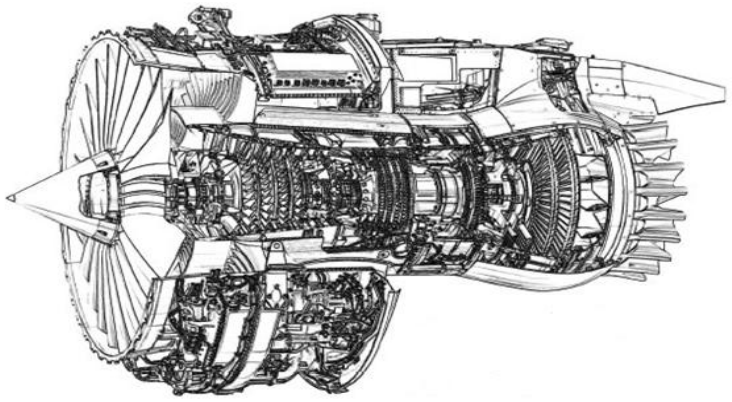

Fig. 1. 1 Gas Turbine Engine

Aeroelastic problem can be categorized in two distinct types. One involves the interaction of aerodynamic and elastic forces, which may exhibit divergent tendencies in a too flexible structure. This divergence leads to failure or an adequately stiff structure. These aerodynamic and elastic forces, convergence is required to reach a stable equilibrium

condition. Problem involving aerodynamic and elastic forces can be categorized as *static or steady* state system. These forces produce aeroelastic phenomena such as divergence and control reversals. Second type of problems can be categorised as *dynamic loading* systems, which involves the inertia of the structure as well as aerodynamic and elastic forces. Dynamic loading systems, of which gust are of primary importance, induce oscillations of structural components. The amplitude of the oscillation may diverge if the natural or resonant frequency of the component is in the region of the frequency of the applied loads, causing failure [1].

Fig. 1. 2 A typical high pressure gas turbine blade

Rotary machines contain rotor blades installed in rotatable hubs or disks in axial orientation. Rotor blades are very commonly used in machine components in hi- tech applications. Rotor assemblies typically contain an aerodynamically shaped blades, or airfoils, which operate at high speeds and in hostile environments [2]. Air flowing over the blades during the gas turbine engine operation varies in term of speed, temperature, pressure and density. Rotor blades in a gas turbine engine are constantly subjected to periodic excitations as a result; the rotor blades are subjected to steady and vibratory loads which generate significant internal and external stresses [2, 3]. These vibration induced stresses which can cause high cycle fatigue (HCF), especially when blades are excited at their resonant frequencies [4].

Vibratory loads are derived from inertial and aerodynamic sources. Inertial loading depends on rotor blade mass and stiffness distribution, and impacts the vibratory response and frequency tuning of the rotary machine. Aerodynamic loading depends on both

steady state and disturbed air flow through the rotary machine. These loads then cause a variety of stresses, such as centrifugal, bending, and torsion, as well as vibratory bending, on the rotary machine [2].

Vibratory stresses increase with the speed and it increases the natural frequency of blade in the range of resonance of running speed or other passing frequencies. The vibratory stresses magnitude becomes proportional to the amount of damping present in the system, when blade vibrates in resonance [5]. For blade failure prevention, the excited resonant response needs to be attenuated to an acceptable level.

1.1 Background

It is desirable for all structures to possess sufficient damping so that their response to the expected excitation is acceptable [6]. Structural vibration, noise and dynamic stresses will be reduced by increasing the damping of the structure. Damping of the blades is also a benefit to reduce vibratory stresses of blades during operation. Damping can be induced in several ways like explained below.

1.1.1 Material / Structural / Hysteresis Damping

All materials dissipate some energy during cyclic deformation. Hysteresis damping, which is also known as material or structural damping, is the result of internal friction in the material of the body during its oscillatory motion. These frictional forces are developed between internal planes that slip and slide during deformation. This type of resistance is independent of the frequency of vibration, but it is considered to be approximately proportional to the amplitude of the deformed body [7].

1.1.2 Aerodynamic Damping

Energy can be dissipated by the air in which a structure vibrates. This can be important for low density structures with large motions. Most damping forces are of a retarding nature which acts against the motion occurring, but situations can arise where the motion itself generates a force that encourages motion. This happens in a structure due to relative motion of the wind, negative aerodynamic damping or aerodynamic instability occurs [6].

1.1.3 Viscous Damping

Viscous damping occurs, when bodies are vibrating in a fluid medium at rather low velocities. The resisting force that is developed from such damping is considered to be proportional to the velocity of the oscillation motion [7].

1.1.4 Coulomb / Dry Friction Damping

Coulomb damping, which is also known as dry friction damping, arises when bodies slide on dry surfaces. For motion to begin there must be force acting upon the body that overcomes the resistance to motion caused by friction. The dry friction force is parallel to the surface and proportional to the force normal to the surface; as shown in figure 1.2, the normal force is equal to the weight "*W"* [8].

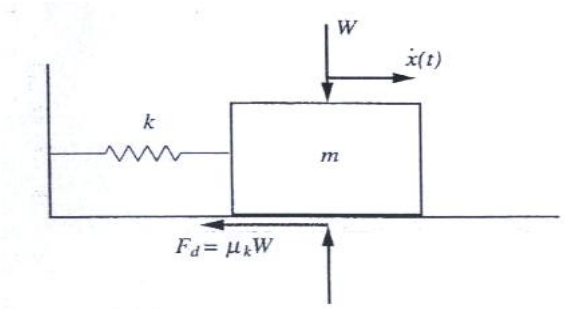

Fig. 1. 3 Mass-Spring System Subjected to Coulomb Damping [8]

1.1.5 Structural Damping Control System

Structural control system can be classified generally into two damping control systems i.e. active and passive damping control system.

1.1.5.1 Active Damping Control System

Active damping system refers to energy dissipation from the system by external means. An active control system is a much more complex system than the passive control systems. Active damping control systems use power actuators, which are located in the structure for applying actuation to counteract the resonant oscillation at right time [9].

The main advantage of active damping control system is that it attains excellent control results. However, there are many drawbacks which are associated with active damping

control systems. These are very expensive systems to design and operate due to the large amount of power needed. They required more space than passive damping control systems [9].

1.1.5.2 Passive Damping Control System

Passive damping control system reduces structural vibration by imparting a force on structure in response to the motion of the structure [9]. Passive damping system refers to as energy dissipation within the structure.

Passive damping control system has many benefits associated with it. No external power is required for the passive system operation. They are smaller in size than active damping control system [9].

1.1.6 Different Damper Types

Several damping approaches have been adopted to suppress blade vibration by providing additional damping through blade dampers. Some damping methods are listed below.

1. Dry Friction Dampers

Dry friction dampers are used to reduce the vibrations in the turbine engine blades. Friction damping plate is attached to the blade underlying. During operation, the plate member rubs against the blade and dissipates the vibrational energy [10]. This result in increased engine weight, and correspondingly engine efficiency reduces. The dry friction damping approach is effective only over a limited engine operating speed [10]. Dry friction dampers, include blade-to-ground, blade-to-blade, and shroud dampers.

2. Blade-to-Ground Damper

Blade-to-ground dampers usually have a moveable member which positioned between the coverplate assembly and the underside of the platform of one or more turbine blades. Upon turbine rotation, the member is displaced radially outwardly by centrifugal forces. This engages the coverplate and underside of the blade platform; thereby perform a damp function [11].

3. Blade-to-Blade Damper

Blade-to-blade dampers have the configuration in which centrifugal load pushes outwardly against the platforms of the two adjacent blades [12]. Each damper extends axially across the disk beneath the platforms. Blade-to-blade dampers effectively damp the rotor blade vibration. The damper geometric configuration provides the longitudinal stiffness and low weight which enables friction damping slippage between the damper and the blade platform [13].

4. Aero-Damping

Aero-damping configuration consists of plurality of spherical damping members, at least one spherical damper being located in each space between rotatable disc and adjacent circumferentially extending blade portion. Rotational spherical damping members centrifugally engage with adjacent circumferentially extended portions during assembly. During the blade assembly, each spherical member centrifugally urges into frictional engagement with undersides blade platform [14]. This arrangement thereby provides the necessary degree of damping.

However, it is well known that the structural damping from dry friction dampers and aero-damping are negligible for high-frequency vibration; and the dominant damping of the blades results from the energy dissipation in the material [15]. Consequently, low material damping results in high vibratory stress, increases failure risk and significantly reduced reliability and safety [16].

5. Viscoelastic Damping

Viscoelastic damping materials are used in rotating blades for the purpose of reducing vibratory stresses in high-frequency stripe modes. Viscoelastic damping has limited damping performance at high temperatures because the optimum damping range of viscoelastic material tends to occur for relatively low temperatures [10]. Temperature limitation of viscoelastic damping materials leads to manufacturing and durability concerns [15]. A surface high-damping coating layer is likely to be more practical.

Usage of thin damping coating systems are attractive from the standpoint of structural integrity, aerodynamic efficiencies and manufacturing, the ability to survive at the operating temperature of gas turbine engine remains the challenge. Protective coating should have the properties which are required at the surface of the component without having a detrimental effect on the mechanical properties of the base material [17]. Additional challenges associated with such coatings include spall resistance under cycling conditions, erosion resistance, impact resistance, high temperature stability and minimum impact on the fatigue lives of the airfoil. Finally maximizing the damping effectiveness of the coating is understood to be an important goal of any damping system.

Magnetomechanical coating material is used for increasing the high-frequency damping of turbine blades [15]. Investigation for the feasibility of using magnetomechanical coating for beams and blade is performed experimentally and through finite element model previously. Models for beams and blades having magnetic coating layer is used for the experiment purpose. The experiment results show that body undergoes maximum vibratory stresses at the bending modes. The fourth bending mode is identified as the worst case at which body undergoes the maximum vibratory stress after performing the force response analysis. Results from the experiment and from finite element model for beams and blades show a significant reduction in vibratory stress with the application of magnetomechanical coating layer.

This research involves formulation of a parametric expression for determining the optimum value of coating layer for a given geometry of a beams, curved plate and turbine blade under dynamic loading conditions. Finite element method (FEM) is used for modeling, simulation and analysis of the parametric model. The resulting parametric expression is verified through comparison with already published experimental data available in literature. This research has a wide ranging application in the areas of gas turbine engines and rotating machinery components.

1.2 Motivation

Vibratory stresses play important role in catastrophic structural failure of many load-carrying systems, such as aircraft gas turbine engines, while operating under severe loading conditions. Turbomachinery blade undergoes highly damaging vibrational forces during their operation. These vibrational forces generate relatively high stresses and vibration in the blade.

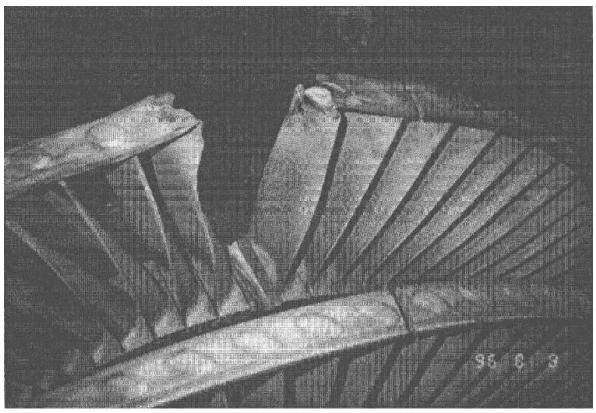

Fig. 1. 4 Blade failure in the rotating Hub

Rotor blade moves with high rotational speed during the gas turbine engine operation. Due to this high rotor speed and the gas flowing between the blades, vibrations are generated in the blades. Preventing the resonance means, the steady state operating speed should not match the system natural frequencies.

Several methods are used to suppress/damp blade vibratory stresses by providing additional damping through blade dampers. Magnetomechanical coating material is used for increasing the high-frequency damping of turbine blades [15]. Surface coating material is selected on its stress or strain dependent damping capability. Other factors which are of critical significance are stiffness, toughness, resistance to corrosion, fatigue and the effect of environmental heating.

1.3 Objectives

The main objective of this research is to explore the feasibility of using a magnetomechanical surface coating material for increasing the high-frequency damping of turbine blades.

Parametric study is performed to determine the optimum material type and thickness for use as coating on plates for stress suppression under dynamic loading conditions.

In the context of the thesis, Finite element technique is used to evaluate the stresses and their corresponding damping properties. Finite element modeling is carried out using HYPERMESH commercial software and analysis is performed using NASTRAN commercial software. HYPERMESH is used for the preprocessing, solution is obtained using NASTRAN and post-processing is performed in HYPERVIEW.

First the cantilever beam which is similar to rotor blade is modeled and its modal analysis is performed to find the natural frequencies of the plate. Stripe mode or fourth bending mode is identified and is analytically verified through Euler-Bernoulli beam equation; frequency response analysis is performed in order to get maximum stresses for the identified stripe mode.

Modeling and analysis is performed with and without magnetomechanical surface coating material. Similarly curved plate and turbine blade are modeled and analyzed, in order to study the real world application.

After the analysis an expression is developed which correlate material type, coating type and their geometric properties. This parametric equation provides the optimum thickness required for coating material.

1.4 Thesis Structure

In this thesis, magnetomechanical surface coating material technique is studies for the suppression of vibratory stresses in rotor blades during their operation. Iterative process is used to obtain the optimum thickness for magnetomechanical surface coating material.

The first chapter includes the introduction to the problem and literature review related to the present problem. Thesis motivation and approach is also discussed.

In chapter 2, vibration principles for the free and forced vibration are discussed. Mathematical modeling of the coated surface is also presented.

In chapter 3, FEA modeling of beam, curved plate and turbine blade is performed. HYPERMESH is used for the preprocessing of beam, curved plate and turbine blade. Their corresponding modeling properties such as material type, constraints / boundary conditions, element type.

In chapter 4, analysis of beam, curved plate and turbine blade is performed. Solution is obtained using NASTRAN for beam, curve plate and turbine blade. Post-processing is carried out using HYPERVIEW for beam, curve plate and blade.

In chapter 5, results are compiled and conclusions are drawn from obtained results. Detailed discussion and comments are made and finally recommendations are given for future work.

Chapter 2. Mathematical Modeling of Damping due to Coating

A vibratory system is a dynamic system for which the variables such as the excitations inputs and responses are time dependent. The response of a vibrating system generally depends on the initial conditions as well as the external excitations. Most practical vibrating systems are very complex, and it is impossible to consider all the details for a mathematical analysis. Only the most important features are considered in the analysis to predict the behavior of the system under specified input conditions [18].

It is necessary to analyze the vibration of structure in order to predict the natural frequencies and the response to the expected excitation. The natural frequencies of the structure must be found because if the structure is exited at one of these frequencies, resonance occur which results in high vibration amplitudes, dynamic stresses and noise levels. The resonance should be avoided and the structure is designed such that it is not encountered during normal conditions; this often means that the structure need only be analyzed over the expected range of excitation [6].

2.1 Euler-Bernoulli Equation

Transverse vibrations of beams and shafts can be either free or forced. Their differential equations of motion are derived by considering the member in Fig 2.1.

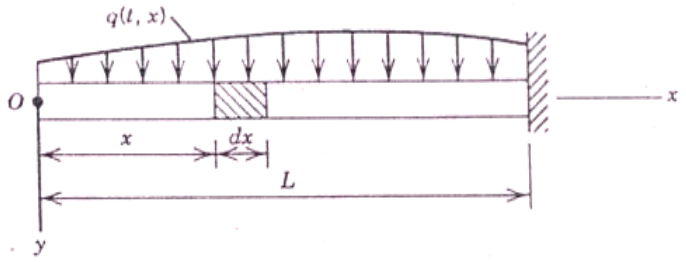

Fig. 2. 1 Uniform Elastic Beam Subjected to Transverse Motions [7]

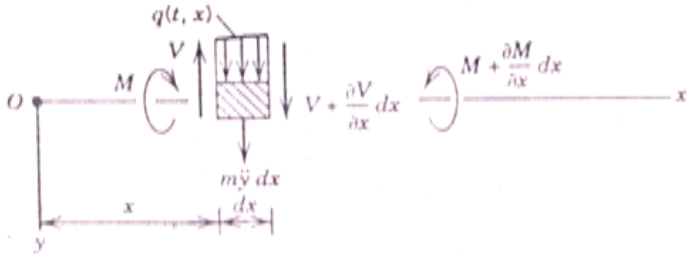

Fig. 2. 2 Free-Body Diagram of an Element of the Beam [7]

In general, the excitation force on the beam is designated as *q (t, x)*, and it can vary with time as well as with x.

The free body diagram of the element is shown in Fig 2.2. In this figure, M and $M + (\partial M/\partial x)\, dx$ are the dynamic moments acting on the sides of the element, V and $V + (\partial V/\partial x)\, dx$ are the dynamic shear forces.

By applying Newton's second law of motion, we get

$$m\ddot{y} - \frac{\partial V}{\partial x} = q(t,x) \tag{2.1}$$

By using the expression

$$V = \frac{\partial M}{\partial x} = -EI\frac{\partial^3 y}{\partial x^3} \tag{2.2}$$

Substituting equation (2.2) into equation (2.1), we find

$$EI\frac{\partial^4 y}{\partial x^4} + m\frac{\partial^2 y}{\partial t^2} = q(t,x) \tag{2.3}$$

If $q(t,x)$ is zero, equation (2.3) yields the expression

$$EI\frac{\partial^4 y}{\partial x^4} + m\frac{\partial^2 y}{\partial t^2} = 0 \tag{2.4}$$

Equation (2.4) is the differential equation of the free undamped vibration of the member. The moment of inertia *I* and modulus of elasticity *E* are considered uniform. It should be noted here that shear and rotational inertia effects are also neglected.

The solution *y (t, x)* of equation (2.4) may be assumed to be composed of a function *Y(x)* which varies only with *x*, and a function *f (t)* that varies only with time *t*; that is

$$y(x,t) = Y(x)f(t) \tag{2.5}$$

By substituting eq. (2.5) into eq. (2.4) and performing the required mathematical operations, we find

$$\frac{EI}{m}\frac{\partial^4 Y(x)/\partial x^4}{Y(x)} = -\frac{\partial^2 f(t)/\partial t^2}{f(t)} \tag{2.6}$$

Equation (2.6) can be satisfied for all values if, and only if, each side of the equation is equal to the same constant. If this constant is taken to be equal to ω^2, we find

$$\frac{EI}{m}\frac{\partial^4 Y(x)/\partial x^4}{Y(x)} = \omega^2$$

$$-\frac{\partial^2 f(t)/\partial t^2}{f(t)} = \omega^2$$

Or

$$\frac{\partial^4 Y(x)}{\partial x^4} - \lambda^4 Y(x) = 0 \tag{2.7}$$

$$\frac{\partial^2 f(t)}{\partial t^2} + \omega^2 f(t) = 0 \tag{2.8}$$

Where

$$\lambda^4 = \frac{m\omega^2}{EI} \tag{2.9}$$

Equation (2.7) is a 4th order partial differential equation and its solution yields the expression for the function *Y(x)*, which defines the shapes of the modes corresponding to free undamped frequencies ω of an elastic beam. Equation (2.8) deals with free, undamped, harmonic vibration of one-degree spring-mass systems. The solutions are written as follows:

$$f(t) = A \sin \omega t + B \cos \omega t \tag{2.10}$$

$$f(t) = C \sin(\omega t + \emptyset) \tag{2.11}$$

The general solution of the free, undamped, transverse vibration of beam spans is given as

$$y(x,t) = (A_1 \cosh \lambda x + A_2 \sinh \lambda x + A_3 \cos \lambda x + A_4 \sin \lambda x) \sin(\omega t + \emptyset) \tag{2.12}$$

The constants A_1, A_1, A_1, A_1, ω, and $\emptyset$, may be determined by using the four boundary conditions of the beam span and the two initial time conditions of the motion, such as initial displacement and velocity at an initial time *t=0*, or $t = t_0$. The frequency ω may be determined from the following expression:

$$\omega = \lambda^2 \sqrt{\frac{EI}{m}} \tag{2.13}$$

The corresponding period of vibration τ is

$$\tau = \frac{2\pi}{\omega} = \frac{2\pi}{\lambda^2} \sqrt{\frac{m}{EI}} \tag{2.14}$$

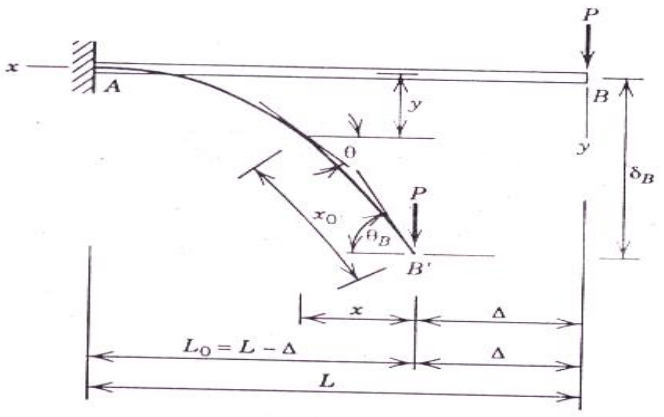

Fig. 2. 3 Large Deformation of a Loaded Uniform Cantilever Beam [7]

If we consider a member which is subjected to large deformations, say, the one shown in Fig 2.3, its general expression regarding the large deformation of the member is represented by the *Euler-Bernoulli equation* as shown below:

$$\frac{y''}{[1+(y')^2]^{3/2}} = -\frac{M_x}{E_x I_x} \tag{2.15}$$

Equation (2.15) is a nonlinear differential equation and represents the exact shape of the deflection curve of a flexible member, which is called elastica.

If the deformations are small, then y' in the denominator of equation (2.15) is very small compared to one, and it can be neglected. Therefore the equation (2.15) may be written as

$$y'' = -\frac{M_x}{E_x I_x} \tag{2.16}$$

Equation (2.16) is a linear differential equation, since we assumed that the deformations are small.

2.2 Commonly Used Methods of Vibration Analysis

It is extremely difficult to obtain exact solutions for more complicated theoretical and practical situations. For such cases, approximate methods of analysis have been developed, which provide reasonable answers for practical applications. The purpose of

all these methods and methodologies is to provide a way for a structure or mechanical component in a safe and functional manner.

The approximate methods of analysis can represent mathematical models based on the simplification of exact solutions or they can be numerical solutions of appropriately derived differential equations of motion. Since all such methods are approximate, the results should be examined carefully to make sure that the physical situation is appropriately represented in the results.

Methods used for vibration analysis are Rayleigh, Stodola's method, Myklestad's method and finite element method.

2.3 Energy Dissipation Method of Damping due to Coating

The energy dissipation concept is applied to examine the effects of the coating damping on the forced response of beams and blades [15]. The energy dissipation mechanism due to the irreversible movement of magnetic domain boundaries has been studied by Smith and Brichak [20, 21]. They divided the energy dissipation density per cycle, ΔU_p, into two regions:

$$\Delta U_p = \frac{K\lambda_m}{\sigma_{loc}^2}\sigma^3 \quad if\ \sigma < \sigma_{cr} \tag{2.17}$$

$$\Delta \mathrm{U_p} = \mathrm{K}\lambda_\mathrm{m}\sigma_\mathrm{loc} \quad if\ \sigma > \sigma_\mathrm{cr} \tag{2.18}$$

Where K is a constant depending on the shape of the hysteresis loop, λ_m is the saturation magnetostriction, σ is the vibratory stress, σ_{loc} is the local internal stress, and σ_{cr} is the stress corresponding to the saturation point of the domain walls irreversible movement.

Using a probabilistic distribution, Smith and Birchok [20, 21] reformulate expression (2.17) and (2.18) to give

$$\Delta U_p = K\lambda_m\sigma_i\{1 - e^{-2r}(1 + 2r + 2r^2)\} \tag{2.19}$$

Where σ_i is the average internal stress, and s is defined by

$$r = \frac{\sigma}{\sigma_i}$$

Therefore the loss factor (μ_c) of the coating material is represented as

$$\mu_c = \frac{K\lambda_m E}{\pi\sigma_i}[1 - e^{-2r}(1 + 2r + 2r^2)]/r^2 \qquad (2.20)$$

where *E* is the Young modulus.

The bending rigidity, $EI(1 - i\mu)$, of the coated beam is calculated from the RKU equation [15].

$$EI(1 - i\mu) = E_q I_q \left\{(1 + i\mu_q) + e_2 h_2^3(1 + i\mu_c) + 3(1 + h_2)^2 \left[\frac{e_2 h_2(1 + i\mu_c)}{1 + e_2 h_2(1 + i\mu_c)}\right]\right\} \qquad (2.21)$$

where

$$e_2 = E_c/E_q\,, \qquad h_2 = h/t\,. \qquad (2.22)$$

and h is the thickness of the coating layer, $2t$ is the thickness of the beam, and $E_q I_q(1 + i\mu_q)$ is the complex bending rigidity of the uncoated portion of the beam.

Chapter 3. The Finite Element Method

The finite element method was originally devised for static stress analysis, but was soon applied to vibration problems as well. It is now used to the exclusion of almost all other methods for setting up the equations of motion of structures.

Its development required no new mathematics, since the basic ideas, essentially the Rayleigh–Ritz concept (1909) of using assumed modes and Lagrange's equations (1788), had been around for a long time. However, because it relies upon extensive calculations and computations, its practical implementation had to wait for the development of high-speed computers, and in practice the use of the method dates from about 1960.

Fundamentally, there are two finite element methods; the force method, where forces are assumed and displacements calculated, and the displacement method where displacements are assumed, and forces are calculated [19].

Vibration stress analysis for plate, beam, curved plate and turbine blade is performed in this thesis using finite element method. For the purpose of vibration analysis, it is performed in three steps.

1. Pre-processing
2. Processing
3. Post-processing

Pre-processing is a step in which the physical problem is modeled. Pre-processing includes preparing geometry, discretization, assigning material properties, application of boundary conditions and the application of loads.

Processing involves solving the finite element system of equations to obtain the required results.

Post processing involves

1. Obtaining the results
2. Plotting the results

3. Interpretation of results

Above listed steps for the vibratory stress analysis are discussed below one by one.

3.1 Technique for Finite Element Modeling

For the present problem, Altair Hypermesh is used for FE modeling. Pre processing involves

1. Defining the type of problem, the problem is structural.
2. Defining control cards.
3. Defining material properties, such as Poisson ratio, stiffness of material and density of material etc.
4. Modeling, the creation of 3D geometry in Hypermesh.
5. Selecting element types such as 3D Hexahedral solid, Shell Quad 4 node Isoparametric element.
6. Meshing, the division of geometry into number of small elements.
7. Application of proper boundary conditions and constraints, generally displacements in case of structural analysis.
8. Defining the analysis card, the free vibration for modal analysis and applying loads like concentrated forces on a point for running frequency response.
9. Defining output card.

As gas turbine engine blade operates under severe conditions, therefore materials are selected with special mechanical properties for the manufacturing of turbine blade. Materials with high proof strength, tensile ductility, and low creep extension, fracture toughness, resistant to crack propagation, resistant to corrosion, and high and low cycle fatigue are more desirable.

3.2 Uncoated Finite Element Modeling of Plate

Gas turbine engine goes under cyclic loading during their operation. Due to these periodic excitations, rotor turbine blades undergo steady and vibratory loads which produce high internal and external stresses. In the context of present problem, plate is modeled in Hypermesh as this is the simplest case to start with vibrational analysis. The main aim of this thesis is to develop the parametric equation which will correlate the material type, coating type and geometric properties. For developing the parametric equation, we start the analysis with plate and then we extend the analysis to beam, curved plate and then finally a turbine rotor blade.

Finite element modeling of simple plate is analyzed with Al 6061 material. Plate is constrained in six degrees of freedom because turbine blade in a rotating disk is also fixed to the rotor. Applying the constraints, the plate model becomes simpler and easier to analysis. Mechanical properties of Al 6061 are listed in table 3.1:

Mechanical Properties of Al 6061	
Property	AL6061
Modulus of Elasticity (E) Psi	1E+07
Density (ρ) lb/in^3	2.52E-04
Shear Modulus (G) Psi	1.11E+07
Poisson's ratio (ν)	0.33

Table 3. 1 Mechanical Properties of Al 6061

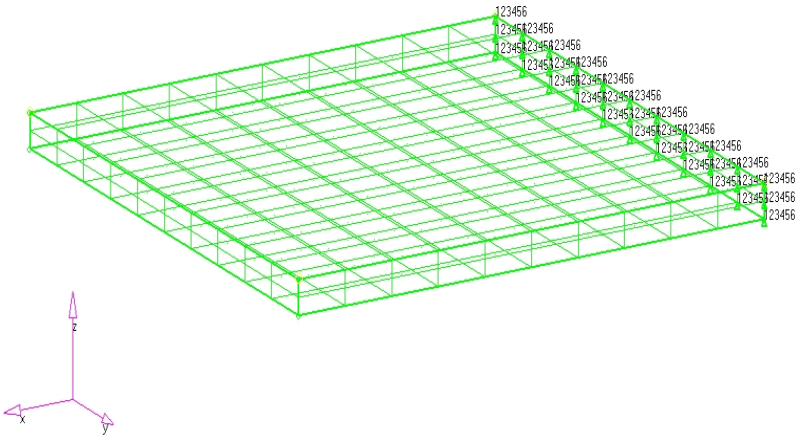

Fig. 3. 1 Finite Element Modeling of 3D Plate

Fig 3.1 presents the 3D plate finite element model in Altair Hypermesh. Mesh density, parameters and element type can be easily controlled by using auto mesh tool. 3D solid Hex element is used for the meshing of simple plate. Plate is constraint in all DOF, in order to capture the proper model of rotor turbine blade. Following steps listed in table 3.2 are performed for the modeling procedure of uncoated plate.

FE Modeling Summary for Uncoated Plate		
Analysis Type	Structural Vibration	Free Vibration
		Forced Vibration
Control Cards	Element Type	3D Hexahedral plane stress
	Property card	Isotropic E = 1E7 Psi, ν = 0.33, ρ = 2.52E-04 lb/in^3 (Al 6061)
Boundary Conditions and Constraints	Constrained in all DOF at one end	Three translational, three rotational
Analysis Card	Free vibration	Modal Analysis
	Forced Vibration	Application of Concentrated Force at free end
Output Card	Modal Analysis	Required mode Frequencies
	Frequency Response	Von Mises Stresses

Table 3. 2 Summary for Plate Modeling

3.3 Coated Finite Element Modeling of Plate

Coating is the application of another material on base material surface with similar or different properties as of the base material. Coating material should be of such type so that it doesn't alter the mechanical properties and behavior of the base material. Coating is generally applied on the pressure side to capturing effectively the vibratory stresses effect. Two different type of coating materials are selected and applied on the base material. Ti 64 and Hastelloy-X are applied on base material of plate i.e. Al 6061. Properties of Al 6061, Ti 64 and Hastelloy-X are listed in the table 3.3:

Properties of Al 6061, Ti 64 and Hastelloy-X			
Property	AL6061	Ti 64	Hastelloy-X
Modulus of Elasticity (E) Psi	1E+07	1.71E+07	2.89E+07
Density (ρ) lb/in^3	2.52E-04	4.14E-04	7.73E-04
Shear Modulus (G) Psi	1.11E+07	6.38E+06	1.12E+07
Poisson's ratio (v)	0.33	0.34	0.034

Table 3. 3 Properties of Al 6061, Ti 64 and Hastelloy-X

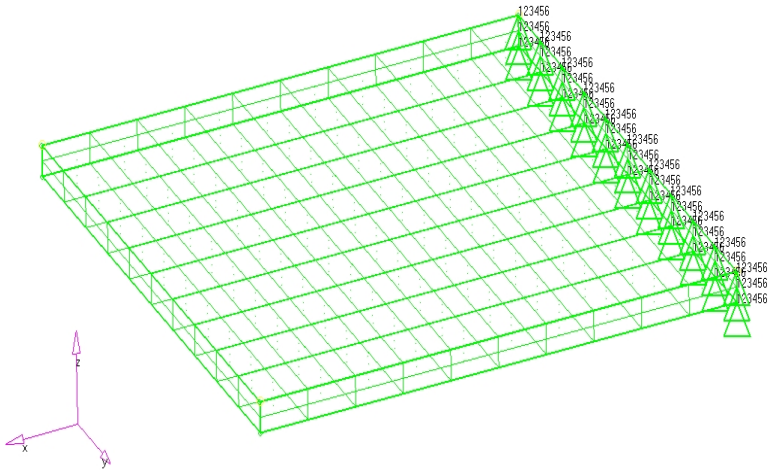

Fig. 3. 2 Meshed and Constraint Coated Plate Model

Meshed Coated plate model with the application of constraints is shown in fig 3.2. Base material is meshed with 3D hex element and coated surface is meshed using shell Quad 4 node isoparametric element. The number of division for the coating material is similar to the number of element division on the upper surface of the base material. Modeling for Ti 64 coating material and Hastelloy-X coating material is performed in similar way. Among the two coating materials, Ti 64 is selected on the basis of better material damping ability then the Hastelloy-X coating material. The steps used for the modeling of coated plate are listed in table 3.4:

FE Modeling Summary for Uncoated Plate		
Analysis type	Structural Vibration	Free Vibration (Modal Analysis)
		Forced Vibration (Frequency Response)
Control Cards	Element Type	3D Hexahedral plane stress Shell Quad 4 node isoparametric
	Property card	Isotropic E = 1E7 Psi, ν = 0.33, ρ = 2.52E-04 lb/in^3 (Al 6061) E = 1.71E7 Psi, ν = 0.34, ρ = 4.14E-04 lb/in^3 (Ti64) E = 2.89E7 Psi, ν = 0.034, ρ = 7.73E-04 lb/in^3 (Hastelloy-X)
Boundary Conditions and Constraints	Constrained in all DOF at one end	Three translational, Three rotational
Analysis Card	Free vibration	Modal Analysis
	Forced Vibration	Application of Concentrated Force at free end
Output Card	Modal Analysis	Required mode Frequencies
	Frequency Response	Von Mises Stresses

Table 3. 4 Steps for FE Modeling of Coated Plate

3.4 Finite Element Modeling of Beam Without Coating

For the current analysis, finite element modeling of uncoated beam is carried out using Aluminum 6061. Aluminum 6061 is generally used for the manufacturing of blades.

All steps listed in the table 3.6 are performed to generate the finite element model for uncoated beam.

FE Modeling Summary for Uncoated Beam		
Analysis type	Structural Vibration	Modal Analysis (Free Vibration)
		Frequency Response (Forced Vibration)
Control Cards	Element Type	3D Hexahedral plane stress
	Material Type and Properties	Isotropic E = 1E7 Psi, ν = 0.33, ρ = 2.52E-04 lb/in^3
Boundary Conditions and Constraints	All nodes of one end are constrained in all 6-DOF	cantilever beam (Three translational, three rotational)
Analysis Card	Free vibration	Modal Analysis
	Forced Vibration	Concentrated Force is applied at free end
Output Card	Modal Analysis	Frequencies for desired modes
	Frequency Response	Von Mises Stresses

Table 3. 5 Summary for Uncoated Beam Modeling

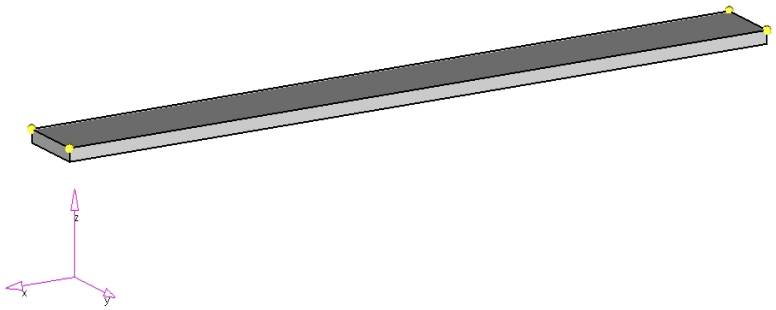

Fig. 3. 3 3D Geometry

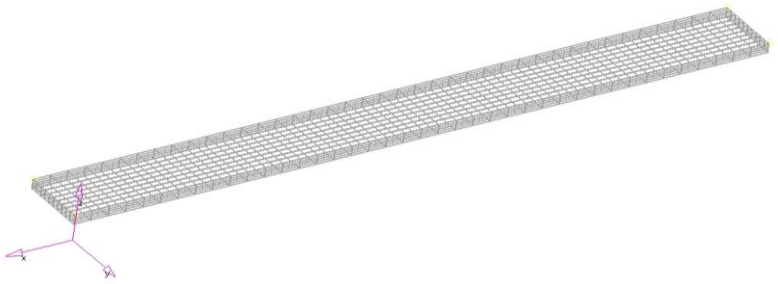

Fig. 3. 4 Meshing of 3D Uncoated Beam

Altair Hypermesh automesh module provides the ability to mesh specified surfaces to a given element edge length. It can also alter mesh density, parameters and element types before accepting the mesh.

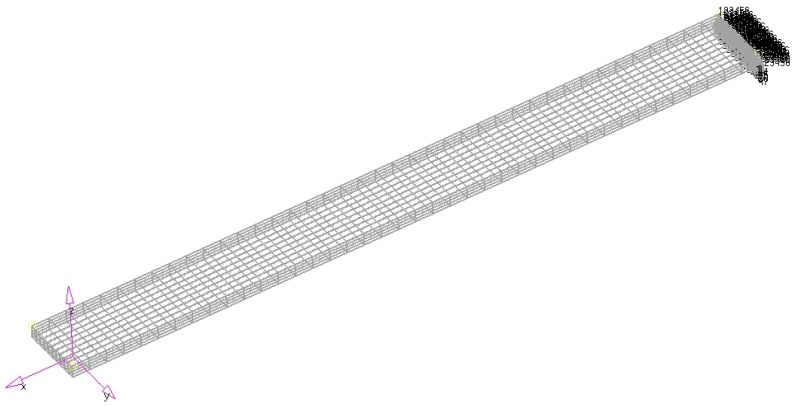

Fig. 3. 5 One End Constraint in all DOF

Figures 3.3, 3.4 and 3.5 show the steps performed for the modeling of beam without coating. First figure shows the 3D model of the beam and second figure shows the meshing after defining the material properties for the beam. Third figure shows the application of constraints, one end is constrained in all direction i.e. three translational and three rotational DOF as in cantilever beam, as cantilever beam depicts the ideal behavior of turbine blade.

3.5 Finite Element Modeling of Beam With Coating

Coating can be defined as the application of additional material layer on the outer surface of the base material. Coating material can be similar to the base material or it can be different from base material. For the present analysis, magnetomechanical material is used as coating on the base material, Al 6061.

Ti64 is the coating material applied on Al 6061 base material. This material is selected on its mechanical properties; method for selecting coating material from several alternative materials to obtain higher structural damping is discussed in [15]. Properties of Al 6061 and coating material Ti64 are listed in table 3.6:

Properties of Al 6061 and Ti64		
Property	AL6061	Ti-64
Modulus of Elasticity (E) Psi	1E+07	1.71E+07
Density (ρ) lb/in^3	2.52E-04	4.14E-04
Shear Modulus (G) Psi	1.11E+07	6.38E+06
Poisson's ratio (ν)	0.33	0.34

Table 3. 6 Properties of Al 6061 and Ti64

Technique used for modeling of coated beam is followed in similar way as for uncoated beam. Shell Quad 4 element is used for the meshing of coating surface and material property card for Ti64 coating material. Procedure followed for modeling of coated beam is shown in the table 3.7:

FE Modeling Summary for Coated Beam		
Analysis type	**Structural vibration**	**Modal Analysis (Free Vibration)**
		Frequency Response (Forced Vibration)
Control Cards	Element Type	3D Hexahedral plane stress Shell Quad 4 node isoparametric for coating surface
	Material Type and Material Properties	Isotropic E = 1E7 Psi, ν = 0.33, ρ = 2.52E-04 lb/in^3 (Al 6061) E = 1.71E7 Psi, ν = 0.34, ρ = 4.14E-04 lb/in^3 (Ti64)
Boundary Conditions and Constraints	All nodes of one end are constrained in all 6-DOF	cantilever beam (Three translational, three rotational)
Analysis Card	Free vibration	Modal Analysis
	Forced Vibration	Concentrated Force is applied at free end
Output Card	Modal Analysis	Frequencies for desired modes
	Frequency Response	Von Mises Stresses

Table 3. 7 Steps for Coated Beam Modeling

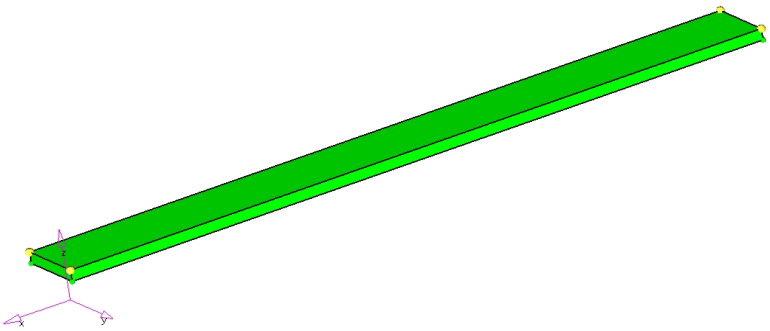

Fig. 3. 6 3D Model of Beam with Coating

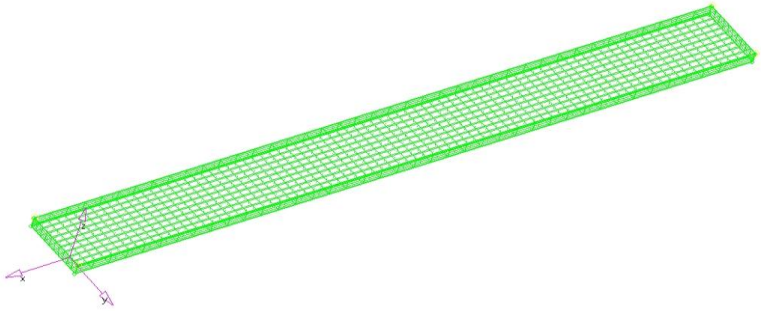

Fig. 3. 7 Meshing of 3D Coated Beam

Meshing for coated beam is performed using auto mesh module, base material is meshed using 3D hexahedral element and coating surface is meshed using Shell Quad 4 isoparametric element. Quad 4 is an isoparametric element with in-plane i.e. plane stress and out of plane i.e. bending capabilities. Same number of elements division is used for shell element as used for meshing of 3D hexahedral element.

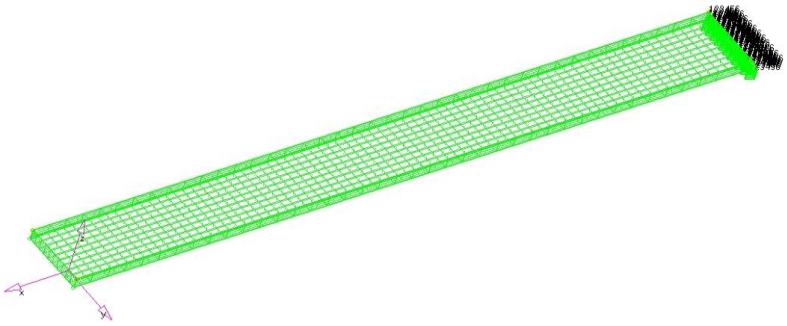

Fig. 3. 8 Constraint in DOF for Coated Beam

Coated beam is constrained in all DOFs at one end. Cantilever beam ideally models the behavior of gas turbine blade mounted in the rotating hub. Therefore, beam is constrained in six DOF, three translational and three rotational.

Four different types of beam have been modeled for the present research. Modeling procedure of beams with and without coating with different dimensions are performed by following the above mentioned techniques, beam with and without coating. Geometric dimensions of four different beams are listed in table 3.8:

Dimensions of Beams used for Analysis	
	Dimensions (inches)
Beam 1	8" × 0.75" × 0.125"
Beam 2	7.087" × 0.3937" × 0.079"
Beam 3	10" × 0.9375" × 0.156"
Beam 4	3.937" × 0.3937" × 0.039"

Table 3. 8 Dimensions of Beams used for Analysis

Chapter 4. Analysis

Finite element modeling of the plate and beam is carried out in pre-processing. The purpose of pre-processing is to obtain the desired output file for the processing step. Hypermesh has the capability to create input files for almost all the famous commercial FE software. Nastran is used as solver for modal and frequency response analysis, for the current problem. Therefore, Nastran profile is selected at start of the FE modeling in Hypermesh. After performing the finite element modeling in Hypermesh, the output files with *.dat extension are created for the Nastran solver. Nastran generally uses the input file having *.dat or *.bdf extension for the analysis purpose.

Nastran solver generally generates two important files with extension *.f06 and *.op2.

- *.f06 file extension contains the results in the form of data/numbers. It can be easily opened in any text editor like Notepad or WordPad. This file contains formatted input data, the specified output results like displacement and stresses and it also has errors and warnings listed if any.

- *.op2 file is the binary output file and can be imported to any post-processing software like Altair FEA Hyperview.

4.1 Uncoated Plate Free Vibration Analysis

In this study, free vibration analysis or modal analysis of plate is performed. The purpose of modal analysis is to identify the desired natural frequency with respect to the mode shapes. About 200 3D hexahedral solid elements are used in the modeling of uncoated plate. Natural frequencies of respective modes are listed in the table 4.1:

Modes for Uncoated Plate	
Mode No.	Al 6061 Frequency (Hz)
1	168.56
2	399.25
3	1009.55
4	1263.33
5	1435.52
6	2094.33
7	2420.14
8	2881.40
9	2912.84
10	3269.28

Table 4. 1 Modes for Uncoated Plate

After the analysis, mode shapes are plotted in Altair Hyperview post-processor. The 1st mode shape is the first bending mode. The 2nd mode shape is a torsional mode. The 3rd mode shape is the 2nd bending mode and the 4th, 5th and 6th mode shapes are again torsional modes. The 7th mode shape is the 3rd bending mode.

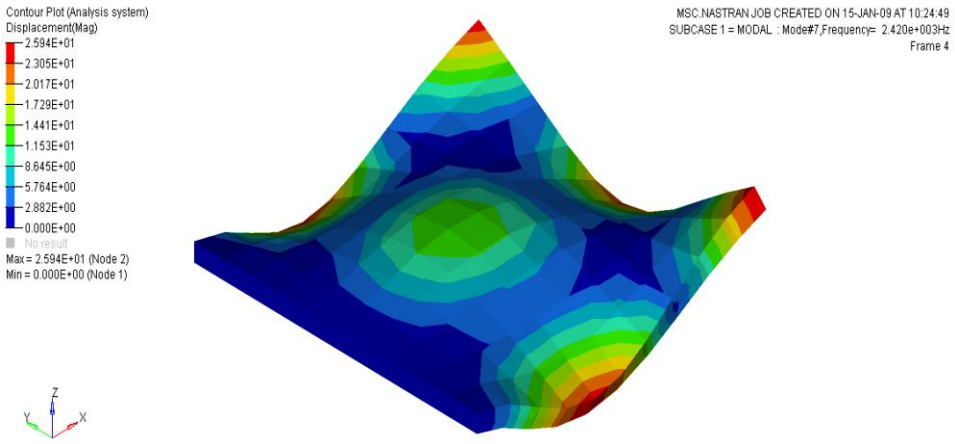

Fig. 4. 1 Al6061 3rd Bending Mode (Without Coating)

The natural frequency of this third bending mode is identified as the stripe mode and is verified from plate theory. The figure 4.1 shows the 3rd bending mode.

4.2 Coated Plate Modal Analysis

The 3rd bending mode natural frequency is identified after performing the modal analysis. Two type of coating material is used for the Al-6061 plate. Coating material can have similar or different material properties to the base material on which coating is applied. Ti64 and Hastelloy-X are used as coating material on Al6061 plate. The properties of these coating materials are listed in table 4.2.

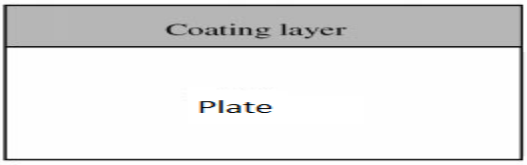

Fig. 4. 2 Plate Cross Section

Modes Natural Frequencies for Ti 64 and Hastelloy-X			
Modes No.	Al 6061 Frequency (Hz)	Al6061_Ti64 Frequency (Hz)	Al6061_HX Frequency (Hz)
1	168.5669	206.8897	212.7001
2	399.2598	484.2725	532.1611
3	1009.553	1214.015	1270.109
4	1263.330	1529.890	1572.977
5	1435.521	1715.211	1827.713
6	2094.332	2100.589	2115.212
7	2420.146	2872.996	3045.535
8	2881.406	3382.509	3392.898
9	2912.844	3413.440	3534.228
10	3269.282	3813.261	3868.737

Table 4. 2 Modes Natural Frequencies for Ti 64 and Hastelloy-X

The natural frequencies for coated plate are obtained and listed in the table 4.2. Similarly identification of 3rd bending mode for the coated plate is made as for the Al6061 uncoated plate. The 1st mode shape is the first bending mode. The 2nd mode shape is a torsional mode. The 3rd mode shape is the 2nd bending mode. The 4th and 5th mode shapes are torsional modes. The 6th mode shape is again torsional mode. The 7th mode shapes is the 3rd bending mode.

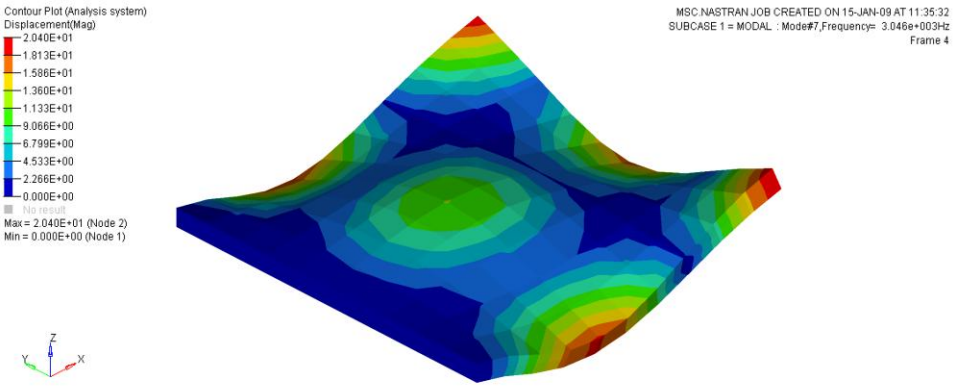

Fig. 4. 3 Al6061_HX 3rd Bending Mode (With Coating)

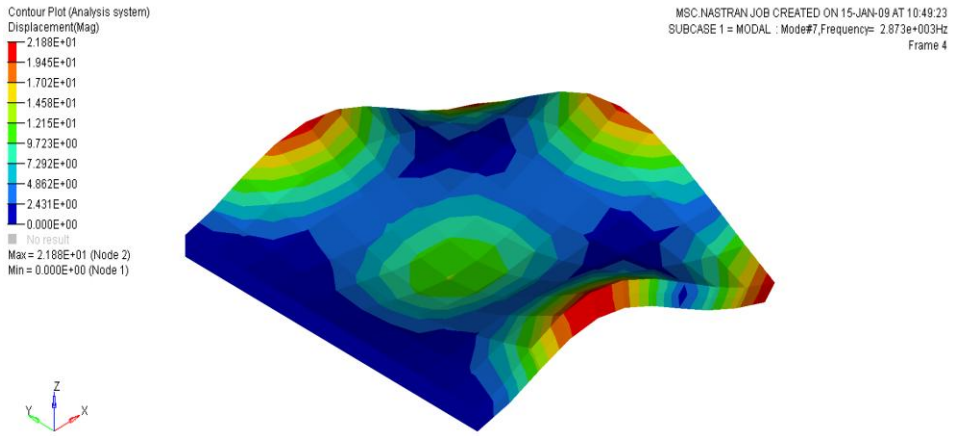

Fig. 4. 4 Al6061_Ti64 4th Bending Mode (With Coating)

Third bending mode for Hastelloy-X and Ti 64 coated plates are plotted and shown if fig 4.3 and 4.4 respectively by using Hyperview.

4.3 Uncoated Plate Frequency Response Analysis

Concentrated force of 1lb is applied at the free end of the plate to perform the frequency response analysis. Natural frequency of identified stripe mode is used for the analysis. After the analysis stresses are obtained for the 3rd bending mode. This is the mode at which body experiences the maximum vibratory stress.

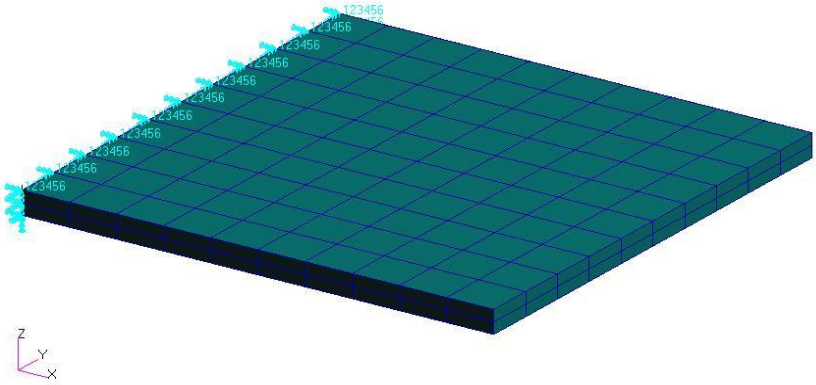

Fig. 4. 5 Uncoated FE model of plate in NASTRAN

The fig 4.5 shows the finite element model in PATRAN. PATRAN is used for generating the forced response input file for NASTRAN analysis. The fig 4.6 shows the application of 1lb tip force. Harmonic excitation is used for the analysis of frequency response. The 3rd bending mode frequency for the forced response analysis is also defined in the PATRAN. This is the modal frequency where body experiences the maximum vibratory stresses.

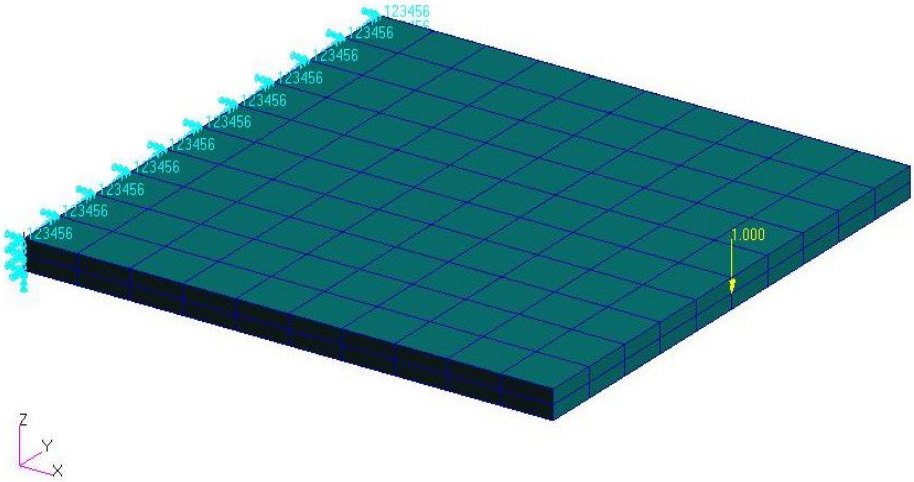

Fig. 4. 6 1lb force application for uncoated plate in NASTRAN

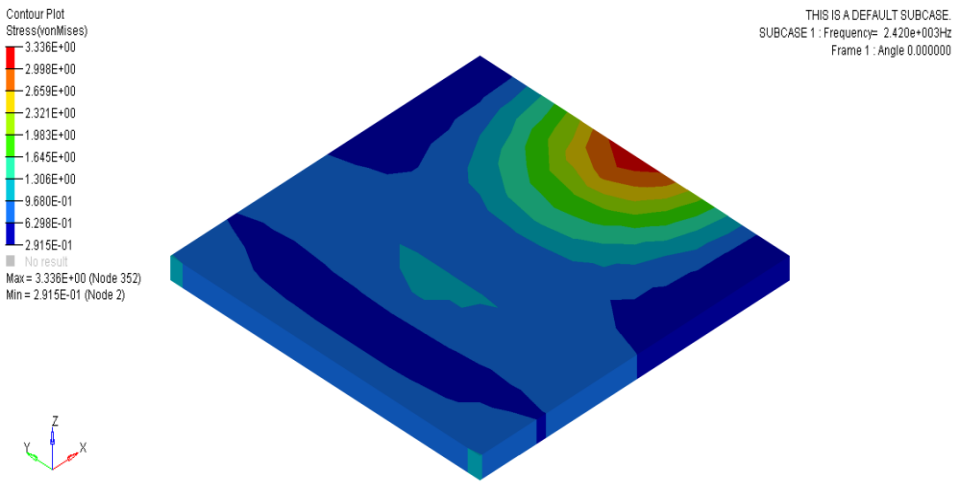

Fig. 4. 7 Al6061 FR (Without Coating)

Performing the analysis in the NASTRAN, results are plotted using the post processor HYPERVIEW. Fig 4.7 shows the variation of stresses on the uncoated plate.

4.4 Coated Plate Frequency Response Analysis

Shell Quad 4 isoparametric element is used for the meshing of coating surface. The frequency response card for the NASTRAN input file is obtained using the PATRAN. Natural frequency for the 4th bending mode is used for the analysis purpose. A force of 1lb is also applied on the free end of the plate to perform the forced response analysis.

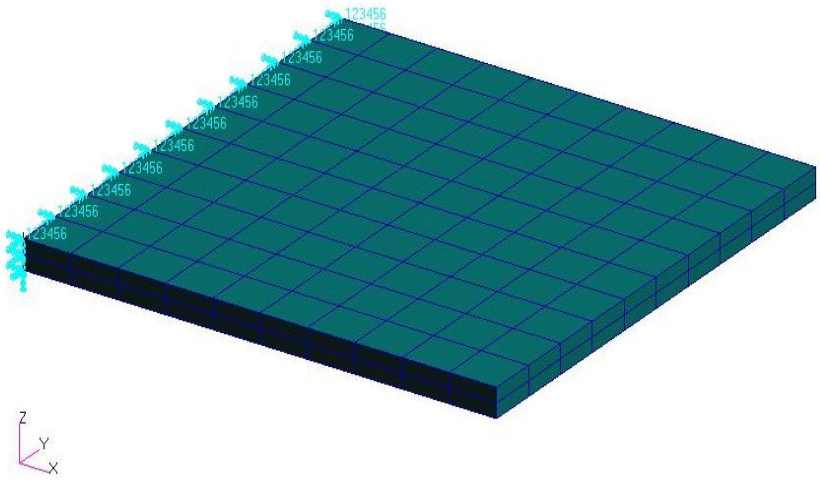

Fig. 4. 8 Coated FE model of plate in NASTRAN

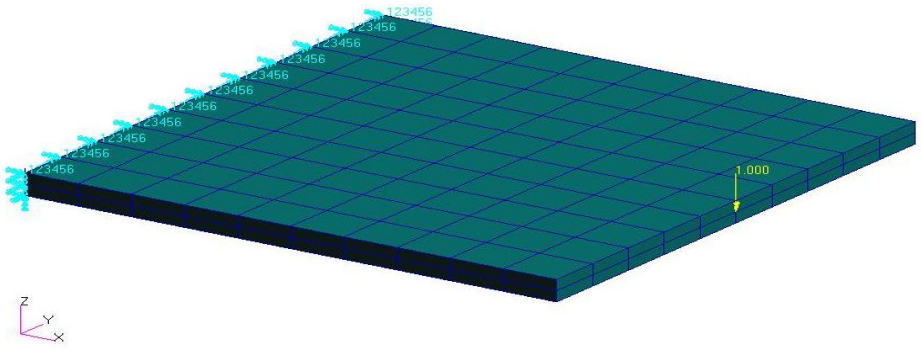

Fig. 4. 9 Frequency Response Model for coated plate

Stripe mode or 3rd bending mode frequency is used for the frequency response analysis. 1lb force is applied at the free end; corresponding vibratory stresses are obtained after the analysis.

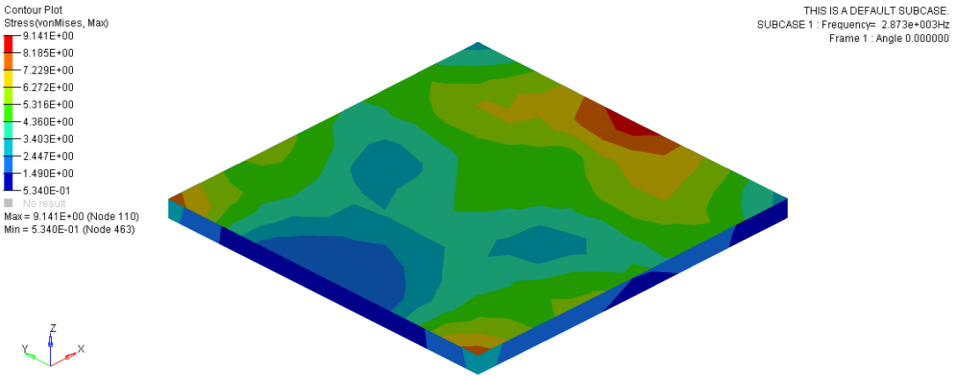

Fig. 4. 10 Al6061_Ti64 FR (With Coating)

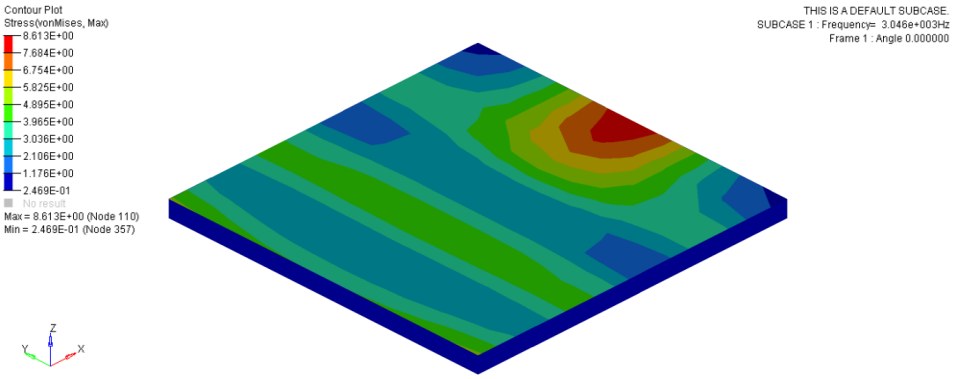

Fig. 4. 11 Al6061_HX FR (With Coating)

Frequency response for Ti 64 and Hastelloy-X coating materials are shown in the fig 4.10 and 4.11 respectively. Stresses are obtained for the two different types of coating. Comparisons for the stress obtained for the uncoated and coated beam is tabulated in table 4.3:

Stress Comparison of coating materials		
	Frequency (Hz)	VonMises Stresses (Max) Psi
Al6061	2420.146	333.6
Al6061_Ti64	2872.996	310.45
Al6061_HX	3045.535	434.94

Table 4. 3 Stress Comparison of coating materials

The purpose of this stress comparison is to select the coating material for Al6061 plate. Result shows that Ti-64 coating material produces less stress than Hastelloy-X coating material. The main objective of this present thesis is to calculate the optimum coating thickness which will result in less vibratory stress then uncoated plate.

This will be more elaborate when the analysis is performed for the beam, curve plate and finally to the actual turbine blade.

4.5 Without Coating Beam Modal Analysis

Cantilever beam is considered for the analysis purpose. Cantilever beam is the simplest model of the gas turbine rotor blade. Al 6061 material properties are used for the finite element model of uncoated beam. Approximately 1600 3D hexahedral solid elements are used for the finite element beam model. For the purpose of analysis, natural frequencies of the respective modes of beam are determined. Modal analysis is performed to obtain the natural frequency of the maximum displacement mode of the beam. This is the mode at which the maximum vibratory stresses are produced. Four different beam sizes are used for the analysis and their dimensions are listed in the table 4.4.

Dimensions of Four Beams used for Analysis	
	Dimensions (inches)
Beam 1	8" × 0.75" × 0.125"
Beam 2	7.087" × 0.3937" × 0.079"
Beam 3	10" × 0.9375" × 0.156"
Beam 4	3.937" × 0.3937" × 0.039"

Table 4. 4 Dimensions of Four Beams used for Analysis

Natural frequencies of the desired modes for the four uncoated beams are obtained by modal analysis. The respective natural frequencies for the uncoated beams are shown in table 4.5.

Uncoated Beams Natural Frequencies				
	Beam 1	Beam 2	Beam 3	Beam 4
Modes	**Al6061 Frequencies (Hz)**	**Al6061 Frequencies (Hz)**	**Al6061 Frequencies (Hz)**	**Al6061 Frequencies (Hz)**
1	63.4	50.9	50.6	81.8
2	376.3	252.7	301.0	512.4
3	397	319.1	317.0	814.9
4	1111.1	893.6	887.4	1436.0
5	1211.7	1561.6	968.0	1518.5
6	2177.3	1599.9	1739.1	2819.5
7	2267.1	1752.1	1813.6	4577.9
8	3600.2	2899.4	2875.7	4673.9
9	3649.1	4279.3	2915.0	4884.2
10	5379.8	4337.7	4297.2	7005.8

Table 4. 5 Without Coating Beams Natural Frequencies

Finite element model bending mode natural frequencies are verified by using the Euler-Bernoulli beam theory. Beam theory calculates the natural frequencies of the bending modes. The comparison of the bending mode natural frequencies for the four beams are listed in the below tables.

Bending Modes Natural Frequencies for Beam_1		
Mode Shapes	Beam Theory	FEM
	Frequency (Hz)	**Frequency (Hz)**
1st bending mode	62.9	63.4
2nd bending mode	393.9	397.0
3rd bending mode	1102.9	1111.1
4th bending mode	2161.2	2177.3
5th bending mode	3572.6	3600.2

Table 4. 6 Bending Modes Natural Frequencies for Beam_1

The mode shapes for FE model of uncoated beam are plotted in post-processor HYPERVIEW. The 1st mode is the 1st bending mode. The 2nd mode shape is the torsional mode. The 3rd and 4th mode shapes are the 2nd and 3rd bending mode respectively. The 5th mode shape is again the torsional mode. The 6th mode shape is the 4th bending mode. This mode shape is also identified as the third stripe mode and is the mode shape at which beam experiences the maximum displacement. The 7th mode is torsional mode. The 8th mode is the 5th bending mode. The natural frequencies for bending modes from beam theory and finite element model are listed in the table 4.6.

In the case of second beam, 1st mode shape is the bending mode. The 2nd mode is the torsional mode. The 3rd mode shape is the 2nd bending mode. The 4th mode shapes is the 3rd bending mode. The 5th and 6th mode shapes are again the torsional mode. The 7th mode is the 4th bending mode. The 8th mode is the 5th bending mode. Natural frequencies calculated from the beam theory and bending natural frequencies for finite element model are shown in the table 4.7.

Bending Modes Natural Frequencies for Beam_2		
Mode Shapes	Beam Theory	FEM
	Frequency (Hz)	**Frequency (Hz)**
1st bending mode	50.6	50.9
2nd bending mode	317.2	319.1
3rd bending mode	888.2	893.6
4th bending mode	1740.5	1752.1
5th bending mode	2877.1	2899.4

Table 4. 7 Bending Modes Natural Frequencies for Beam_2

The third beam mode shapes are also plotted in HYPERVIEW. The 1st mode is the bending mode. The 2nd mode is the torsional mode. The 3rd mode is the 2nd bending mode. The 4th mode shapes is the 3rd bending mode. The 5th mode is again the torsional mode. The 6th mode shape is the 4th bending mode. The 7th mode is again the torsional mode. The 8th mode is the 5th bending mode. Bending mode natural frequencies for the beam theory and finite element model are listed in table 4.8.

Bending Modes Natural Frequencies for Beam_3		
Mode Shapes	Beam Theory	FEM
	Frequency (Hz)	**Frequency (Hz)**
1st bending mode	50.3	50.6
2nd bending mode	315.1	317.0
3rd bending mode	882.3	887.4
4th bending mode	1729.0	1739.1
5th bending mode	2858.1	2875.7

Table 4. 8 Bending Modes Natural Frequencies for Beam_3

The fourth beam modes are viewed in HYPERVIEW. The 1st and 2nd mode shapes are the 1st and 2nd bending modes respectively. The 3rd mode is the torsional mode. The 4th mode shape is the 3rd bending mode. The 5th mode is the torsional mode. The 6th mode shape is the 4th bending mode. The 7th mode is again the torsional mode. The 8th mode is the 5th bending mode. Beam theory and finite element model bending mode natural frequencies are listed below in the table 4.9.

Bending Modes Natural Frequencies for Beam_4		
Mode Shapes	Beam Theory	FEM
	Frequency (Hz)	**Frequency (Hz)**
1st bending mode	81.0	81.8
2nd bending mode	507.4	512.4
3rd bending mode	1420.8	1436.0
4th bending mode	2784.2	2819.5
5th bending mode	4602.4	4673.9

Table 4. 9 Bending Modes Natural Frequencies for Beam_4

The 4th bending mode is also identified as 3rd stripe mode. The 3rd stripe mode is the mode shapes where body vibrates with patterns of worst case scenario and experiencing maximum deflection. The above tables show that the analytical bending mode frequencies obtained from beam theory have close values as compared with bending mode frequencies for the finite element model.

Comparison of bending mode shapes obtained from the beam theory and the mode shapes obtained from FE model are shown below.

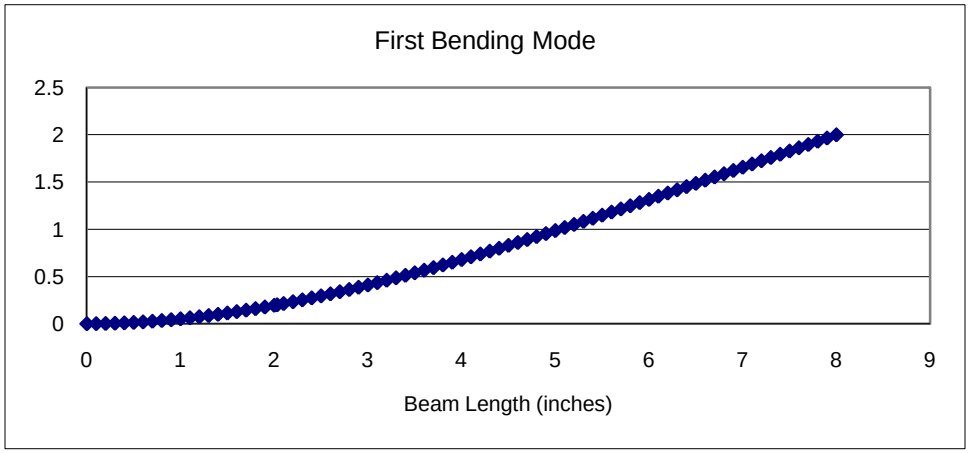

Fig. 4. 12 The 1st Bending Mode (Beam Theory)

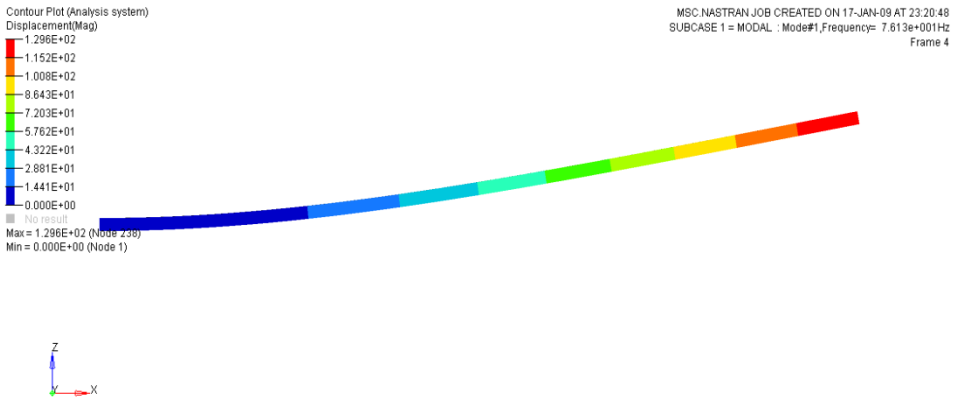

Fig. 4. 13 The 1st Bending Mode (FE model)

The 1st bending mode shape pattern for beam theory and finite element model is shown in fig 4.12 and 4.13.

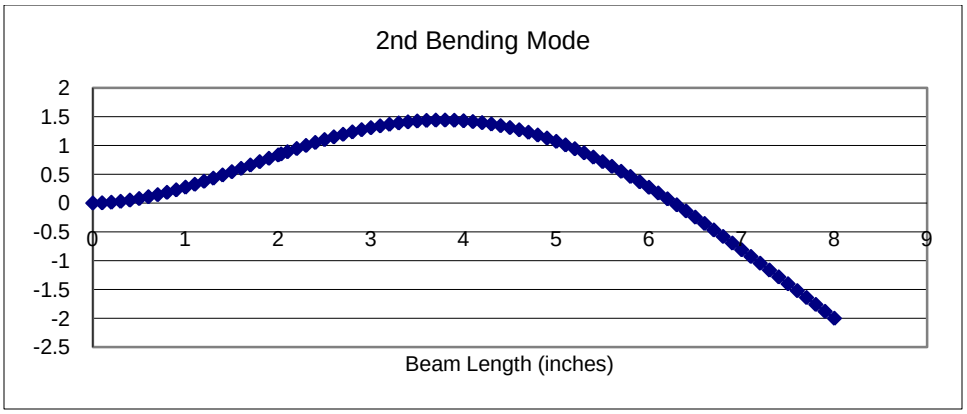

Fig. 4. 14 The 2nd Bending Mode (beam theory)

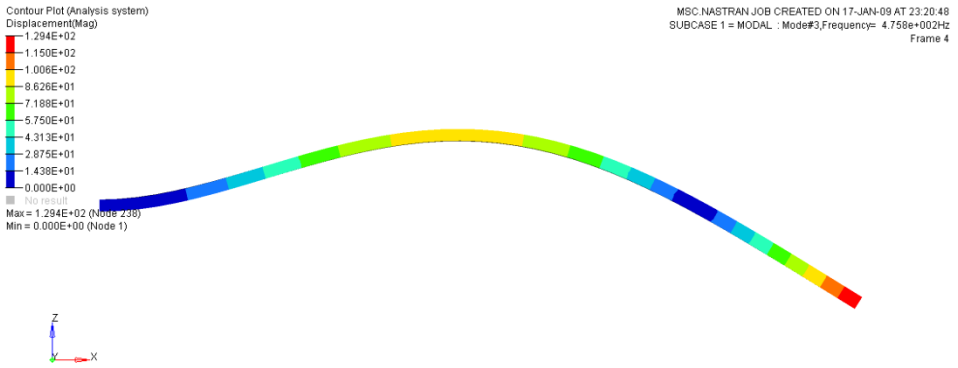

Fig. 4. 15 The 2nd Bending Mode (FE model)

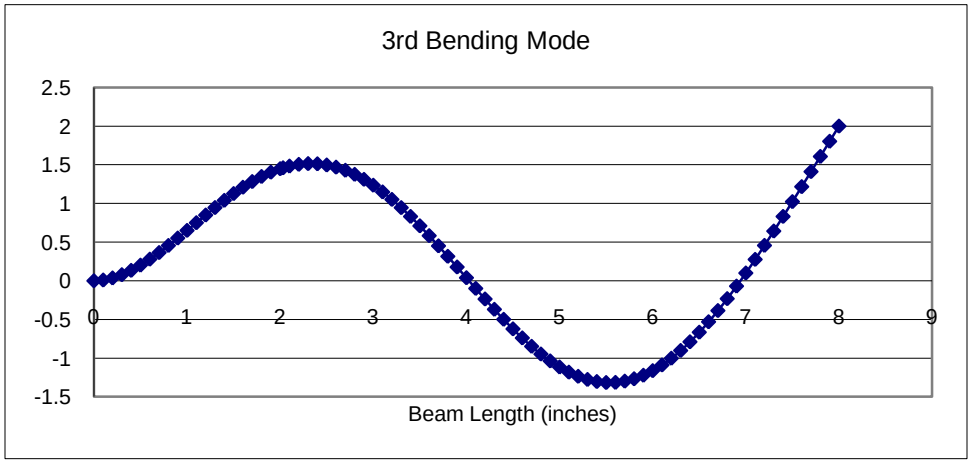

Fig. 4. 16 The 3rd Bending Mode (beam theory)

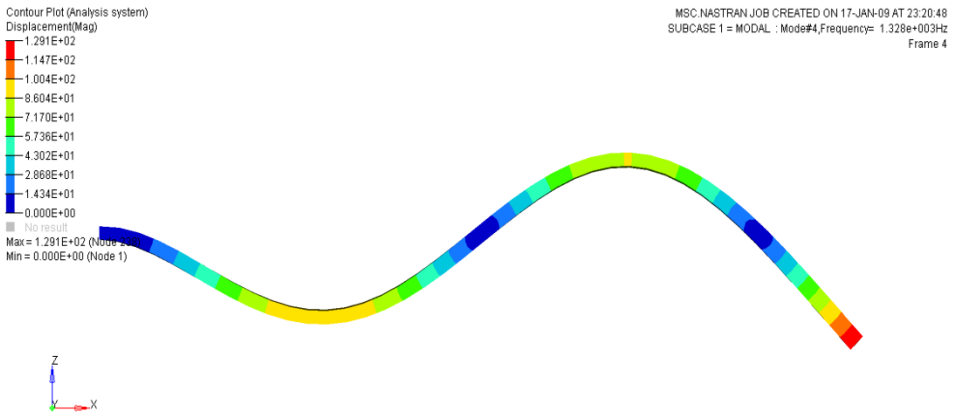

Fig. 4. 17 The 3rd Bending Mode (FE model)

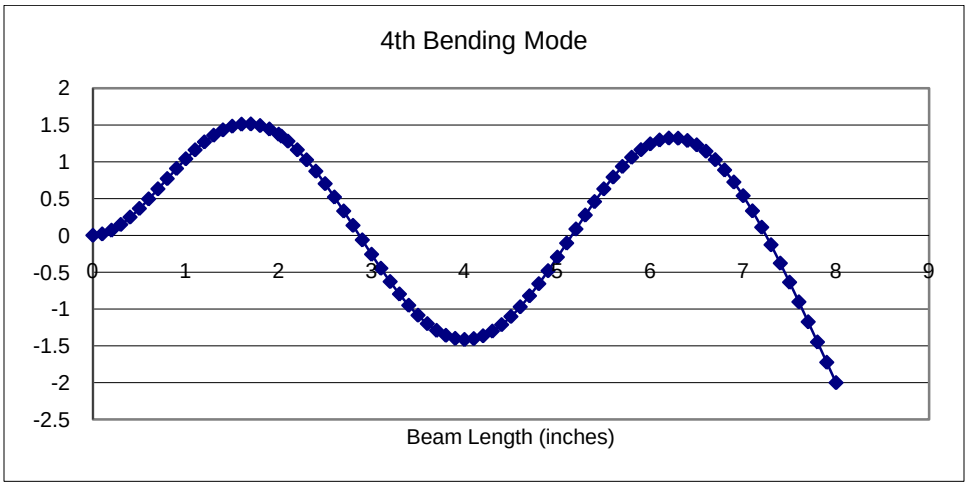

Fig. 4. 18 The 4th Bending Mode (beam theory)

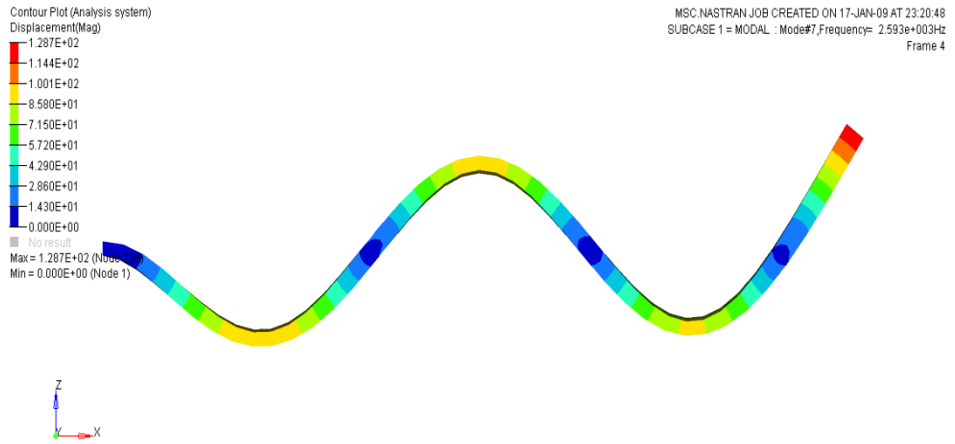

Fig. 4. 19 The 4th Bending Mode (FE model)

The main purpose of modal analysis is to obtain the natural frequency for the 4th bending mode or 3rd stripe mode. Body experiences the maximum stresses at this mode.

4.6 Coated Beam Modal Analysis

Application of thin layer of material on the surface of base material having similar or different properties than the base material is defined as coating. Two types of surface coating materials are used i.e. Ti-64 and Hastelloy-X. Analysis for the coated plate using these coating material shows that Ti-64 is better than Hastelloy-X for the suppression of vibratory stresses. Therefore, beam with Ti-64 coating material is used for coated beam analysis.

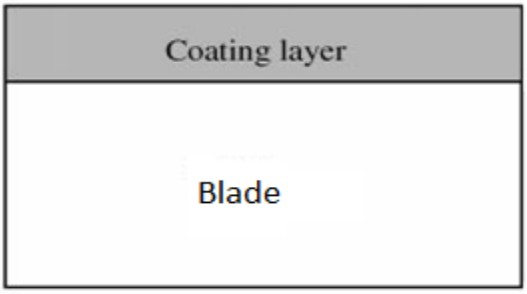

Fig. 4. 20 Beam Cross Section

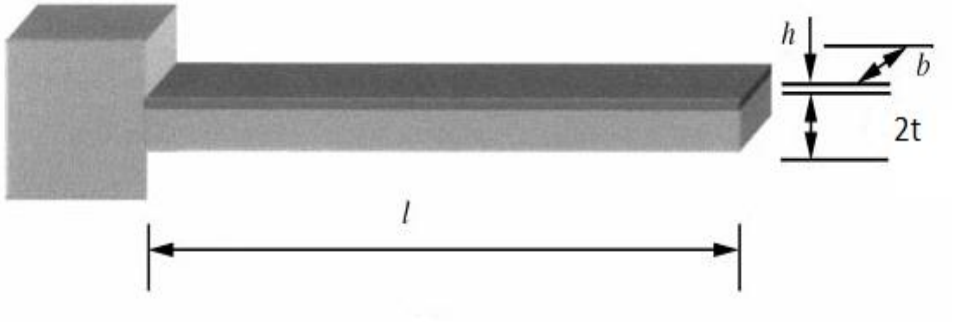

Fig. 4. 21 Coated Cantilever Beam

The fig 4.21 shows the application of coating on the cantilever beam. Coating is applied at the entire pressure side to capture the vibratory stress patterns. Shell Quad 4 element is used for the meshing of coating surface. Base material is meshed with 3D hexahedral element. The frequency range of 1- 10k Hz are used for the calculation of mode shapes. Nearly 2400 elements are used to capture the effect of coating on third stripe mode

frequency. Four beams with different dimensions are used and beams dimensions are listed in the table 4.10.

Dimensions of Beams	
	Dimensions (inches)
Beam 1	8" × 0.75" × 0.125"
Beam 2	7.087" × 0.3937" × 0.079"
Beam 3	10" × 0.9375" × 0.156"
Beam 4	3.937" × 0.3937" × 0.039"

Table 4. 10 Dimensions of Beams

Rectangular beam with dimensions 8.0 in×0.75 in×0.125 in is used for the modal analysis. Natural frequencies for the various coatings is obtained and listed in table 4.11-4.17.

Natural Frequencies for Beam_1 with Various Coating Thicknesses			
Mode No.	Al 6061	Al 6061 with Ti-64 Coating thickness (0.002 in)	Al 6061 with Ti-64 Coating thickness (0.003 in)
	Frequency (Hz)	**Frequency (Hz)**	**Frequency (Hz)**
1	63.42	66.66	68.12
2	376.34	376.67	376.82
3	397.00	417.14	426.15
4	1111.11	1166.72	1191.60
5	1211.75	1265.07	1288.36
6	2177.34	2269.08	2270.00
7	2267.10	2284.12	2331.84
8	3600.25	3772.12	3848.84
9	3649.12	3809.20	3879.08
10	5379.87	5628.17	5738.84

Table 4. 11 Natural Frequencies for Beam_1 with Various Coating Thicknesses (a)

Natural Frequencies for Beam_1 with Various Coating Thicknesses			
Al 6061 with Ti-64 Coating thickness (0.004 in)	Al 6061 with Ti-64 Coating thickness (0.005 in)	Al 6061 with Ti-64 Coating thickness (0.006 in)	Al 6061 with Ti-64 Coating thickness (0.007 in)
Frequency (Hz)	**Frequency (Hz)**	**Frequency (Hz)**	**Frequency (Hz)**
69.47	70.75	71.94	73.07
376.97	377.11	377.24	377.36
434.58	442.47	449.90	456.91
1214.83	1236.60	1257.07	1276.38
1309.70	1329.31	1347.36	1364.05
2270.87	2271.70	2272.49	2273.24
2376.38	2418.08	2457.27	2494.19
3920.37	3987.29	4050.10	4105.93
3943.09	4001.86	4055.96	4109.22
5841.92	5938.24	6018.42	6020.40

Table 4. 12 Natural Frequencies for Beam_1 with Various Coating Thicknesses (b)

Natural Frequencies for Beam_1 with Various Coating Thicknesses			
Al 6061 with Ti-64 Coating thickness (0.008 in)	Al 6061 with Ti-64 Coating thickness (0.009 in)	Al 6061 with Ti-64 Coating thickness (0.01 in)	Al 6061 with Ti-64 Coating thickness (0.012 in)
Frequency (Hz)	**Frequency (Hz)**	**Frequency (Hz)**	**Frequency (Hz)**
74.14	75.16	76.13	77.93
377.48	377.60	377.71	377.91
463.55	469.84	475.82	486.97
1.294.63	1311.94	1328.38	1359.01
1.379.53	1393.93	1407.40	1431.91
2.273.96	2274.65	2275.31	2276.55
2529.07	2562.11	2593.49	2651.83
4152.24	4195.35	4235.61	4308.87
4165.02	4217.82	4267.90	4360.87
6022.29	6024.08	6025.80	6029.01

Table 4. 13 Natural Frequencies for Beam_1 with Various Coating Thicknesses (c)

Natural Frequencies for Beam_1 with Various Coating Thicknesses			
Al 6061 with Ti-64 Coating thickness (0.015 in)	Al 6061 with Ti-64 Coating thickness (0.018 in)	Al 6061 with Ti-64 Coating thickness (0.02 in)	Al 6061 with Ti-64 Coating thickness (0.022 in)
Frequency (Hz)	**Frequency (Hz)**	**Frequency (Hz)**	**Frequency (Hz)**
80.35	82.52	83.84	85.09
378.19	378.44	378.59	378.73
501.98	515.36	523.55	531.25
1400.18	1436.81	1459.20	1480.22
1463.87	1491.49	1508.06	1523.44
2278.23	2279.72	2280.63	2281.47
2730.12	2799.58	2841.94	2881.66
4404.31	4486.72	4536.11	4581.95
4485.28	4595.31	4662.22	4724.85
6033.31	6037.09	6039.35	6041.43

Table 4. 14 Natural Frequencies for Beam_1 with Various Coating Thicknesses (d)

Natural Frequencies for Beam_1 with Various Coating Thicknesses			
Al 6061 with Ti-64 Coating thickness (0.023 in)	Al 6061 with Ti-64 Coating thickness (0.024 in)	Al 6061 with Ti-64 Coating thickness (0.025 in)	Al 6061 with Ti-64 Coating thickness (0.027 in)
Frequency (Hz)	**Frequency (Hz)**	**Frequency (Hz)**	**Frequency (Hz)**
85.69	86.27	86.84	87.94
378.80	378.87	378.93	379.05
534.94	538.53	542.02	548.77
1490.28	1500.07	1509.61	1527.98
1530.74	1537.82	1544.69	1557.86
2281.87	2282.25	2282.63	2283.34
2900.65	2919.11	2937.08	2971.67
4603.71	4624.79	4645.23	4684.43
4754.75	4783.78	4812.02	4866.30
6042.41	6043.35	6044.25	6045.96

Table 4. 15 Natural Frequencies for Beam_1 with Various Coating Thicknesses (e)

Natural Frequencies for Beam_1 with Various Coating Thicknesses			
Al 6061 with Ti-64 Coating thickness (0.028 in)	Al 6061 with Ti-64 Coating thickness (0.03 in)	Al 6061 with Ti-64 Coating thickness (0.035 in)	Al 6061 with Ti-64 Coating thickness (0.037 in)
Frequency (Hz)	**Frequency (Hz)**	**Frequency (Hz)**	**Frequency (Hz)**
88.46	89.49	91.89	92.80
379.10	379.21	379.45	379.54
552.03	558.34	573.13	578.71
1536.85	1554.03	1594.18	1609.32
1564.19	1576.41	1604.85	1615.55
2283.68	2284.32	2285.78	2286.31
2988.35	3020.62	3095.90	3124.23
4703.26	4739.59	4824.02	4855.74
4892.45	4942.96	5060.52	5104.67
6046.77	6048.29	6051.68	6052.89

Table 4. 16 Natural Frequencies for Beam_1 with Various Coating Thicknesses (f)

Natural Frequencies for Beam_1 with Various Coating Thicknesses		
Al 6061 with Ti-64 Coating thickness (0.04 in)	Al 6061 with Ti-64 Coating thickness (0.05 in)	Al 6061 with Ti-64 Coating thickness (0.06 in)
Frequency (Hz)	**Frequency (Hz)**	**Frequency (Hz)**
94.12	98.22	102.02
379.66	380.01	380.27
586.79	611.90	635.22
1631.04	1679.36	1724.94
1631.23	1699.17	1762.15
2287.05	2289.17	2290.94
3165.20	3291.92	3409.14
4901.62	5044.10	5177.16
5168.42	5365.11	5546.65
6054.60	6059.73	6065.06

Table 4. 17 Natural Frequencies for Beam_1 with Various Coating Thicknesses (g)

The above tables 4.11-4.17 list the natural frequencies for the variation of Ti-64 coating on Al 6061 base material. The natural frequency for the uncoated beam is also listed. Mode shape pattern for varying thickness of the coating material is plotted in HYPERVIEW. The 1st mode of coated plate is 1st bending mode. The 2nd mode is the torsional mode. The 3rd and 4th modes are the 2nd and 3rd bending modes respectively. The 5th and 6th modes are again torsional modes. The 7th mode is the 4th bending mode. The 4th bending mode is also known as 3rd stripe mode and shown in fig 4.22.

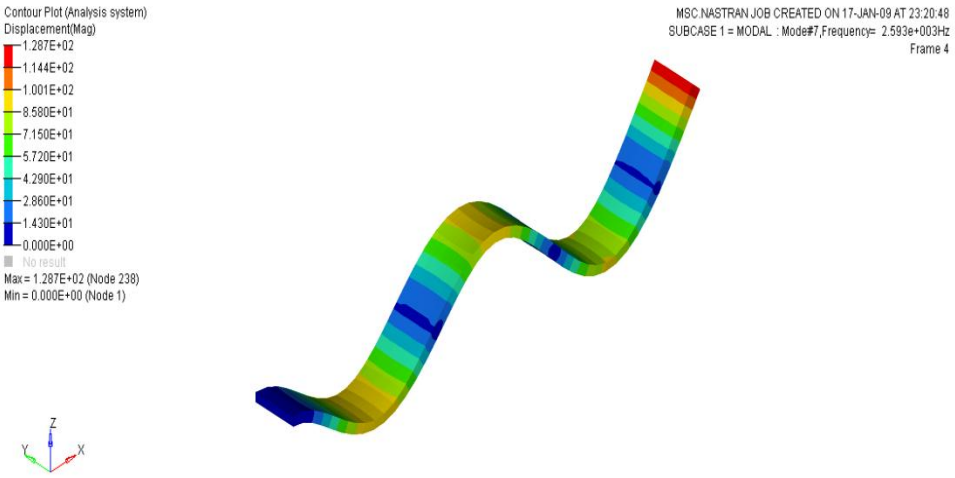

Fig. 4. 22 4th Bending or 3rd Stripe Mode Beam_1

3rd Stripe Mode Frequencies for Beam_1			
Coating Thickness (in)	Height with coating (in)	%age thickness relative to height	3rd Stripe mode Frequency (Hz)
0.002	0.127	1.6	2284.12
0.003	0.128	2.4	2331.84
0.004	0.129	3.2	2376.38
0.005	0.13	4	2418.08
0.006	0.131	4.8	2457.27
0.007	0.132	5.6	2494.19
0.008	0.133	6.4	2529.07
0.009	0.134	7.2	2562.11
0.01	0.135	8	2593.49
0.012	0.137	9.6	2651.83

0.015	0.14	12	2730.12
0.018	0.143	14.4	2799.58
0.02	0.145	16	2841.94
0.022	0.147	17.6	2881.66
0.023	0.148	18.4	2900.65
0.024	0.149	19.2	2919.11
0.025	0.15	20	2937.08
0.027	0.152	21.6	2971.67
0.028	0.153	22.4	2988.35
0.03	0.155	24	3020.62
0.035	0.16	28	3095.90
0.037	0.162	29.6	3124.23
0.04	0.165	32	3165.20
0.05	0.175	40	3291.92
0.06	0.185	48	3409.14

Table 4. 18 3rd Stripe Mode Frequencies for Beam_1

The 4th bending or 3rd third stripe mode frequencies for the various coatings are listed in table 4.18. This table also shows the percentage of coating thickness relative to the height of the beam. The 3rd stripe mode natural frequencies for the coated beam are used for the forced response analysis to get the maximum vibratory stresses.

For the present analysis, four different dimensions of beams are used. The 3rd stripe mode frequencies for the other three beams are also listed in the tables 4.19-4.21.

3rd Stripe Mode Frequencies for Beam_2			
Coating Thickness (in)	Height with coating (in)	%age thickness relative to height	3rd Stripe mode Frequency (Hz)
0.001	0.08	1.2	1821.78
0.002	0.081	2.5	1883.71
0.003	0.082	3.7	1939.37
0.004	0.083	5	1989.82
0.005	0.084	6.3	2035.87
0.006	0.085	7.5	2078.20
0.007	0.086	8.8	2117.34

0.008	0.087	10.1	2153.73
0.009	0.088	11.3	2187.72
0.01	0.089	12.6	2219.63
0.011	0.09	13.9	2249.70
0.012	0.091	15.1	2278.16
0.013	0.092	16.4	2305.20
0.014	0.093	17.7	2330.96
0.015	0.094	18.9	2355.60
0.016	0.095	20.2	2379.23
0.017	0.096	21.5	2401.95
0.018	0.097	22.7	2423.87
0.019	0.098	24	2445.06
0.02	0.099	25.3	2465.59
0.021	0.1	26.5	2485.53
0.023	0.102	29.1	2523.86
0.027	0.106	34.1	2595.57
0.03	0.109	37.9	2646.12
0.04	0.119	50.6	2803.02

Table 4. 19 3rd Stripe Mode Natural Frequencies Beam_2

The mode shapes are viewed using HYPERVIEW. The 1st mode is the first bending mode. The 2nd mode shows the torsion. The 3rd and 4th mode patterns are the 2nd and 3rd bending modes. The 5th and 6th modes are torsional modes. The 7th mode is the 4th bending mode. This is the bending mode where body experiences the maximum deflection. This 4th bending mode is identified as 3rd stripe mode.

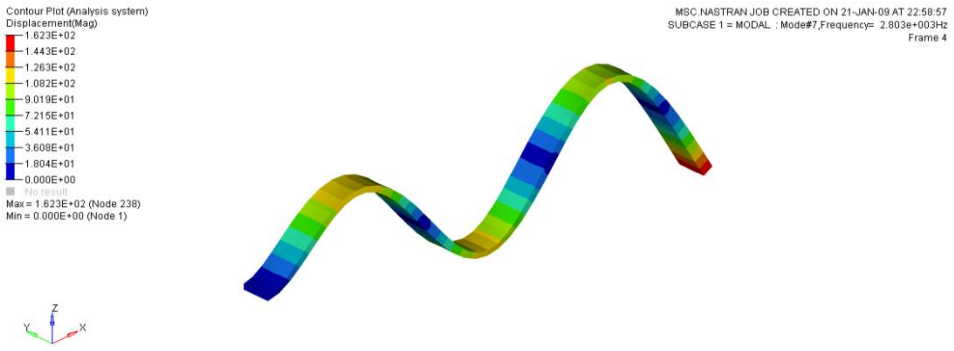

Fig. 4. 23 3rd Stripe Mode for Coated Beam_2

3rd Stripe Mode Frequencies for Beam_3			
Coating Thickness (in)	Height with coating (in)	%age thickness relative to height	3rd Stripe mode Frequency (Hz)
0.001	0.15725	0.6	1774.89
0.003	0.15925	1.9	1840.14
0.007	0.16325	4.4	1950.72
0.01	0.16625	6.4	2020.43
0.013	0.16925	8.3	2081.62
0.016	0.17225	10.2	2136.06
0.018	0.17425	11.5	2169.26
0.02	0.17625	12.8	2200.37
0.022	0.17825	14.1	2229.63
0.026	0.18225	16.6	2283.48
0.028	0.18425	17.9	2308.42
0.03	0.18625	19.2	2332.23
0.032	0.18825	20.5	2355.03
0.034	0.19025	21.7	2376.93
0.038	0.19425	24.3	2418.40
0.04	0.19625	25.6	2438.11
0.044	0.20025	28.2	2475.85
0.048	0.20425	30.7	2511.66
0.049	0.20525	31.4	2520.36
0.05	0.20625	32	2528.96
0.054	0.21025	34.6	2562.54
0.06	0.21625	38.4	2610.79
0.07	0.22625	44.8	2687.18

Table 4. 20 3rd Stripe Mode Natural Frequencies Beam_3

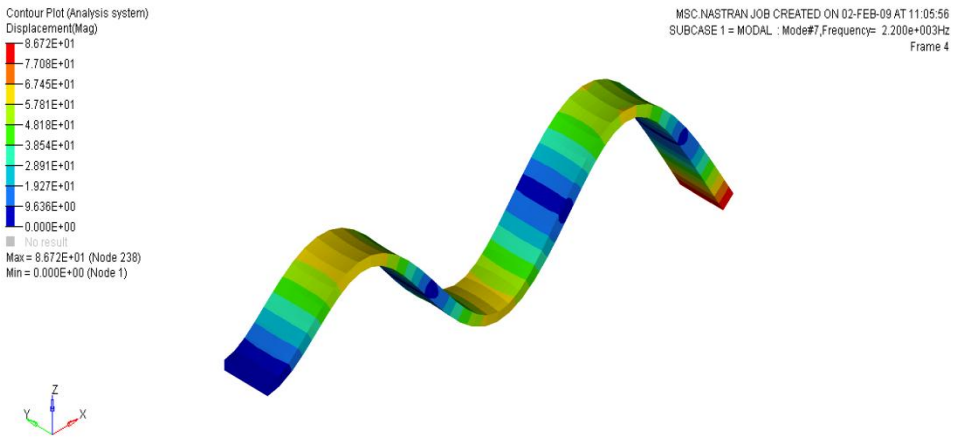

Fig. 4. 24 3rd Stripe Mode for Coated Beam_3

3rd Stripe Mode Frequencies for Beam_4			
Coating Thickness (in)	Height with coating (in)	%age thickness relative to height	3rd Stripe mode Frequency (Hz)
0.0006	0.0396	1.5	2954.11
0.0007	0.0397	1.7	2974.74
0.0008	0.0398	2	2994.90
0.0009	0.0399	2.3	3014.61
0.001	0.04	2.5	3033.90
0.002	0.041	5.1	3206.52
0.003	0.042	7.6	3350.15
0.004	0.043	10.2	3472.77
0.005	0.044	12.8	3579.72
0.006	0.045	15.3	3674.69
0.007	0.046	17.9	3760.36
0.008	0.047	20.5	3838.68
0.009	0.048	23	3911.15
0.01	0.049	25.6	3978.91
0.011	0.05	28.2	4042.86
0.012	0.051	30.7	4103.71
0.015	0.054	38.4	4272.80
0.017	0.056	43.5	4377.99
0.02	0.059	51.2	4529.28

Table 4. 21 3rd Stripe Mode Natural Frequencies Beam_4

The 1st and 2nd modes are the two bending modes. The 3rd mode is the torsional. The 4th mode is the 3rd bending mode. The 5th mode is again torsional mode. The 6th mode is the 4th bending mode.

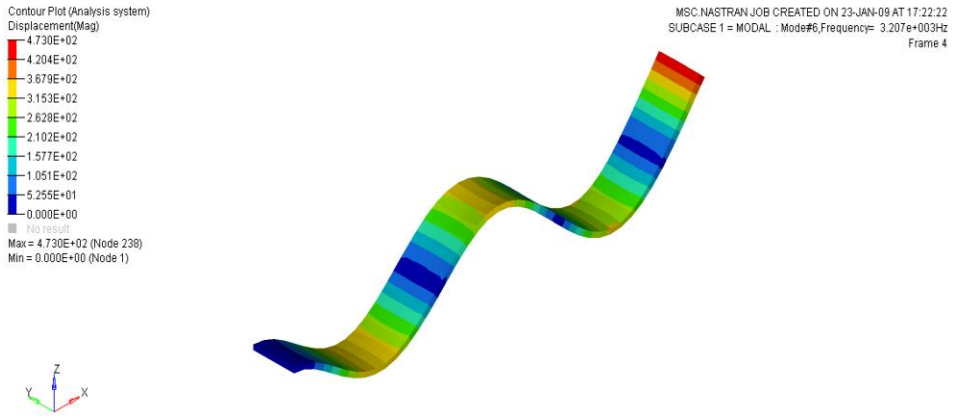

Fig. 4. 25 3rd Stripe Mode for Coated Beam_4

The 3rd stripe mode pattern is viewed in HYPERVIEW. This is the mode which experiences the maximum vibratory stresses.

4.7 Forced Response Analysis of Uncoated Beam

In this thesis, free vibration analysis for the uncoated beam is performed to identify the natural frequencies of the system. The pattern of mode shapes is plotted in HYPERVIEW. These mode shapes include the bending and torsional modes. Identification of bending mode with maximum deflection among the all the other bending modes is made. It has been already established through experiments that these maximum deflection modes or high bending modes produce the maximum vibratory stresses in the system during the operation.

The 4th bending mode is identified as the maximum vibratory stress mode. Forced response analysis is performed for this bending mode frequency. A 3D model of the beam is shown in the figure 4.26.

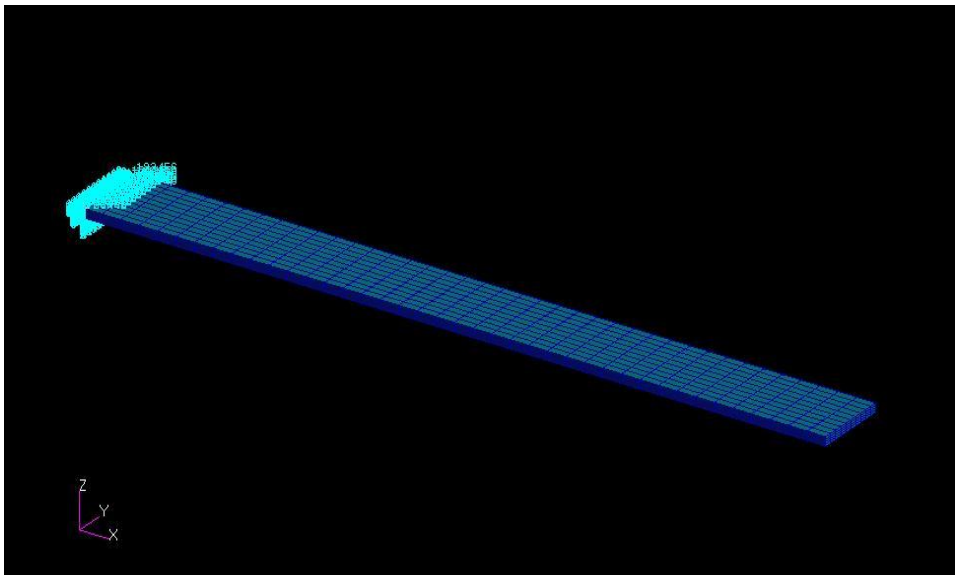

Fig. 4. 26 3D Beam Model in NASTRAN

Harmonic excited force of 1lb is applied at the tip of the beam. PATRAN is used to prepare the force response input file for the NASTRAN solver. Input file contains the information about the geometry, material type and the 4^{th} bending mode's natural frequency.

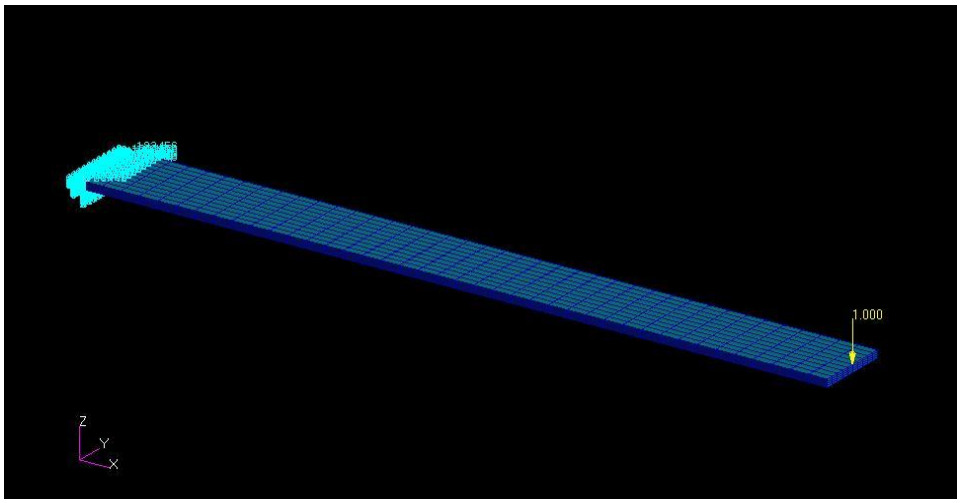

Fig. 4. 27 Harmonic Excitation Force at the Free End of Cantilever

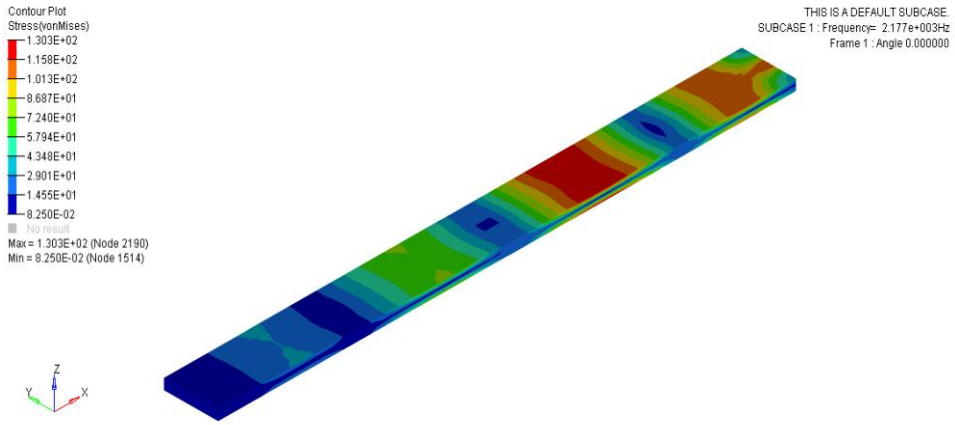

Fig. 4. 28 VonMises Stress Pattern for Beam_1

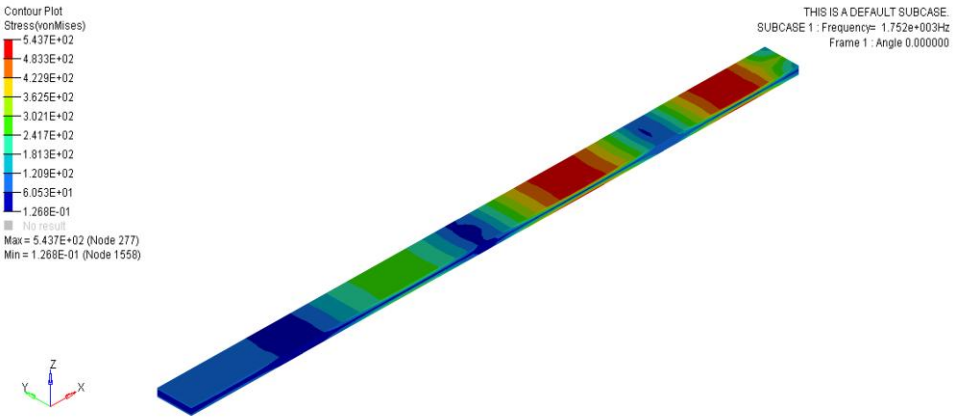

Fig. 4. 29 VonMises Stress Pattern for Beam_2

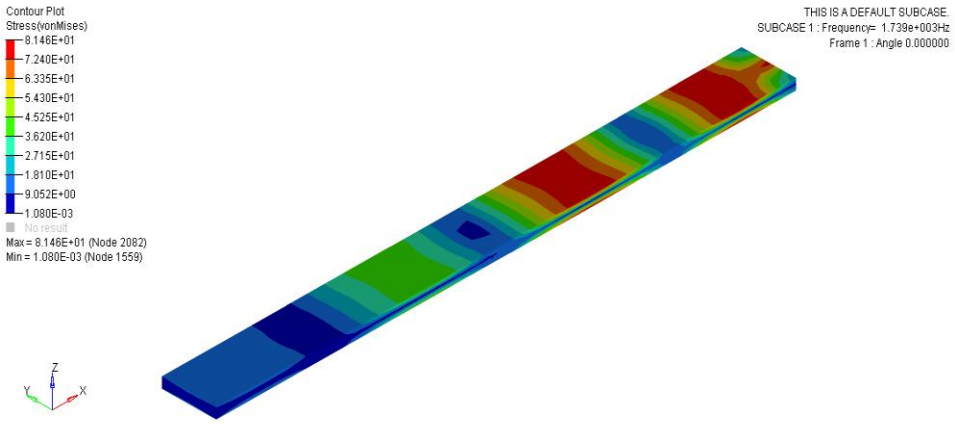

Fig. 4. 30 VonMises Stress Pattern for Beam_3

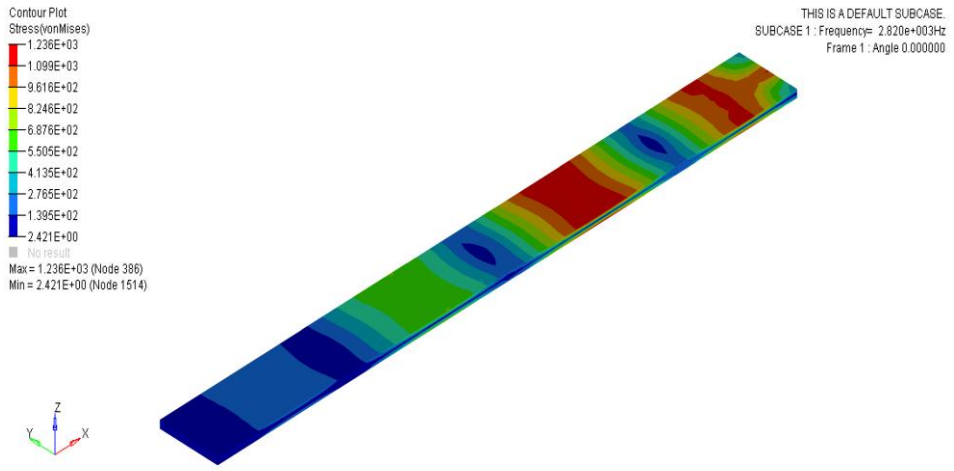

Fig. 4. 31 VonMises Stress Pattern for Beam_4

VonMises stresses patterns of the four beams are shown in above fig 4.28-4.31. It is expected that maximum stresses are generated at the constraint and free end. The stress patterns show the variation of stresses in the form regions. The variation of stresses has the form of sinusoidal wave. Maximum stress is observed at or near the free end in all the cases of beam.

4.8 Forced Response Analysis of Coated Beam

It is required that vibratory stresses should remain in the acceptable limit so that system doesn't fail under the severe operating conditions. Magnetomechanical coating technique is applied to suppress the vibratory stresses. Shell Quad 4 isoparametric element is used for the meshing of coating surface. Base material is meshed by using 3D hexahedral solid element. PATRAN is used for obtaining the forced response analysis file. Concentrated harmonic force of 1lb is applied at the free end of the cantilever beam. Input files for the analysis by NASTRAN with various coating thicknesses are prepared.

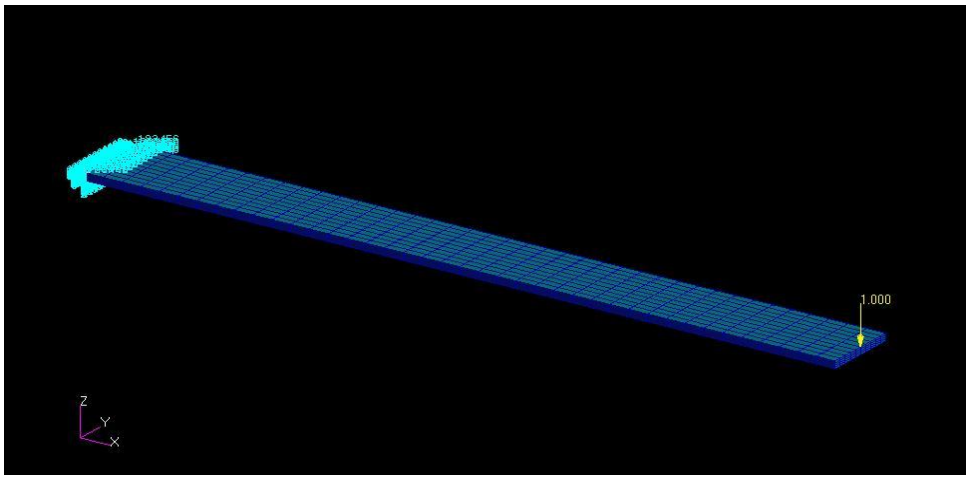

Fig. 4. 32 Concentrated Harmonic Force at the Free End of Coated Beam

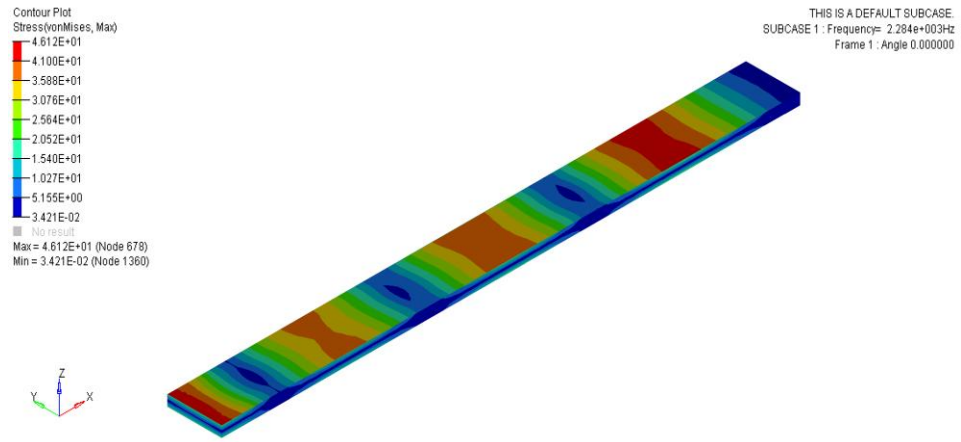

Fig. 4. 33 Coated Beam_1 with 0.002 in Coating VonMises Stress Pattern

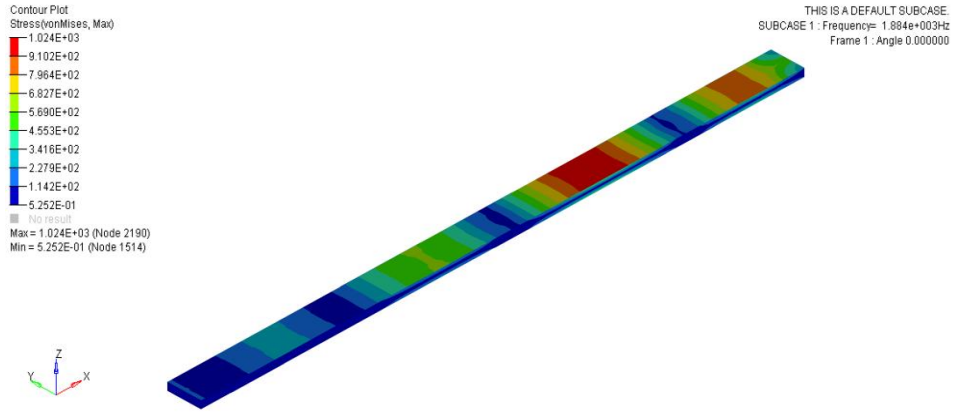

Fig. 4. 34 Coated Beam_2 with 0.002 in Coating VonMises Stress Pattern

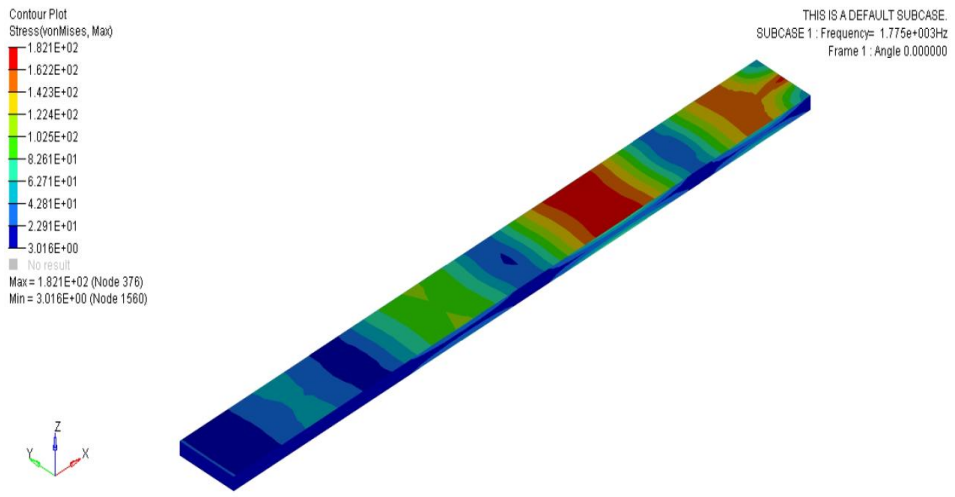

Fig. 4. 35 Coated Beam_3 with 0.001 in Coating VonMises Stress Pattern

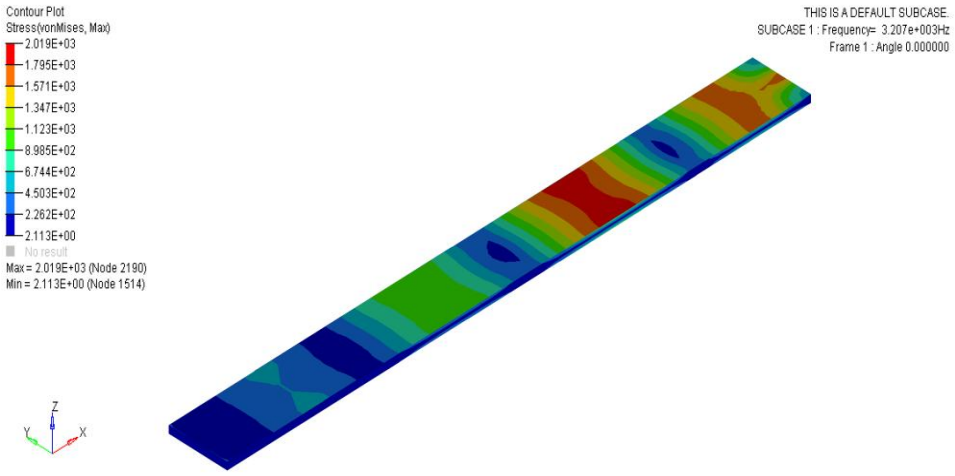

Fig. 4. 36 Coated Beam_4 with 0.002 in Coating VonMises Stress Pattern

The above fig 4.33-4.36 show the pattern variation of VonMises stresses for the four beams. The coating application helps in reduction of the VonMises stresses. At the 4^{th} bending mode three stripes of VonMises stress variation are observed. Due to these three stripes, 4^{th} bending mode is also known as the 3^{rd} stripe mode frequency.

4.9 Curved Plate Forced Response Analysis

Curved plate finite element modeling is performed in the similar way as of plate and beam finite element modeling is carried out. A curved plate having dimension 7 in x 3in

x 0.35 in is used for the free and forced vibration analysis. Beam is the simplest representation of turbine blade and curved plate is the nearest model of the turbine blade.

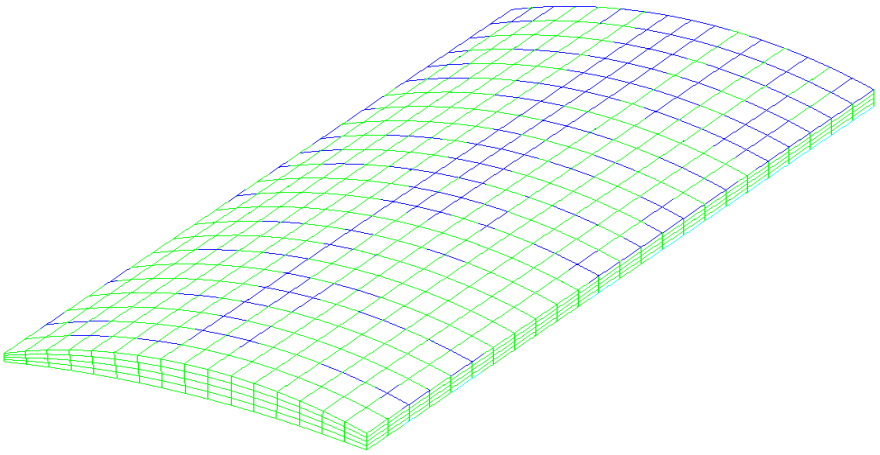

Fig. 4. 37 3D Finite Element Model of Curved Plate

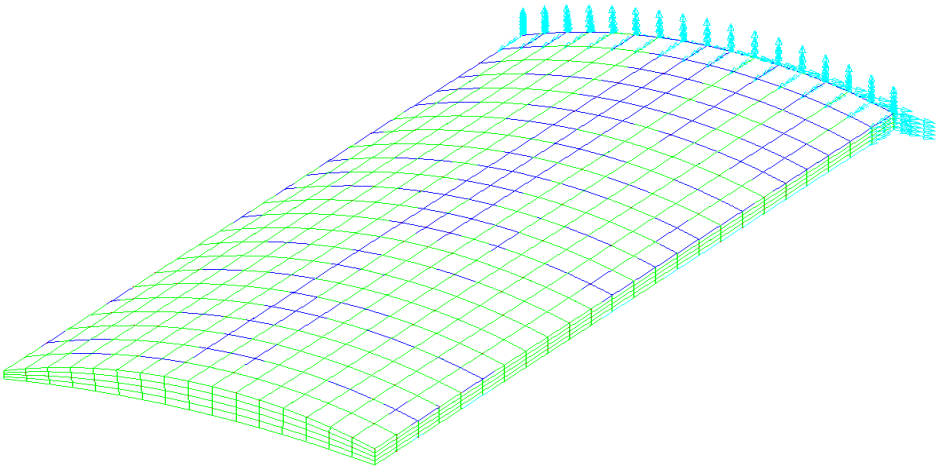

Fig. 4. 38 Constraint Finite Element Model of Curved Plate

Finite element model meshing for the curved is performed using 3D Hexahedral and shell quad isoparametric elements. Approximately 2400 element are used to capture the effect of vibratory stresses pattern with the various coating thicknesses. A tip force of 20lb is applied at the free end of the curved plate to perform the forced response analysis.

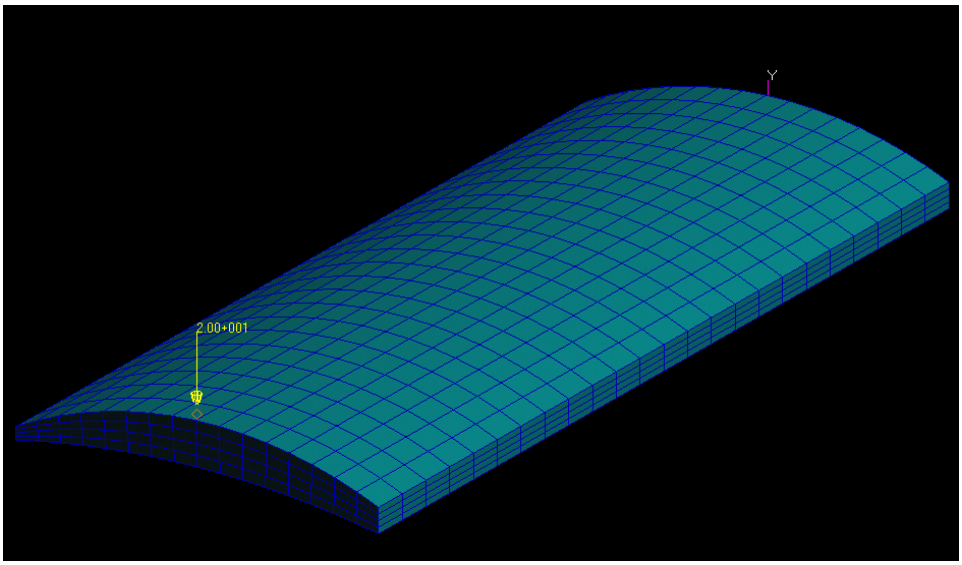

Fig. 4. 39 Concentrated Harmonic Force at the Free End of Coated Curved Plate

4.10 Blade Forced Response Analysis

Actual turbine blade model is performed using the 3D Hexahedral, shell quad and penta elements. A force of 50lb is applied for the frequency response analysis.

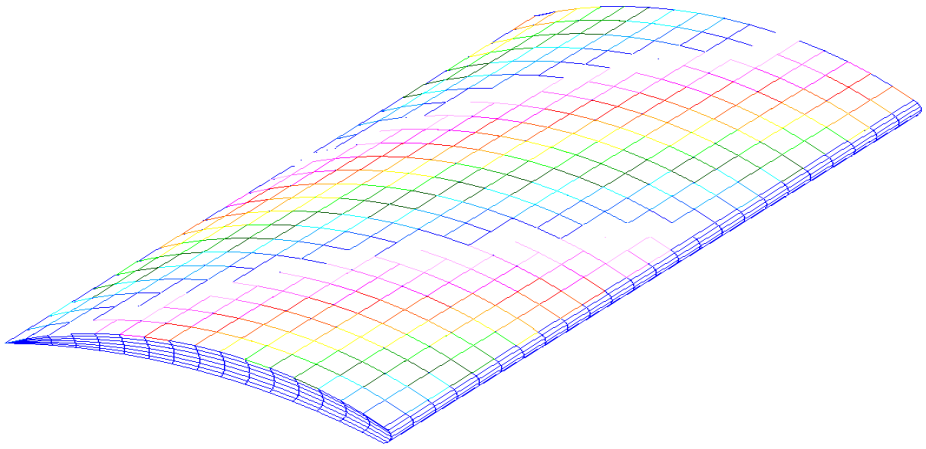

Fig. 4. 40 3D Finite Element Model of Turbine Blade

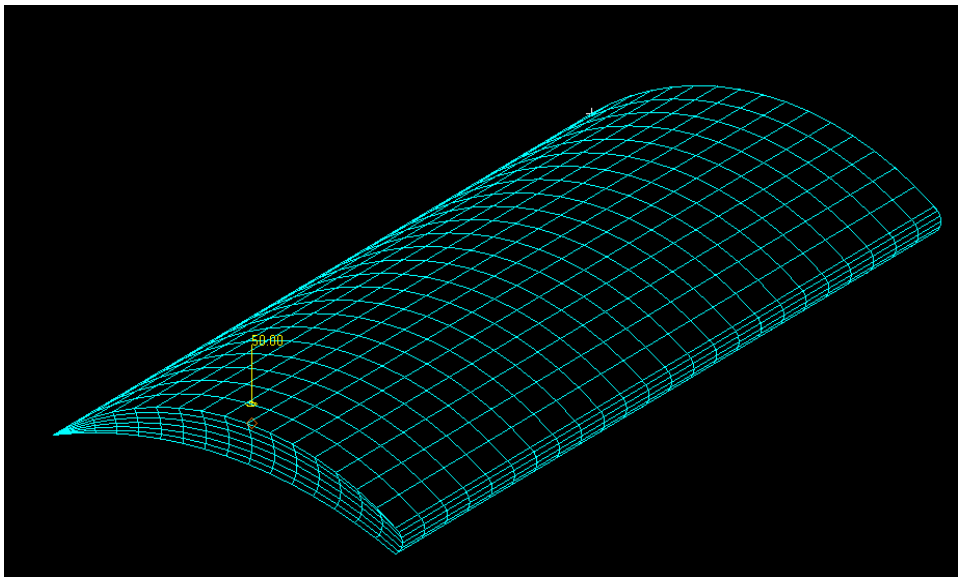

Fig. 4. 41 Concentrated Harmonic Force at the Free End of Coated Turbine Blade

Chapter 5. Discussion and Conclusion

The main aim of this research is to increase the high frequency damping of turbine blade by using magnetomechanical coating. Variation of coating means that coating thickness is correlated with geometric properties, coating type and material type. Aluminum 6061 is used as base material and two different types of coating material are used, Ti-64 and Hastelloy-X. The selection procedure for the coating material to obtain the maximum structural damping is discussed in [15].

5.1 Forced/Frequency Response for Coated Plate

In the context of present thesis, modeling of plate with and without coating for the selection of coating material is performed. Natural frequencies of the uncoated and coated plate are obtained for the dynamic analysis model. Harmonic excitation is applied for the forced analysis. The 3rd bending mode is identified as the 3rd stripe mode. Plate experiences the worst scenario of structural vibration and maximum deflection in this bending mode. Around 200 3D hexahedral elements are used for capturing the natural frequencies especially for stripe modes of uncoated plate. Coated plate is modeled with approximately 400 3D hexahedral and shell Quad 4 elements. Concentrate tip force of 1lb is applied at the free end for the forced response analysis. Frequency range of 1-10k Hz is used to capture the effect of stripe modes for uncoated and coated plate. Plate without coating is analyzed first to identify the worse bending mode and maximum stresses for the corresponding mode. This worse bending mode is also known as stripe mode. Variation of stresses is shown in the figure below for the uncoated plate. Stresses present the pattern of stripes therefore 3rd bending mode is also known as stripe mode bending.

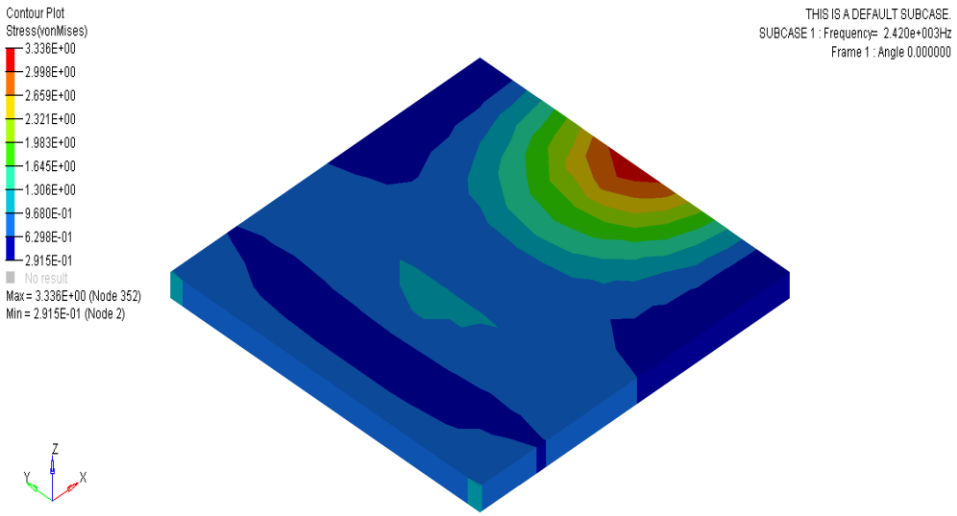

Fig. 5. 1 Al6061 frequency response

The above fig 5.1 shows the variation of VonMises stresses on the uncoated plate. Plate is constrained at one end. VonMises stress for the 3rd bending mode at constrained end has minimum value. Vibratory stress at the free end has the maximum value. Maximum VonMises stress is located at the application of the concentrated tip force. This maximum value of stress at the tip force area is due to localized effect.

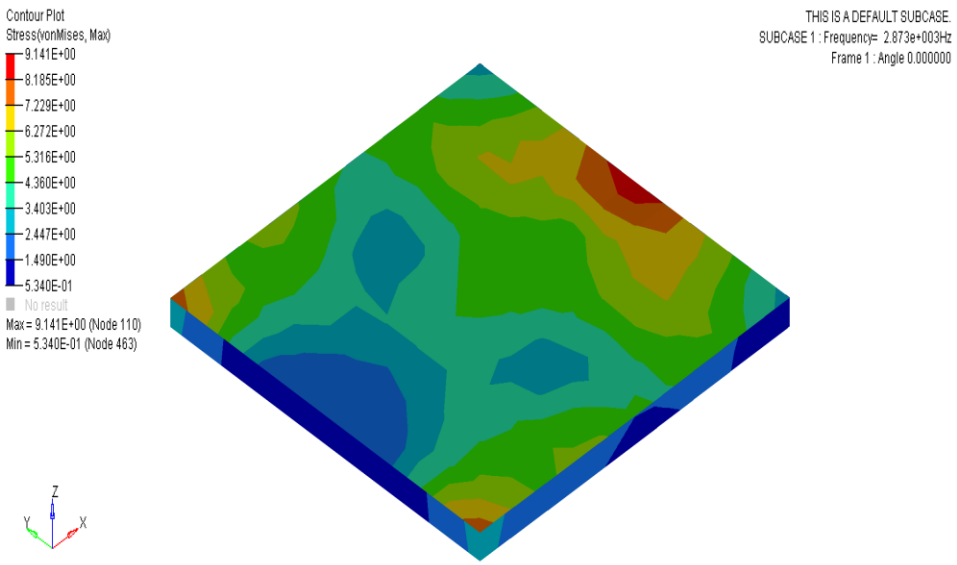

Fig. 5. 2 Al6061_Ti64 FR (With Coating)

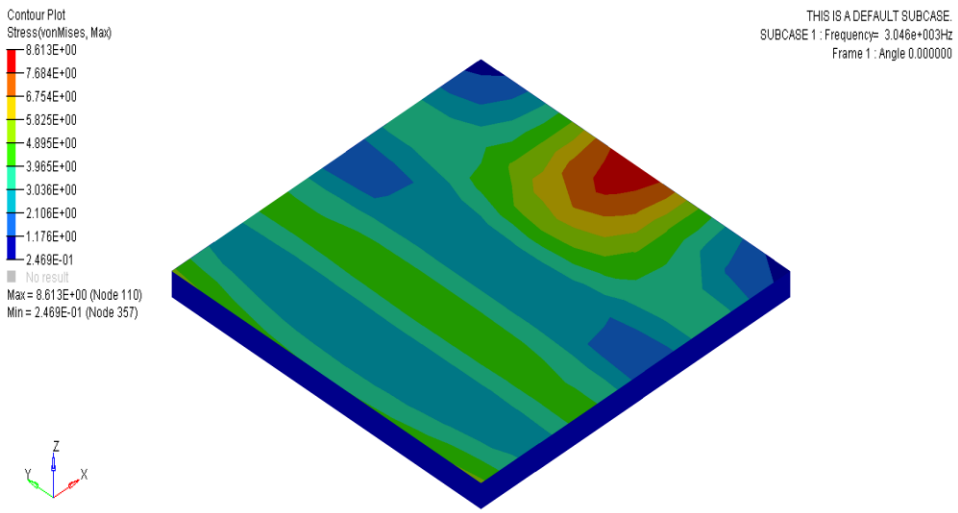

Fig. 5. 3 Al6061_HX FR (With Coating)

Two materials are selected for the coating purpose on Al 6061 plate. The purpose for the application of coating is to enhance the localized damping ability of the material while operating at higher frequency range. Analysis of coated plate for the selection of coating material is performed. Ti-64 and Hastelloy-X are applied and their forced response analysis is performed at the 4^{th} bending or 3^{rd} stripe mode. After the analysis stress pattern for Ti-64 and Hastelloy-X coating material is seen in post-processor HYPERVIEW and shown in above two figures 5.2 and 5.3.

Minimum VonMises stress is seen at the constrained end and maximum VonMises stress is observed at free end for both coating materials. VonMises stress patterns are also observed and these patterns are in the form of stripes. Maximum stress is located at the application of concentrated force and it also shows the localized effect. After performing the analysis, NASTRAN generates the result file having *.f06 extension. This file contains the result of element stress values. Normalization of these stress values are required to obtain the VonMises stresses generated on the upper and lower surface of the coating. VonMises stresses are calculated using the formula

$$\sigma_{von} = \sqrt{\frac{1}{2}\left(\left(\sigma_x - \sigma_y\right)^2 + (\sigma_x)^2 + \left(\sigma_y\right)^2 + \left(\tau_{xy}\right)^2\right)} \qquad (5.1)$$

where

σ_x = Normal Stress Component for Plane Stress

σ_y = Normal Stress Component for Plane Stress

τ_{xy} = Shear-Stress Component for Plane Stress

Maximum VonMises stresses are calculated for the two coating materials separately. The maximum stress value for Ti-64 and Hastelloy-X is listed in table 5.1:

Maximum VonMises Stresses for Ti-64 and Hastelloy-X		
	Al6061 with Ti-64 Coating	Al6061 with Hastelloy-X Coating
Frequency (Hz)	2872.99	3045.53
VonMises Stresses (Max) Psi	310.45	434.94
Coating Thickness (inches)	0.002"	0.002"

Table 5. 1 Maximum VonMises Stresses for Ti-64 and Hastelloy-X

Coating thickness of 0.002 inch is applied on base material Al6061. The analysis results for two coating materials is shown in above table 5.1, it is concluded that Ti-64 produces less vibratory stresses than Hastelloy-X. Therefore, Ti-64 is selected as coating material for the analysis of coated cantilever beam.

5.2 Forced/Frequency Response for Coated Beam

In this thesis, the effect of geometric variation of magnetomechanical plasma graded coating on beam is analyzed. This passive technique is used for enhancing the high frequency damping ability of the system. Ti-64 is used as the coating material on the base material. The selection of coating material is made on the basis of material damping properties. After the selection of coating material, dynamic analysis for the beam is performed by varying the thickness of coating material.

In the context of thesis, finite element uncoated beam modal analysis is performed to identify the worse case bending mode frequency. The bending modes frequencies for the uncoated beam are also analytically calculated from Euler-Bernoulli beam equation. The

4^{th} bending mode is identified as maximum displacement mode and hence the maximum vibratory stresses occur in this mode.

Finite element modeling of the coated beam is performed by using 3D hexahedral solid and shell Quad 4 node element. Approximately 2400 elements are used to capture the damping ability of coating material. Modal analysis and forced response analysis are performed at the frequency range of 1-10k Hz. Dynamic analysis is performed by applying 1lb harmonic load at the free end of the coated beam.

Empirical relation which correlates material type, coating type and geometric properties is obtained by using four different dimensions of beam. Beam dimensions are given in table 5.2:

Beam Dimensions for Analysis	
	Dimensions (inches)
Beam 1	8" × 0.75" × 0.125"
Beam 2	7.087" × 0.3937" × 0.079"
Beam 3	10" × 0.9375" × 0.156"
Beam 4	3.937" × 0.3937" × 0.039"

Table 5. 2 Beam Dimensions for Analysis

The beam having 8 in × 0.75 in × 0.125 in is analyzed with plasma graded coating layer. After identifying the worst bending mode using finite element model and uniform Euler-Bernoulli beam equation for uncoated plate, coated plate dynamic model is analyzed for the varying coating thickness. It is also important that coating layer thickness should remain in the acceptable limit relative to the beam thickness, so that the strain level for the upper and lower coating surface remains the same.

VonMises stresses are obtained by normalizing the elements stress values. Variation in contours of stresses on the upper and lower surface is also observed. Stripes of stress pattern are formed for the 4^{th} bending mode dynamic response analysis. Hence this 4^{th} bending mode is also known as 3^{rd} stripe mode as three stripe variations in the stresses are observed after the forced analysis.

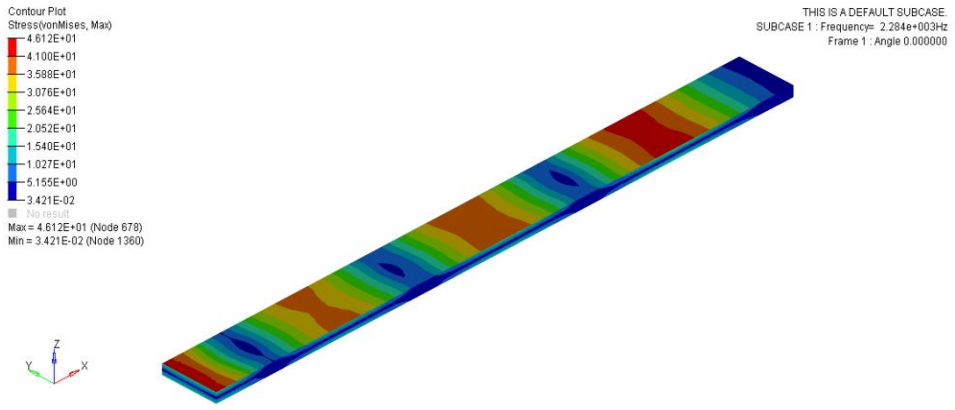

Fig. 5. 4 Beam_1 Al6061 with Ti-64 0.002 in Coating Thickness

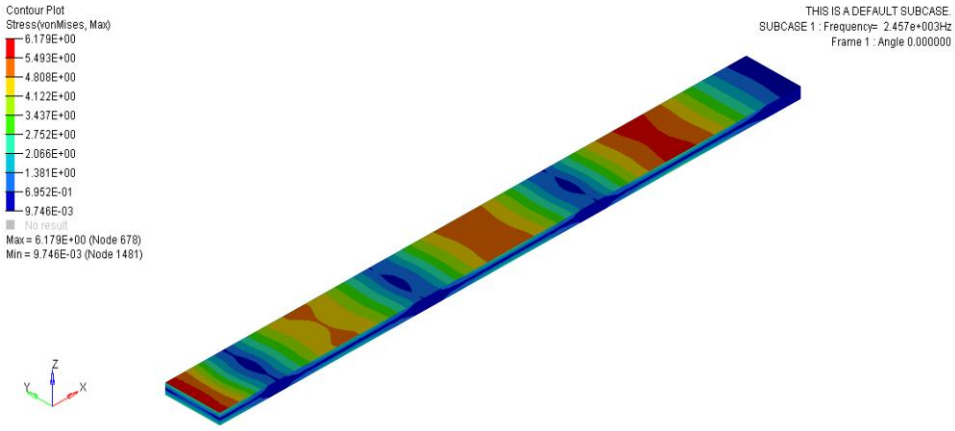

Fig. 5. 5 Beam_1 Al6061 with Ti-64 0.006 in Coating Thickness

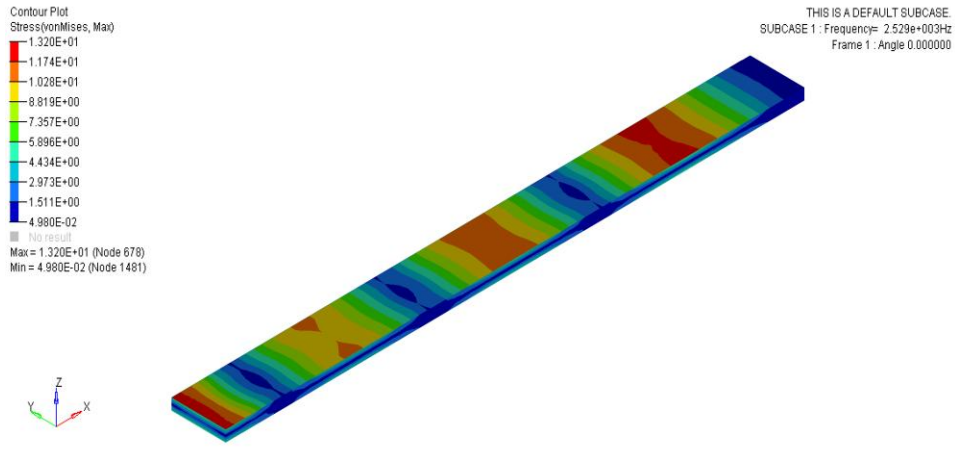

Fig. 5. 6 Beam_1 Al6061 with Ti-64 0.008 in Coating Thickness

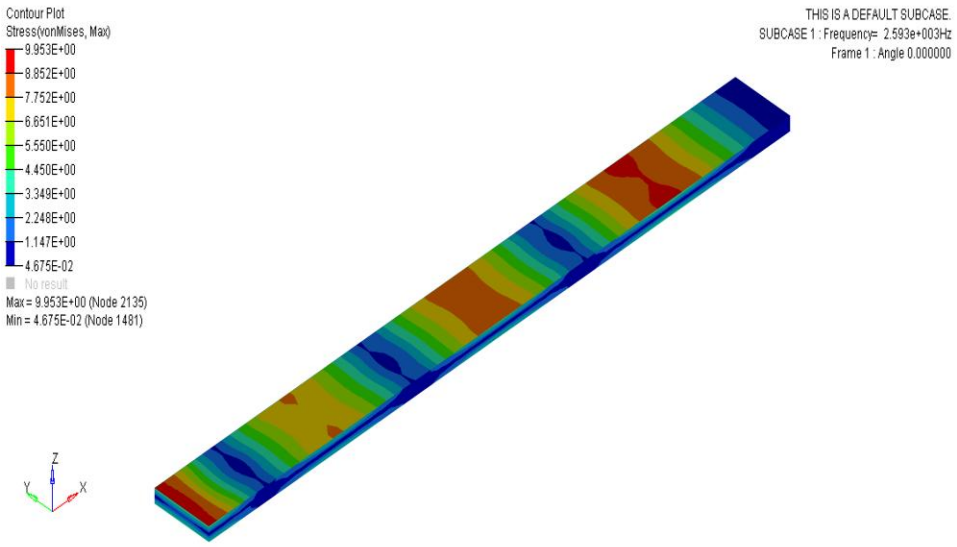

Fig. 5. 7 Beam_1 Al6061 with Ti-64 0.01 in Coating Thickness

Vibratory stress for up to 8% coating thickness is shown in the above figures 5.4 - 5.7. It is expected that maximum vibratory stresses occur near the clamped and trailing edges. In the above figure it is observed that maximum vibratory stresses occur at the constrained end. The variation of stresses is seen throughout the coating surfaces. VonMises stresses vary from maximum at constrained end to minimum and then maximum to minimum.

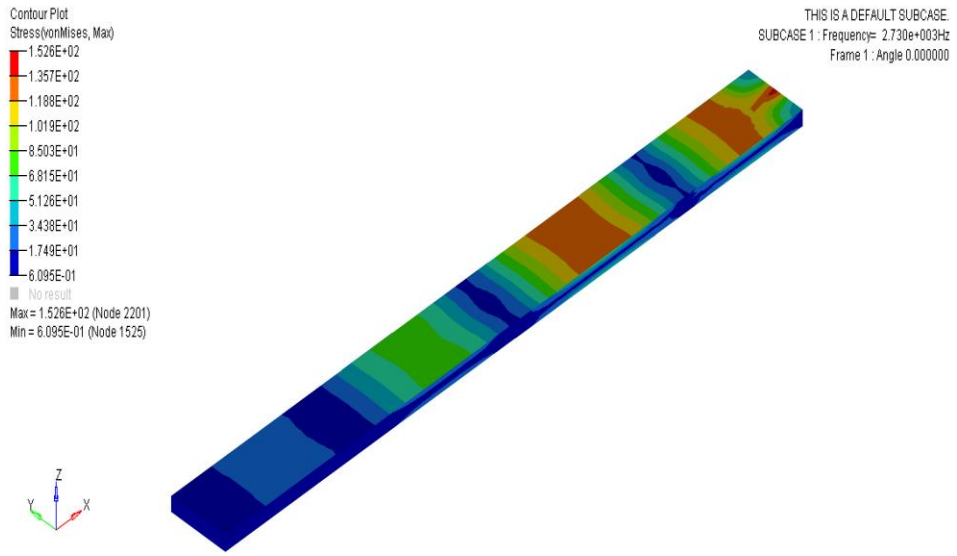

Fig. 5. 8 Beam_1 Al6061 with Ti-64 0.015 in Coating Thickness

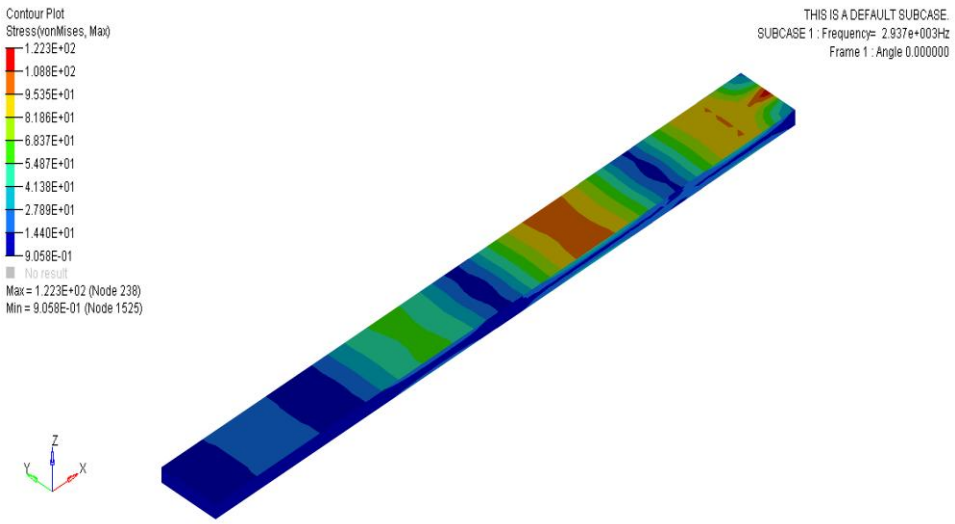

Fig. 5. 9 Beam_1 Al6061 with Ti-64 0.025 in Coating Thickness

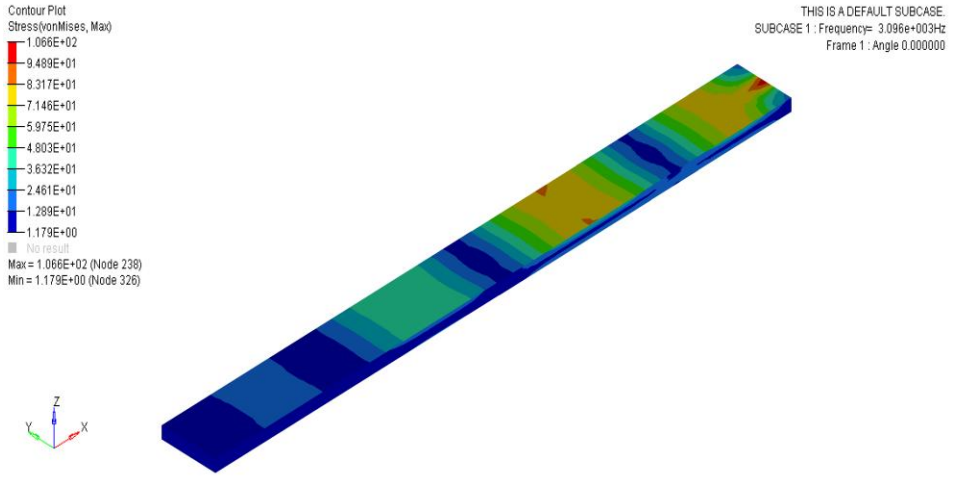

Fig. 5. 10 Beam_1 Al6061 with Ti-64 0.035 in Coating Thickness

After the application of up to 28% coating thickness relative to the beam height, contours of vibratory stresses are shown in the above figures 5.8 – 5.10. Maximum VonMises stress is observed at the trailing edge at the application point of harmonic load. Three stripes of stress variation starting from the constraint end are observed. With the increase of coating thickness, vibratory stresses reduce but the coating thickness limitation is also important. Displacement is also reduced as coating is applied on the pressure side of the

beam for the 3rd stripe mode, but with the application of various coating thicknesses the vibratory stress minimize for the dynamic model.

Beam_1 3rd Stripe Mode Frequencies				
Coating Thickness (in)	Height with Coating (in)	%age thickness relative to height	3rd Stripe mode Frequencies (Hz)	VonMises Stresses (Ksi)
0.002	0.127	1.6	2284.12	39.01
0.003	0.128	2.4	2331.84	36.60
0.004	0.129	3.2	2376.38	34.46
0.005	0.13	4	2418.08	32.55
0.006	0.131	4.8	2457.27	30.81
0.007	0.132	5.6	2494.19	29.24
0.008	0.133	6.4	2529.07	27.81
0.009	0.134	7.2	2562.11	26.49
0.01	0.135	8	2593.49	25.28
0.012	0.137	9.6	2651.83	23.12
0.015	0.14	12	2730.12	20.40
0.018	0.143	14.4	2799.58	18.15
0.02	0.145	16	2841.94	16.85
0.022	0.147	17.6	2881.66	15.69
0.023	0.148	18.4	2900.65	15.15
0.024	0.149	19.2	2919.11	14.63
0.025	0.15	20	2937.08	14.14
0.027	0.152	21.6	2971.67	13.23
0.028	0.153	22.4	2988.35	12.80
0.03	0.155	24	3020.62	11.99
0.035	0.16	28	3095.90	10.24
0.037	0.162	29.6	3124.23	9.63
0.04	0.165	32	3165.20	8.80
0.05	0.175	40	3291.92	6.54
0.06	0.185	48	3409.14	4.85

Table 5. 3 Beam_1 3rd Stripe Mode Frequencies

Normalization of element stresses are required to get the VonMises stress for the varying coating thickness. VonMises stresses corresponding to the coating thickness for the 4th bending or 3rd stripe mode is listed in the above table 5.3.

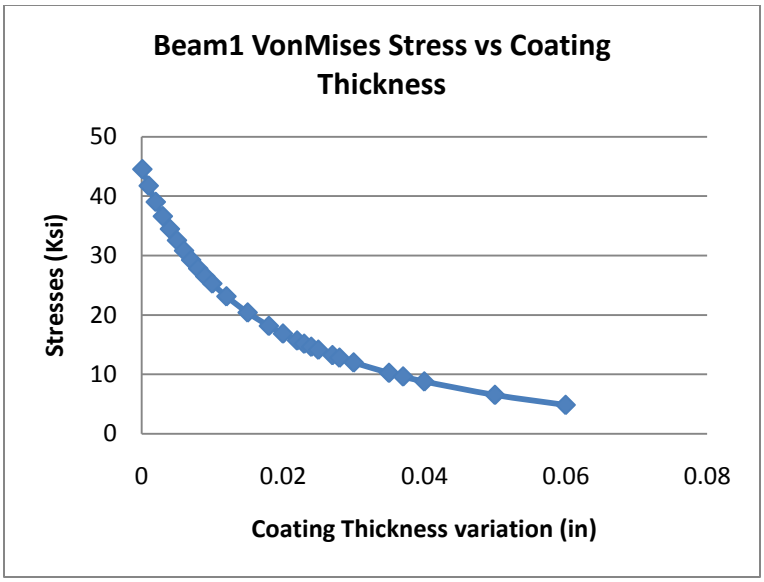

Fig. 5. 11 Beam_1 VonMises Stresses vs. Coating Thickness

Vibratory stresses are plotted against the geometric variation of the coating thickness as shown in fig 5.11. It is observed that vibratory stress decreases with the increase of the thickness of the coating. This variation of stresses is significant upto 16 percent coating thickness but after that there is no significant change in the vibratory stresses by increasing coating thickness. This shows that coating material also has the limitation for the suppression of vibratory stresses.

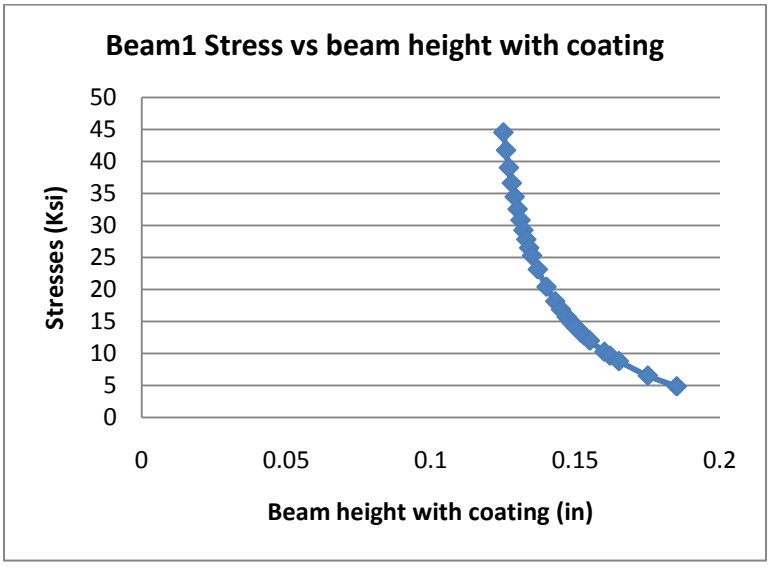

Fig. 5. 12 Beam_1 VonMises Stresses vs. Beam Height with Coating

Beam thickness with coating is plotted against vibratory stresses as shown in above fig 5.12. Suppression of vibratory stresses is observed with the increase of the coating thickness. It is also necessary that coating thickness should remain in the acceptable limit relative to the beam height or beam thickness. After the VonMises stress analysis for the varying geometric coating thickness, an empirical relation is developed for the correlation of the coating type, material type and geometric properties. Correlation for the varying coating thickness is stated as

$$t = (0.0004/y)^{1/5.574} - h \qquad (5.2)$$

where

t = Thickness in inches

y = Yield Stress in Ksi

h = Height or Thickness in inches

A second beam with 7.087 in × 0.3937 in × 0.079 in dimension is analyzed for the development of empirical relation. The 4th bending mode frequency is used for the forced response analysis of the beam. The 4th bending mode natural frequency of finite element model is verified by Euler-Bernoulli beam equation. The variation of coating thickness for the reduction of the vibratory stresses is shown in the figures 5.13 and 5.14.

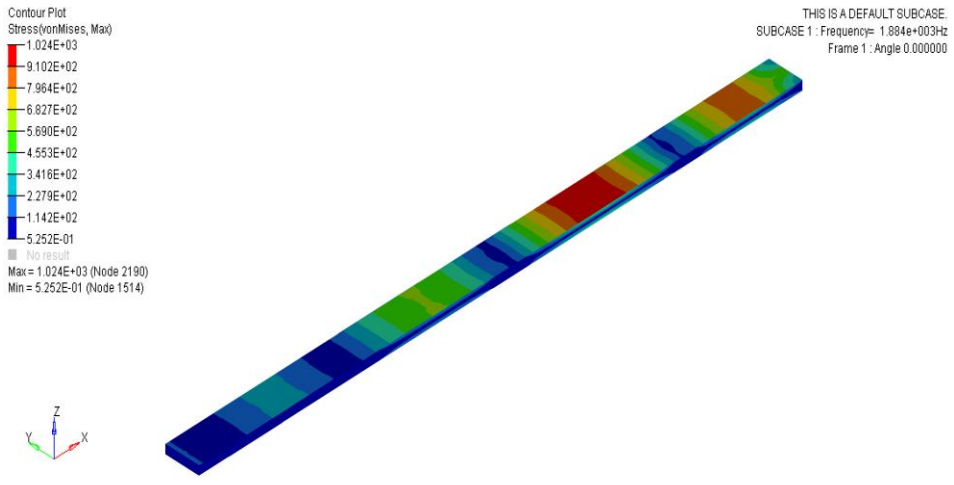

Fig. 5. 13 Beam_2 Al6061 with Ti-64 0.002 in Coating Thickness

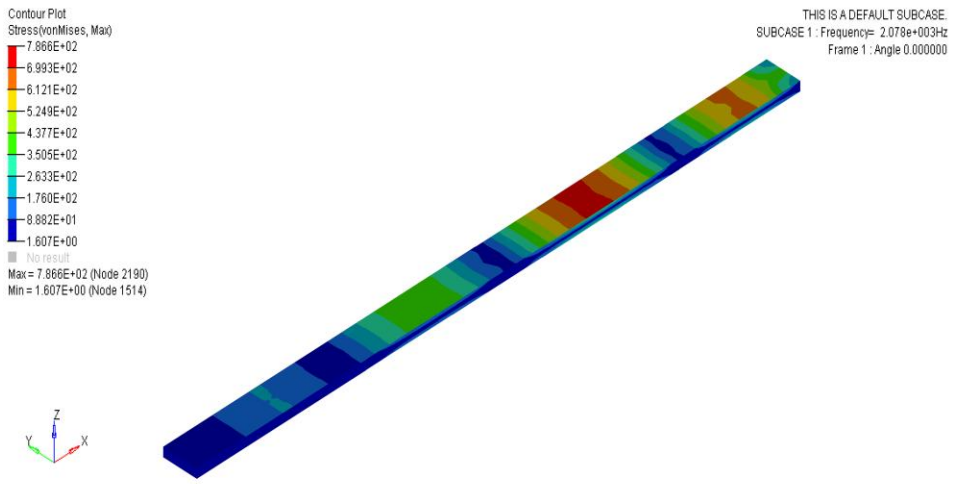

Fig. 5. 14 Beam_2 Al6061 with Ti-64 0.006 in Coating Thickness

Vibratory stress reduces with the increase of coating thickness. The 3rd stripe mode patterns are obtained by using pre-processor HYPERVIEW. Stress pattern for the coating thickness up to 8 percent is shown in above figures. These VonMises stress counters or patterns are observed on the upper coating surface due to localized damping ability of coating material. VonMises stress is minimum at the constrained end and has higher stress value near the tip of the beam.

As the coating thickness increases, the localized damping of coating material starts to decrease at the upper surface and increase at the lower surface. Coating thickness variation up to 25 percent is shown in the figures 5.15, 5.16 and 5.17. The maximum VonMises stress patterns are observed at the lower surface of the coating material.

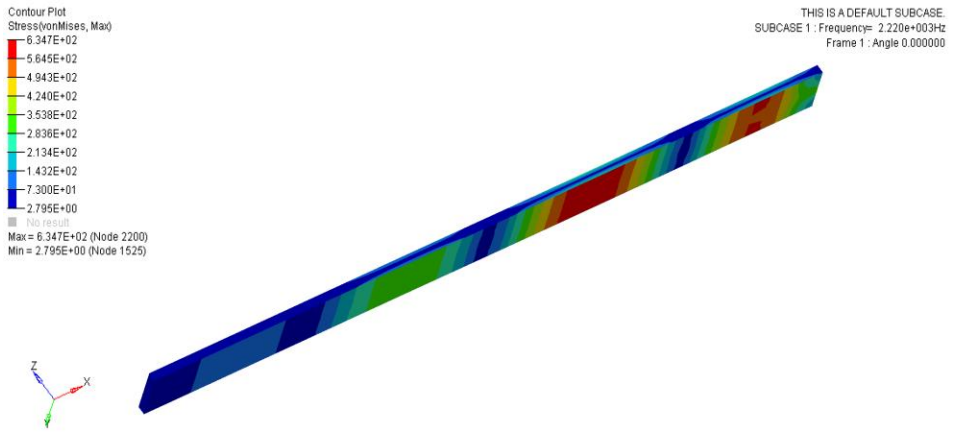

Fig. 5. 15 Beam_2 Al6061 with Ti-64 0.01 in Coating Thickness

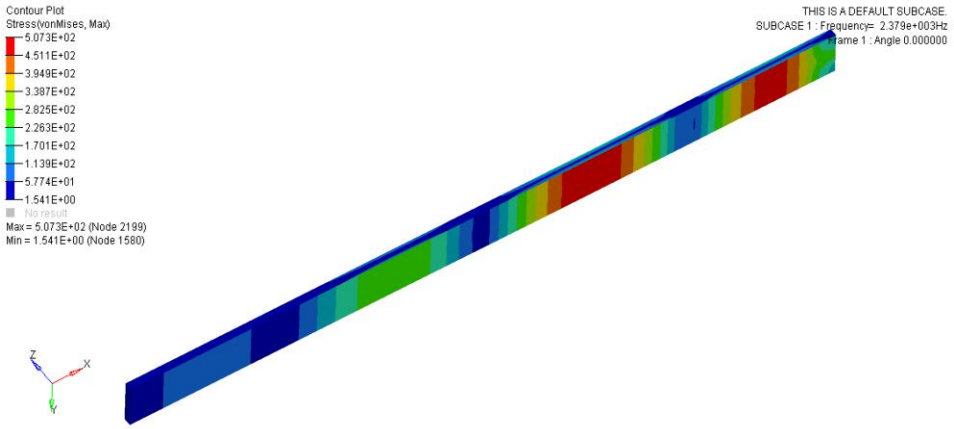

Fig. 5. 16 Beam_2 Al6061 with Ti-64 0.016 in Coating Thickness

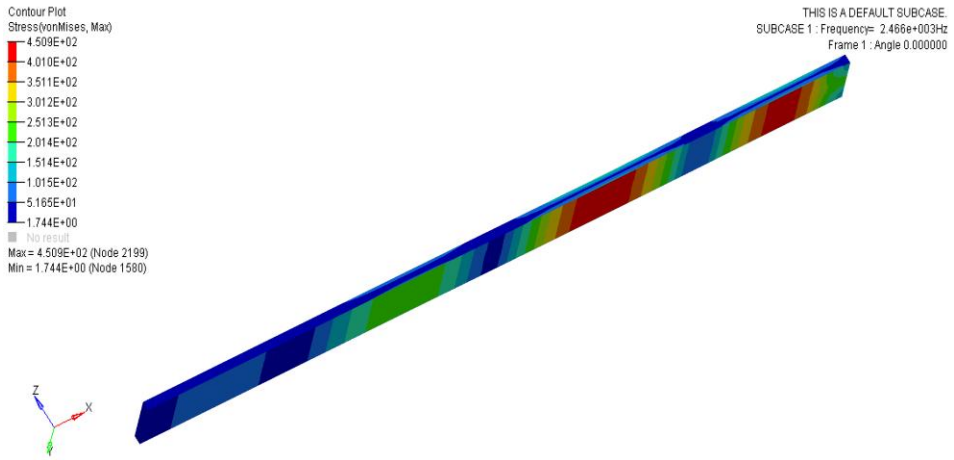

Fig. 5. 17 Beam_2 Al6061 with Ti-64 0.02 in Coating Thickness

Beam_2 3rd Stripe Mode Natural Frequencies				
Coating Thickness (in)	Height with Coating (in)	%age thickness relative to height	3rd Stripe mode Frequencies (Hz)	VonMises Stresses (Ksi)
0.001	0.08	1.2	1821.78	167.74
0.002	0.081	2.5	1883.71	151.59
0.003	0.082	3.7	1939.37	138.16
0.004	0.083	5	1989.82	126.78
0.005	0.084	6.3	2035.87	116.99
0.006	0.085	7.5	2078.20	108.47
0.007	0.086	8.8	2117.34	100.98
0.008	0.087	10.1	2153.73	94.32
0.009	0.088	11.3	2187.72	88.36
0.01	0.089	12.6	2219.63	82.99
0.011	0.09	13.9	2249.70	78.12
0.012	0.091	15.1	2278.16	73.68
0.013	0.092	16.4	2305.20	69.61
0.014	0.093	17.7	2330.96	65.87
0.015	0.094	18.9	2355.60	62.41
0.016	0.095	20.2	2379.23	59.21
0.017	0.096	21.5	2401.95	56.23
0.018	0.097	22.7	2423.87	53.45
0.019	0.098	24	2445.06	50.86
0.02	0.099	25.3	2465.59	48.42
0.021	0.1	26.5	2485.53	46.14
0.023	0.102	29.1	2523.86	41.97
0.027	0.106	34.1	2595.57	34.92
0.03	0.109	37.9	2646.12	30.53
0.04	0.119	50.6	2803.02	19.68

Table 5. 4 Beam_2 3rd Stripe Mode Natural Frequencies

Maximum VonMises stress for the corresponding coating thickness is listed in the above table 5.4. Stripe mode frequency is also listed in the table. Forced response analyses are performed for their respective stripe mode frequency. As discussed earlier, this is bending mode at which body undergoes maximum vibratory stresses along with maximum displacement.

Coating thickness with their respective maximum VonMises stresses are shown in the figure 5.18. This figure also shows that VonMises stresses are reduced with the application of coating. This reduction increases with the increase of the coating surface. Damping ability of the coating material has also its limitations. The effect of coating significantly reduces stresses till 16 percent coating thickness.

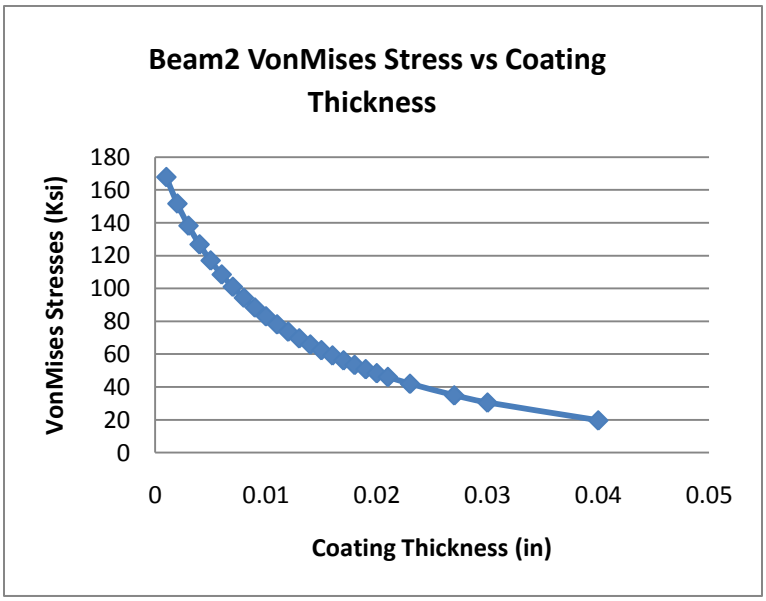

Fig. 5. 18 Beam_2 VonMises Stresses vs. Coating Thickness

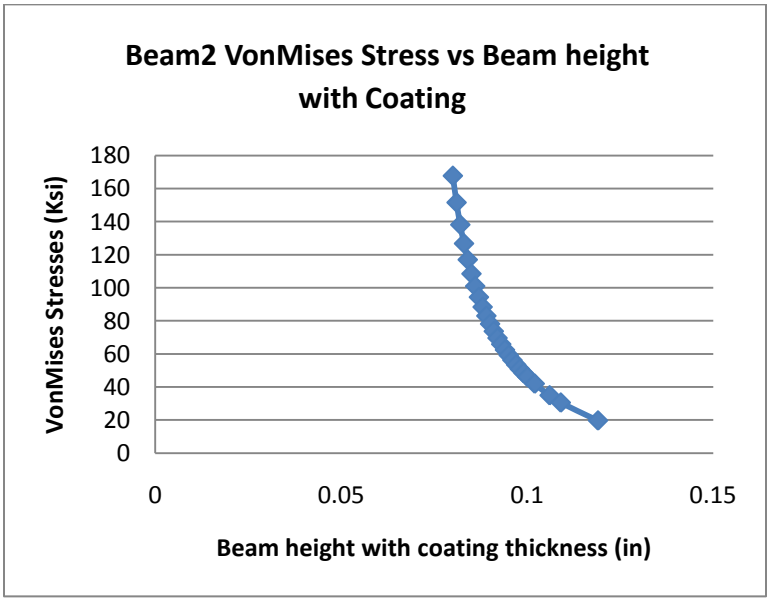

Fig. 5. 19 Beam_2 VonMises Stresses vs. Beam Height with Coating

Maximum vibratory stresses results are plotted against the beam height added with the coating height shown in fig 5.19. This data is used for the correlation which correlates geometric properties, coating and material type.

$$t = (0.0002/y)^{1/5.301} - h \tag{5.3}$$

where

t = Thickness in inches

y = Yield Stress in Ksi

h = Height or Thickness in inches

A third beam with dimensions 10 in × 0.9375 in × 0.156 in is used for the coating thickness variation analysis. The 4th bending mode natural frequencies are used for the forced response analysis.

Contours of stresses are observed for different coating thicknesses. Maximum vibratory stresses are expected at free or constrained ends. Patterns for the VonMises stress has the form of sinusoidal in which there is a maximum and minimum value as shown in the figures 5.20-5.25. Constrained end has minimum stress value, stress increases and decreases in the form of regular patterns. Maximum VonMises stresses are observed at the free end of the beam.

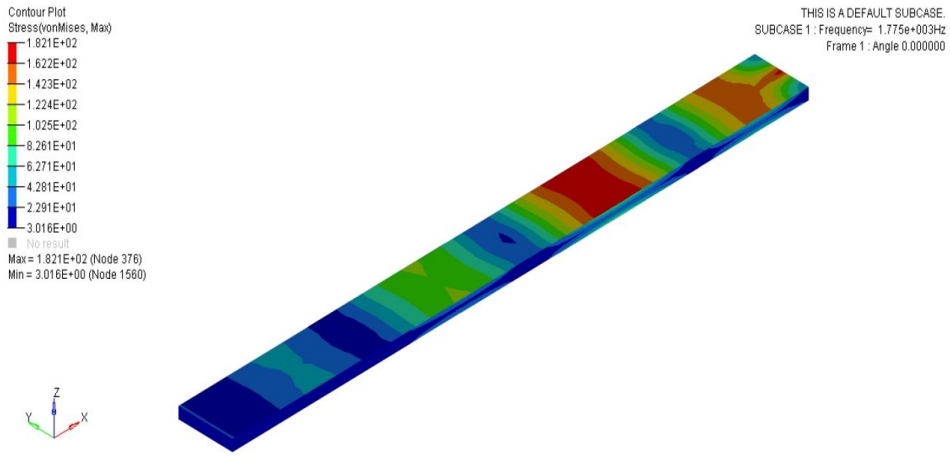

Fig. 5. 20 Beam_3 Al6061 with Ti-64 0.001 in Coating Thickness

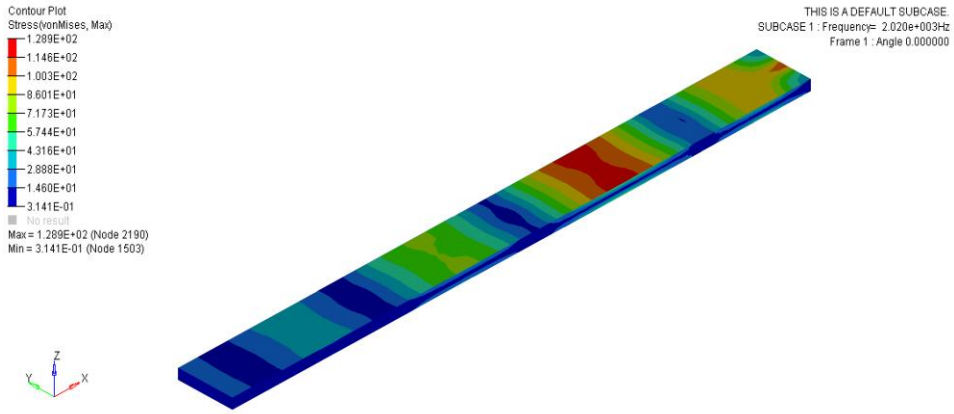

Fig. 5. 21 Beam_3 Al6061 with Ti-64 0.01 in Coating Thickness

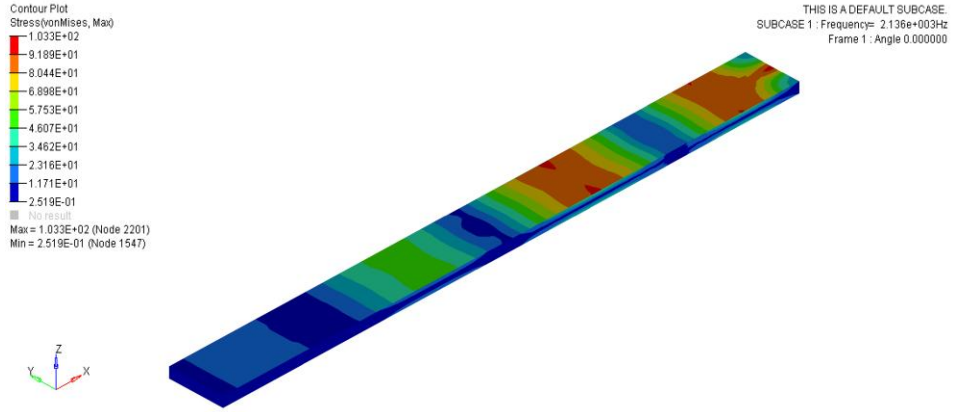

Fig. 5. 22 Beam_3 Al6061 with Ti-64 0.016 in Coating Thickness

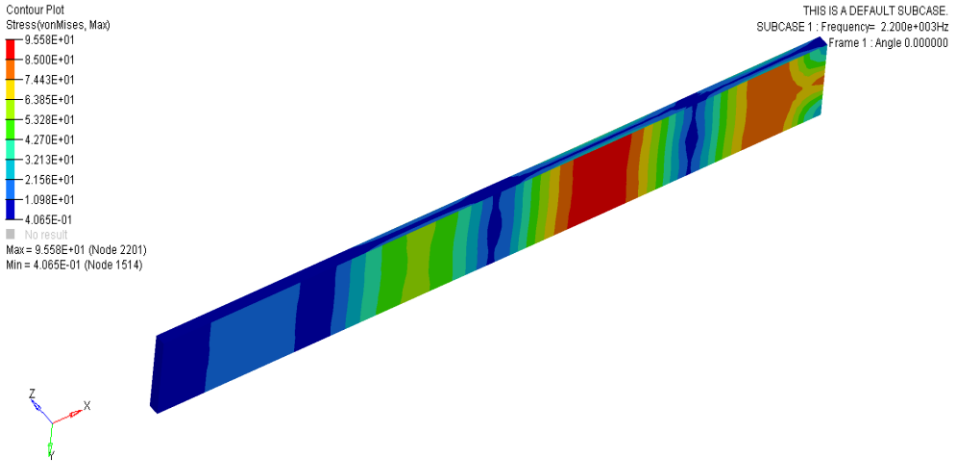

Fig. 5. 23 Beam_3 Al6061 with Ti-64 0.02 in Coating Thickness

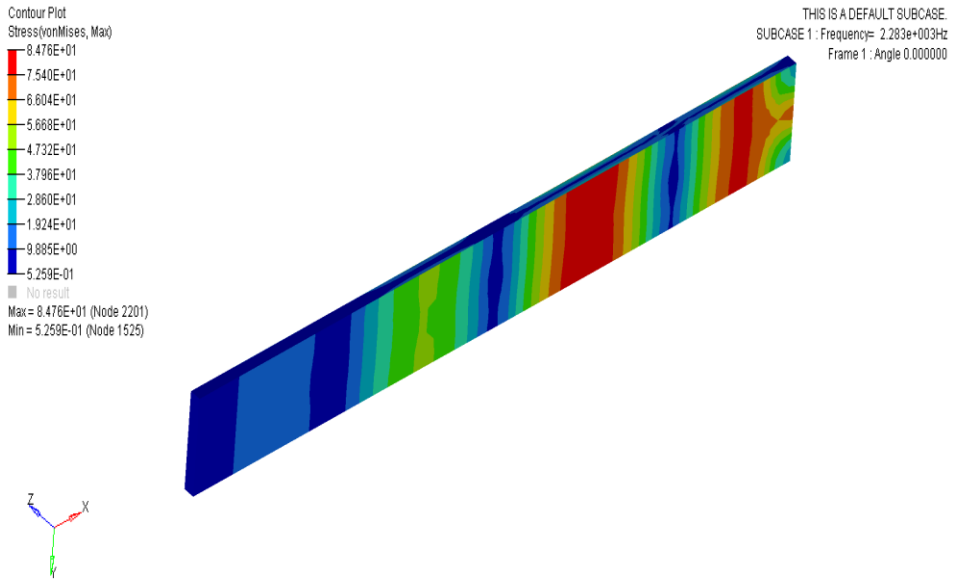

Fig. 5. 24 Beam_3 Al6061 with Ti-64 0.026 in Coating Thickness

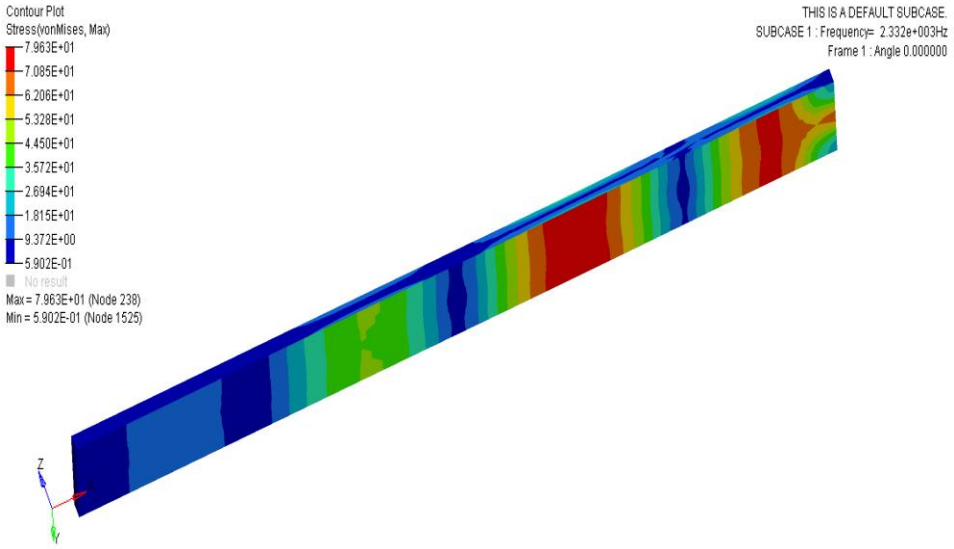

Fig. 5. 25 Beam_3 Al6061 with Ti-64 0.03 in Coating Thickness

It has been observed from the above figures 5.20-5.25 that maximum stresses are located near the mid span of the beam and average value at the free end of the beam. Maximum stress value has large contribution in the mid span and with the application of coating these VonMises stresses are reduced to acceptable level.

Coating material percentage thickness relative to the height of the beam is listed in the table 5.5. Maximum VonMises stresses data for the coating thickness are also listed.

Beam_3 4th Bending Mode Natural Frequencies				
Coating Thickness (in)	Height with Coating (in)	%age thickness relative to height	3rd Stripe mode Frequencies (Hz)	VonMises Stresses (Ksi)
0.001	0.15725	0.6	1774.89	27.17
0.003	0.15925	1.9	1840.14	24.40
0.007	0.16325	4.4	1950.72	20.20
0.01	0.16625	6.4	2020.43	17.84
0.013	0.16925	8.3	2081.62	15.92
0.016	0.17225	10.2	2136.06	14.33
0.018	0.17425	11.5	2169.26	13.41
0.02	0.17625	12.8	2200.37	12.57
0.022	0.17825	14.1	2229.63	11.82
0.026	0.18225	16.6	2283.48	10.50
0.028	0.18425	17.9	2308.42	9.92
0.03	0.18625	19.2	2332.23	9.38
0.032	0.18825	20.5	2355.03	8.88
0.034	0.19025	21.7	2376.93	8.42
0.038	0.19425	24.3	2418.40	7.59
0.04	0.19625	25.6	2438.11	7.21
0.044	0.20025	28.2	2475.85	6.53
0.048	0.20425	30.7	2511.66	5.92
0.049	0.20525	31.4	2520.36	0.91
0.05	0.20625	32	2528.96	0.89
0.054	0.21025	34.6	2562.54	0.81
0.058	0.21425	37.1	2594.95	0.75
0.06	0.21625	38.4	2610.79	0.72
0.07	0.22625	44.8	2687.18	0.53
0.08	0.23625	51.2	2760.34	0.47

Table 5. 5 Beam_3 4th Bending Mode Natural Frequencies

VonMises stress reduces gradually with the increase of coating height relative to the beam height. The figure 5.26 shows the drop of vibratory stress and it is concluded that thickness of about 15 percent significantly reduces the VonMises stresses. Engineering

judgment is also required to use the coating thickness of acceptable limit, so that reduction in vibratory stresses is achieved.

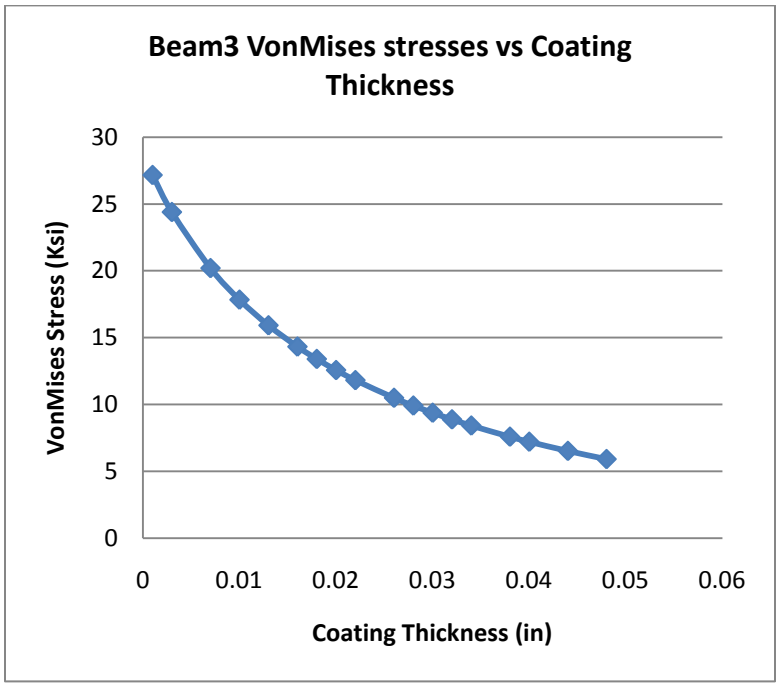

Fig. 5. 26 Beam_3 VonMises Stresses vs. Coating Thickness

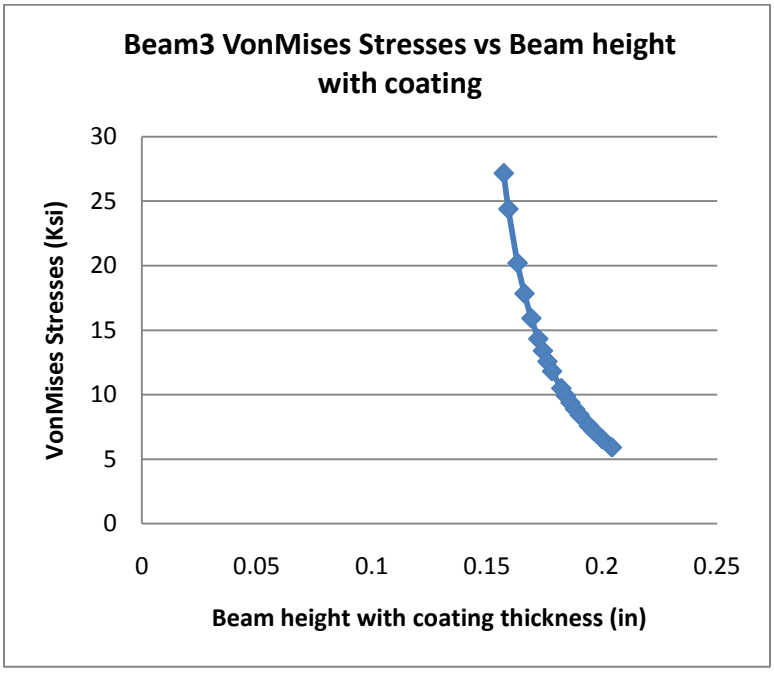

Fig. 5. 27 Beam_3 VonMises Stresses vs. Beam Height with Coating

Empirical correlation for the correlation of geometric properties, coating type and material is developed by plotting the VonMises stress with the change of thickness shown in fig 5.27. Curve fitting is used to get the correlation for the obtained data from the iterative analysis process. The empirical relation obtained for the beam three is written as

$$t = (0.0007/y)^{1/5.687} - h \quad (5.4)$$

where

t = Thickness in inches

y = Yield Stress in Ksi

h = Height or Thickness in inches

The coating thickness analysis for the fourth beam with dimensions 3.937 in × 0.3937 in × 0.039 in is performed. Optimum coating height as compared with the beam height is obtained, which suppresses the vibratory stress in the desired range for that beam. It is expected that maximum vibratory stresses occur near the clamped and free end. The counters of VonMises stresses are shown in figures 5.28-5.32 with the variation of coating thickness.

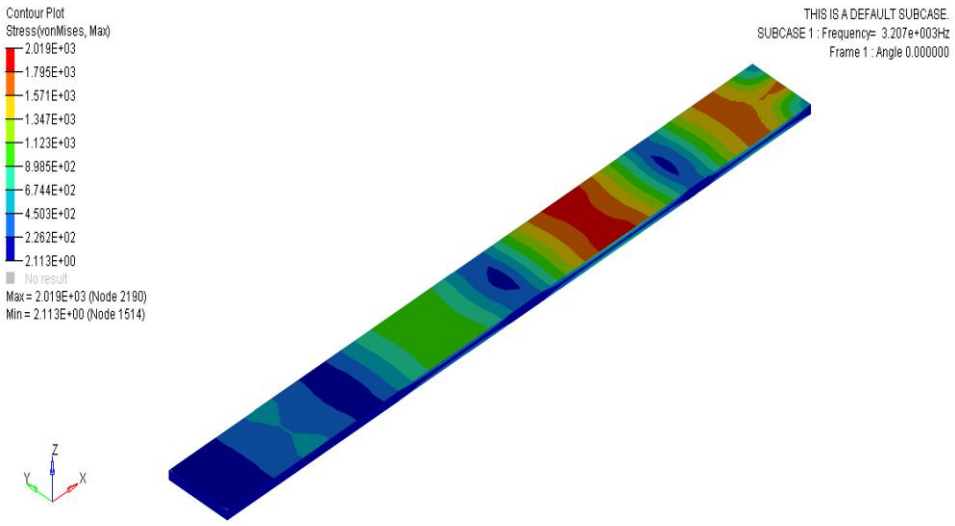

Fig. 5. 28 Beam_4 Al6061 with Ti-64 0.002 in Coating Thickness

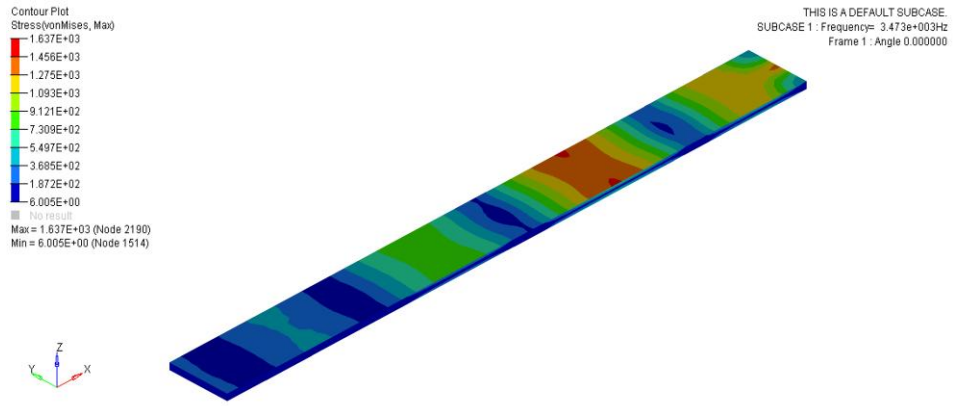

Fig. 5. 29 Beam_4 Al6061 with Ti-64 0.004 in Coating Thickness

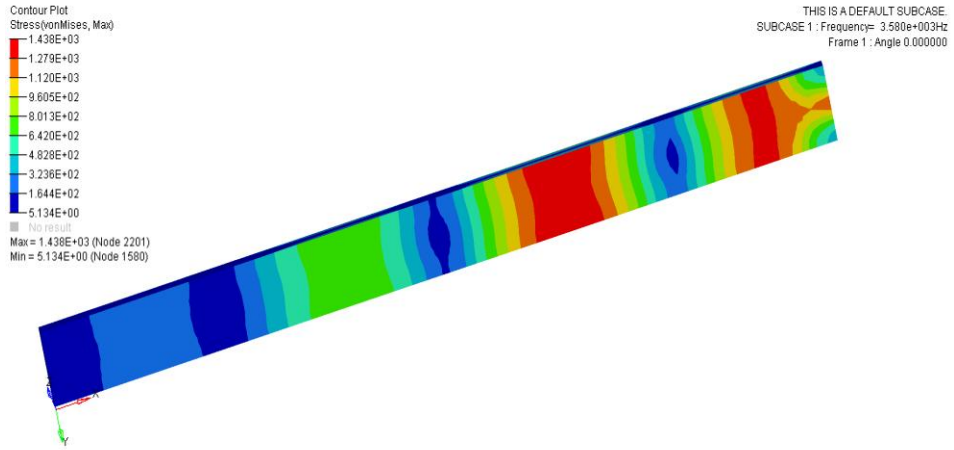

Fig. 5. 30 Beam_4 Al6061 with Ti-64 0.005 in Coating Thickness

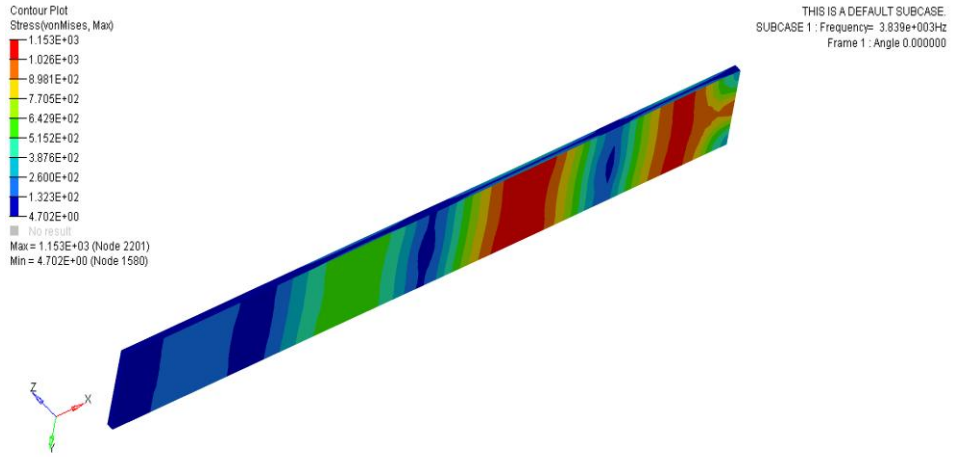

Fig. 5. 31 Beam_4 Al6061 with Ti-64 0.008 in Coating Thickness

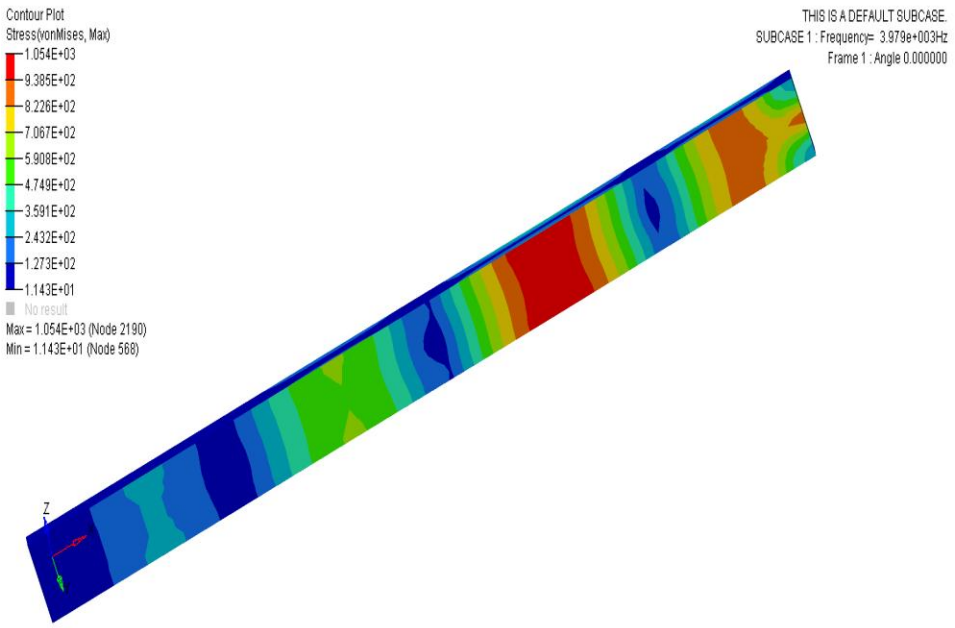

Fig. 5. 32 Beam_4 Al6061 with Ti-64 0.01 in Coating Thickness

These stress patterns show that the stress varies in the form of stripe and three stripes are observed for the beam. As coating is applied on the pressure side of beam therefore maximum stresses are also observed on the upper and lower coating surfaces. For the thickness less than 10 percent, maximum stress is observed on the upper coating surface but with the increase of coating thickness, maximum VonMises stresses are observed on the lower surface of the coating. Due to the application of coating, maximum stress are reduced at the constrained and free end of the beam.

These VonMises stresses are obtained from the stresses of elements which were obtained from the NASTRAN result file. The file having *.op2 extension is also generated by the NASTRAN. This file is used by the pre-processor HYPERVIEW to observe the effect of coating on VonMises stress visually. After normalizing the element stresses, VonMises stresses are obtained for the respective thickness. These stresses for the coating thickness are listed in the table 5.6.

Beam_4 3rd Stripe Mode Natural Frequencies				
Coating Thickness (in)	Height with Coating (in)	%age thickness relative to height	3rd Stripe mode Frequencies (Hz)	VonMises Stresses (Ksi)
0.0006	0.0396	1.5	2954.11	378.46
0.0007	0.0397	1.7	2974.74	370.75
0.0008	0.0398	2	2994.90	363.33
0.0009	0.0399	2.3	3014.61	356.20
0.001	0.04	2.5	3033.90	349.32
0.002	0.041	5.1	3206.52	292.15
0.003	0.042	7.6	3350.15	249.97
0.004	0.043	10.2	3472.77	217.35
0.005	0.044	12.8	3579.72	191.24
0.006	0.045	15.3	3674.69	169.79
0.007	0.046	17.9	3760.36	151.80
0.008	0.047	20.5	3838.68	136.46
0.009	0.048	23	3911.15	123.21
0.01	0.049	25.6	3978.91	111.63
0.011	0.05	28.2	4042.86	101.43
0.012	0.051	30.7	4103.71	92.37
0.015	0.054	38.4	4272.80	70.42
0.017	0.056	43.5	4377.99	59.04
0.02	0.059	51.2	4529.28	45.41

Table 5. 6 Beam_4 3rd Stripe Mode Natural Frequencies

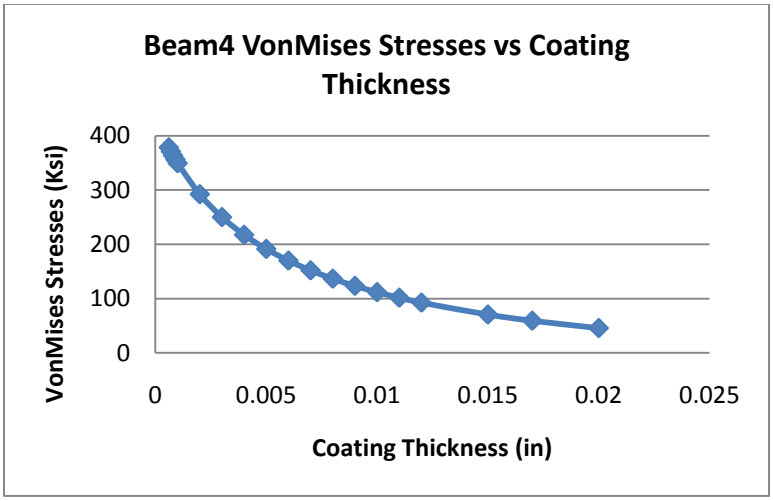

Fig. 5. 33 Beam_4 VonMises Stresses vs. Coating Thickness

Vibratory stresses relative to the coating height are shown in the above fig 5.33. In this case as well, coating material reduces the stresses with the increase of the coating thickness. Coating material also has the damping ability limitation. It is also desirable that coating thickness should remains in the acceptable limit.

To obtain the correlation of geometry with coating type and material type VonMises stresses are plotted against the beam height added with the coating height and shown in the fig 5.34. The obtained correlation gives the coating thickness for the desirable stress value.

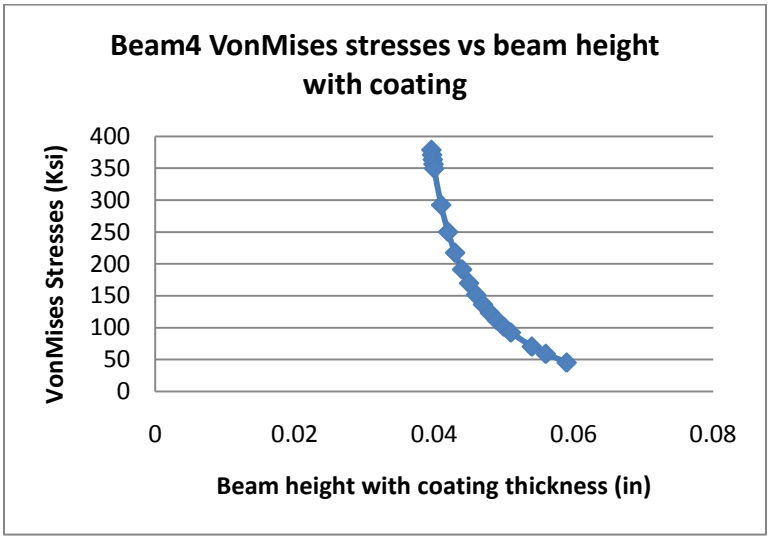

Fig. 5. 34 Beam_4 VonMises Stresses vs. Beam Height with Coating

The correlation for this beam is written as

$$t = (0.00001/y)^{1/5.315} - h \qquad (5.5)$$

where

t = Thickness in inches

y = Yield Stress in Ksi

h = Height or Thickness in inches

Coating thickness for the required vibratory stresses is obtained from the use of these empirical relations. The above equations correlate the geometric properties, coating type

and material type for obtaining the required thickness of the coating materials. These correlations for the four beam cases have the same trend. VonMises stress data for the four beams are shown in figures 5.35-5.36.

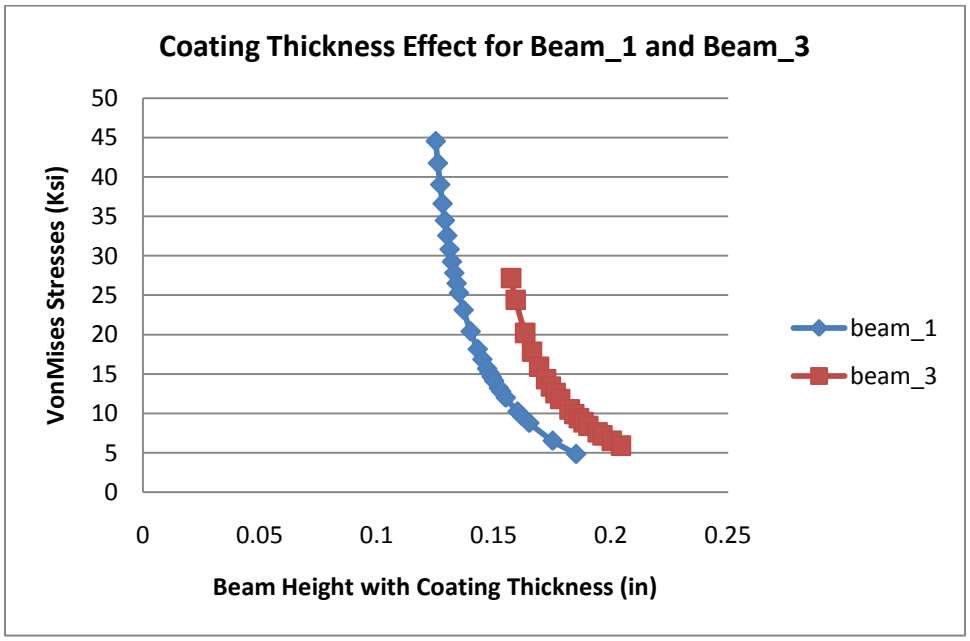

Fig. 5. 35 Effect of Coating Thickness for Beam_1 and Beam_3

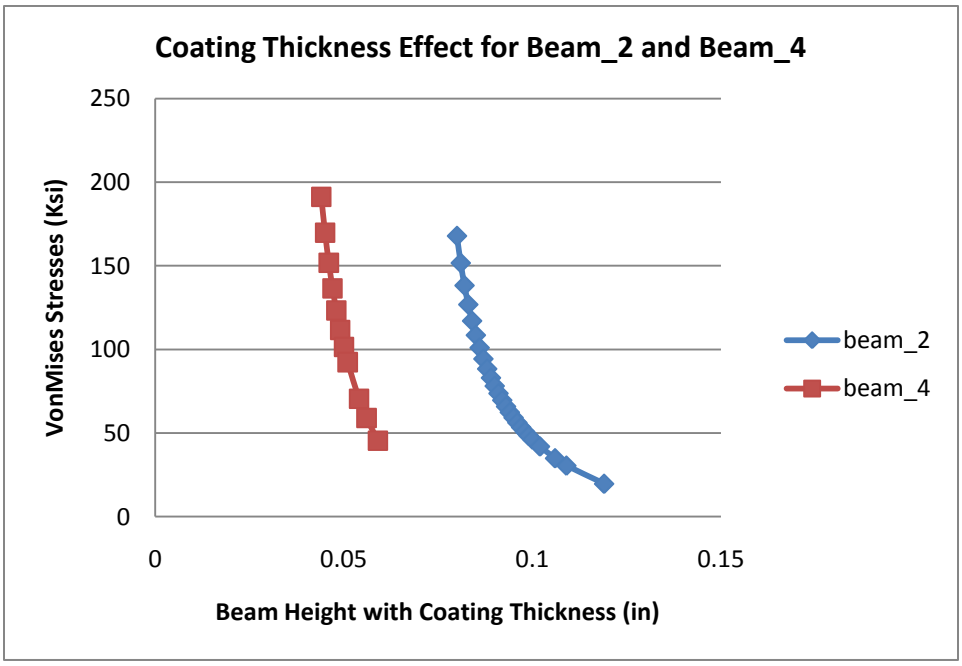

Fig. 5. 36 Effect of Coating Thickness for Beam_2 and Beam_4

The coated beam analysis shows that the coating thickness of about 15 to 20 percent relative to the beam heights significantly reduces the vibratory stresses. It is also desirable that under dynamic loading beam material remains in their yield limit to prevent the beam failure. The vibratory stresses during the operation are reduced with coating application. Coating is applied to the beam so that beam does not fail during the application of excited harmonic loads. Reducing these vibratory stresses also reduces the high cycle fatigue during the gas turbine rotor blade operation.

The main aim of these analyses is to overcome the iterative process and formulate such empirical relation which develops correlation between geometric properties, material type and coating type. Similar procedure is adopted to obtain the empirical relation for curved plate and actual blade.

5.3 Frequency/Forced Response for Coated Curved Plate

Coated curved plate with dimensions 7 in x 3 in x 0.35 in is analyzed to obtain empirical relation. Frequency response analysis for the 3rd stripe frequency of coated curved plate is performed to obtain the empirical relation for the optimum coating thickness. VonMises stress pattern for the curved plate are shown in figures 5.37-5.39. Coating variation on the curved plate is listed in table 5.7. VonMises stresses variations for the various coating thicknesses are also listed in the table 5.7.

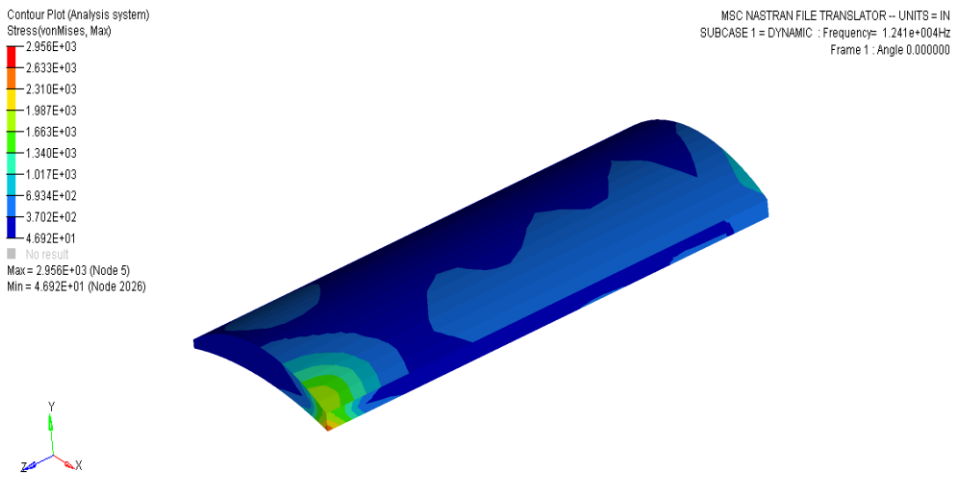

Fig. 5. 37 Curved Plate with 0.035 in Coating Thickness

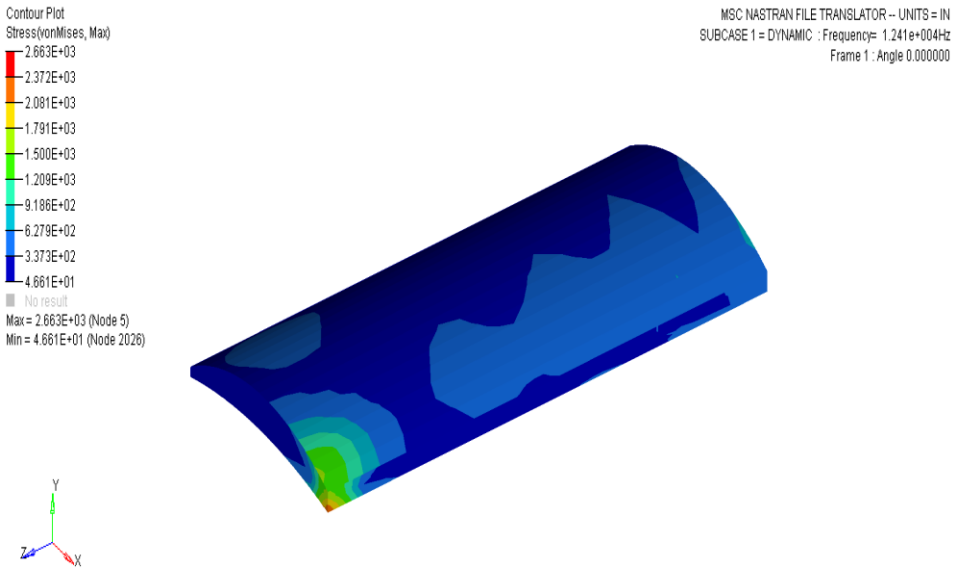

Fig. 5. 38 Curved Plate with 0.05 in Coating Thickness

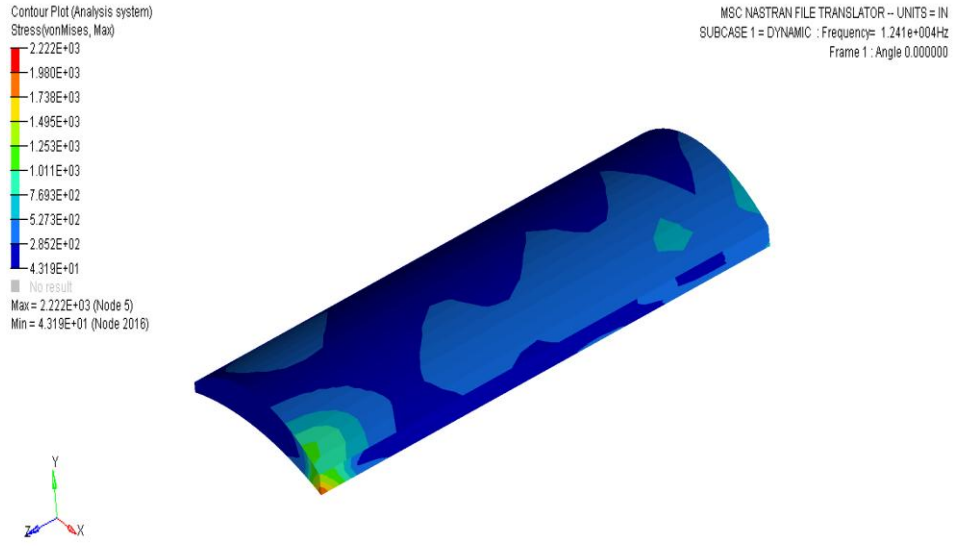

Fig. 5. 39 Curved Plate with 0.08 in Coating Thickness

Curved Plate 3rd Stripe Mode Natural Frequencies			
Coating Thickness (in)	Height with Coating (in)	%age thickness relative to height	VonMises Stresses (Ksi)
0.01	0.36	2.85	4.37
0.014	0.364	4	3.95
0.018	0.368	5.1	3.64
0.025	0.375	7.1	3.27
0.035	0.385	10	2.95
0.042	0.392	12	2.80
0.05	0.4	14.3	2.66
0.06	0.41	17.1	2.50
0.07	0.42	20	2.36
0.08	0.43	23	2.22
0.1	0.45	28	1.93

Table 5. 7 Curved Plate 3rd Stripe Mode Natural Frequencies

VonMises stress variation with the coating thickness is plotted in Fig 5.37. The vibratory stress significantly reduces for coating thickness upto 12% relative to the curved plate height. The VonMises stress suppression after coating thickness of 12% of the curved plate height becomes saturated and the further increase in coating thickness does not yield any significant improvement.

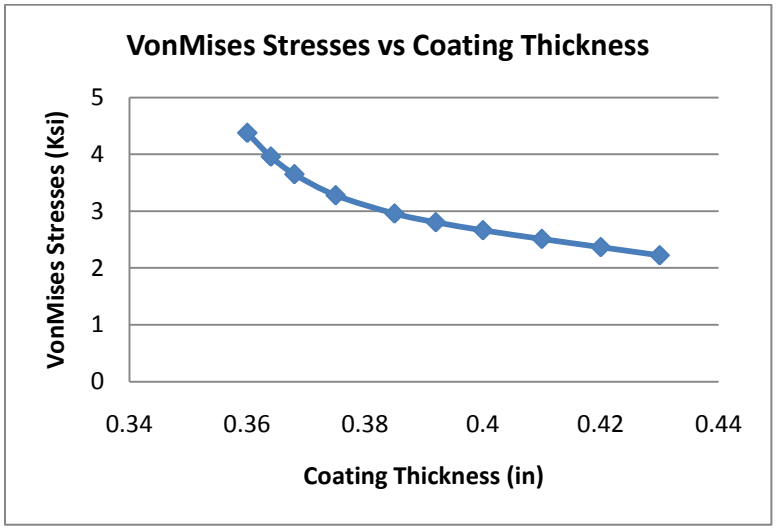

Fig. 5. 40 Curved Plate VonMises stresses vs. coating thickness

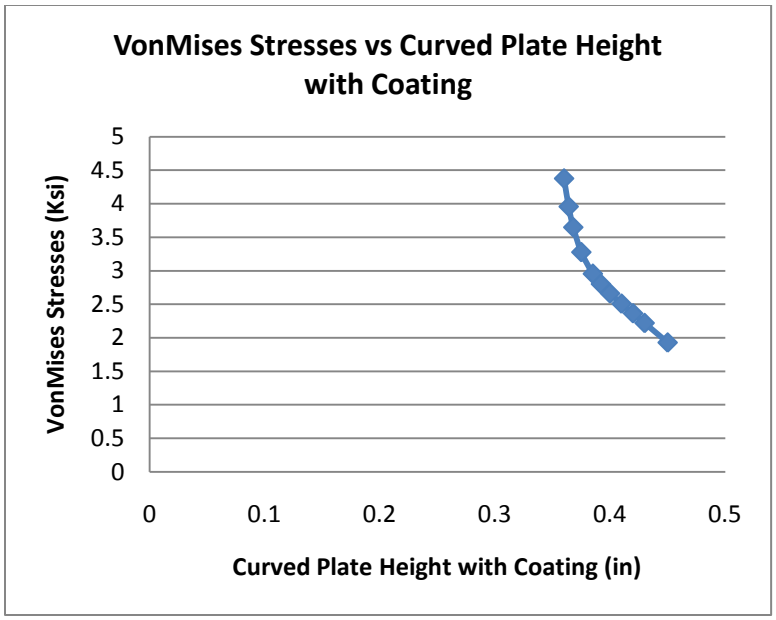

Fig. 5. 41 Curved Plate VonMises stresses vs. Beam height with coating

In order to develop the correlation for the coating thickness and the geometric properties, coating thickness along with height of the curved plate plotted against the VonMises stresses. These stresses are obtained from the application of various coating thicknesses through iterative analysis and these variations are shown in the Fig 5.38. The empirical correlation developed for the curved plate after the analysis is

$$t = (0.1221/y)^{1/3.404} - h \qquad (5.6)$$

where

t = Thickness in inches

y = Yield Stress in Ksi

h = Height or Thickness in inches

5.4 Frequency/Forced Response for Coated Turbine Blade

Empirical relation to correlate the geometric properties of blade with 7 in x 3 in x 0.34 in dimensions is obtained by the similar procedure, as adopted for the cantilever beam and curved plate. VonMises stress patterns for the blade are shown in figures5.42- 5.44.

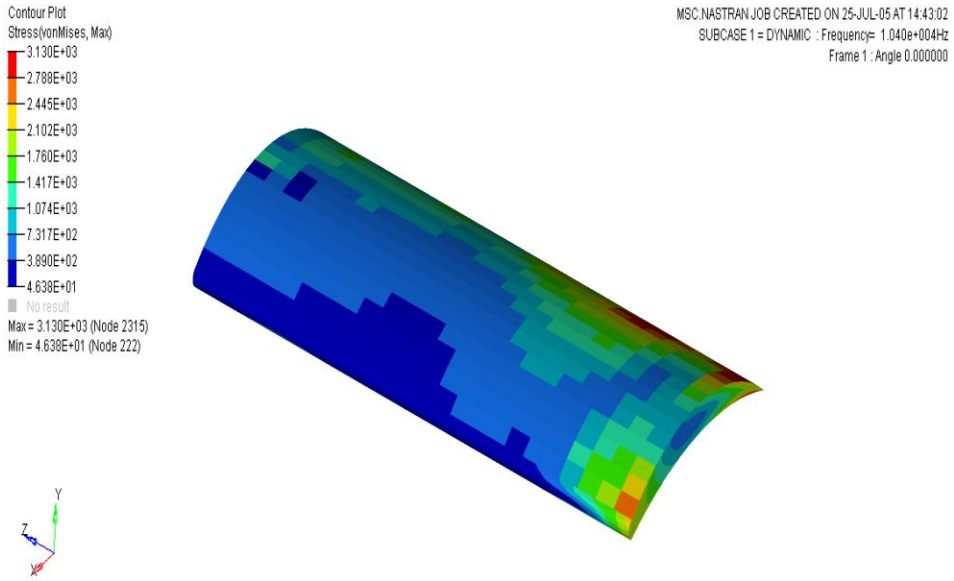

Fig. 5. 42 Blade with 0.02 in Coating Thickness

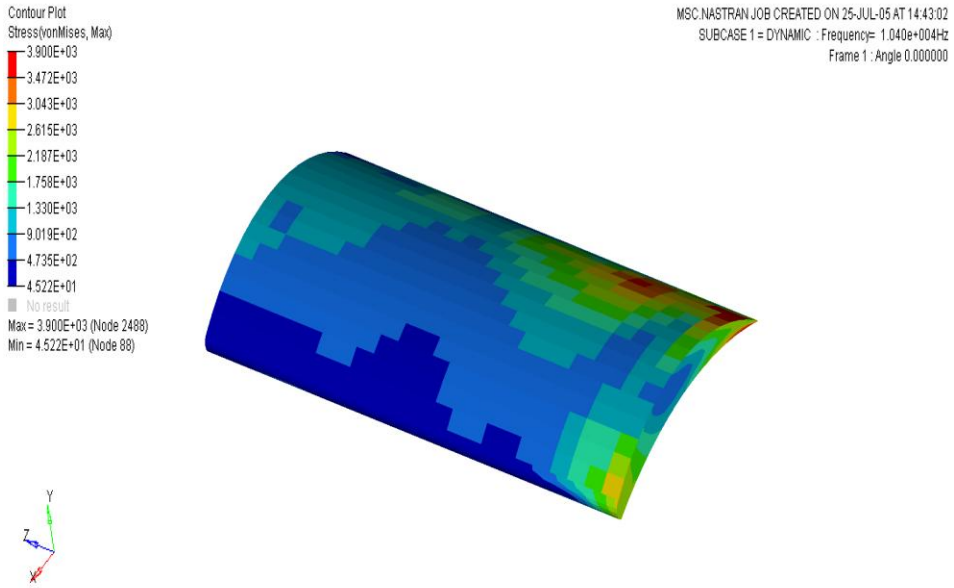

Fig. 5. 43 Blade with 0.04 in Coating Thickness

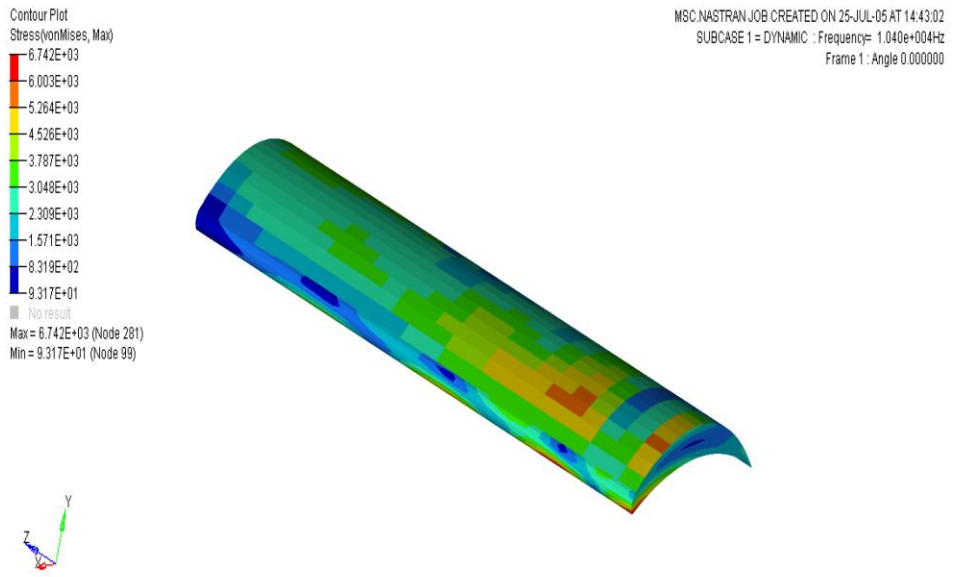

Fig. 5. 44 Blade with 0.1 in Coating Thickness

The figures 5.42- 5.44 shows the variation of VonMises stresses on the upper and lower surface of the blade. The maximum VonMises stress for the variation of coating thickness is obtained by normalizing the normal stresses. The correlation which correlates the coating type and the geometric properties is given below

$$t = (0.7891/y)^{1/1.304} - h \qquad (5.7)$$

where

t = Thickness in inches

y = Yield Stress in Ksi

h = Height or Thickness in inches

5.5 Conclusions

The magnetomechanical surface coating is a passive technique to reduce the vibratory stresses for beams and blades. It is already established that magnetomechanical coating is effective in reducing the vibratory stresses developed in the beams and blades during the operation. Empirical relation for correlating material type, coating type and

corresponding geometric properties for beam and blade is not available in the literature. Analysis for coated beams, curved plate and blade is performed using the harmonic excitation force.

For this research, an iterative process is used to develop an empirical relation for beam, curved plate and blade which correlates geometric properties, coating type and material type. This correlation can be used as an effective tool in the design studies related to vibratory stresses in the gas turbine blades. Finite element analysis for forced response shows that stripe mode stresses are reduced by increasing the coating thickness, which shows the dependence of coating layer on stress or strain level. Present methodology can easily be used for the actual twisted and varying cross section turbine blades.

5.6 Future Work

- Extending this research to Rotor Dynamics
- Co-relating geometry and damping

REFERENCES

[1]. Megson T.H.G., "Aircraft Structures for Engineering Students", 3rd Edition, Arnold, London, 1999.

[2]. Violette, John A., Mashey, Thomas, United Technologies Corp., "Rotor Blade Retention", No. 5017092, 21 May. 1991.

[3]. Bakhle, Milind A., "Calculation and Correlation of the Unsteady Flowfield in a High Pressure Turbine". NASA/TM--2002-211475, 2002.

[4]. Darolia, Ramgopal, Weaver, Matthew Mark, Corbly, Dennis Martin, Movchan, Boris Alexeevich, Ustinov, Anatolii Ivanovich, General Electric Company, "Coating System and Method for Vibrational Damping of Gas Turbine Engine Airfoils", No. 20060078432, 13 April. 2006.

[5]. Barb, Kevin Joseph, General Electric Company, "Mixed Tuned Hybrid Bucket and Related Method", No. 6854959, 15 Feb. 2005.

[6]. Beards C. F., "Structural Vibration: Analysis and Damping", Arnold, London, 1996.

[7]. Demeter G. Fertis, "Mechanical and Structural Vibrations", John Wiley & Sons, Inc. 1995.

[8]. Leonardo Meirovitch, "Fundamentals of Vibrations", McGraw-Hill, Inc. 2001.

[9]. Lynch, Jerome Peter, "Active Structural Control", Kajima Corporation, Stanford University, 17 Sep. 1998.

[10]. Lewis, Thomas M., Jones I, David G., "Turbine Engine Dampers", No. 6514040, 4 Feb. 2003.

[11]. Bulgrin, Charles A., Struthers, John O., United Technologies Corp., "Offset Center of Gravity Radial Damper", No. 6042336, 28 March. 2002.

[12]. Dietz, Philip W., Staker, John R., General Electric Company, "Retention Devices for turbine Blade Damper", No. 5261790, 16 Nov. 1993.

[13]. Mueller, Peter W., Stevenson, Joseph T., Panovsky, Josef, Glynn, Christopher C., Park, Sang Y., Wines, Daniel E., General Electric Company, "Blade damper", No. 5226784, 13 July. 1993.

[14]. Bonn, Brian, Diepersloot, Dave, Terastor Corporation, "Method and apparatus for dampening disk vibrations", No. 6560192, 6 May. 2003.

[15]. Yen, H. Y., Shen, Herman M. H., "Passive Vibration Suppression of Beams and Blades Using Magnetomechanical Coating", Journal of Sound and Vibration vol. 245, 701-714, 2001.

[16]. Ascher, U. M., Mattheij, R. M. M., Russell, R. D., "Numerical Solution of Boundary Value Problems for Ordinary Differential Equations", Englewood Cliffs, Prentice-Hall Inc., 1988.

[17]. Smith, John, Chandra, Sharad, "Coatings for Turbine Blades", No. WO/2005/106064, 11 Oct. 2005.

[18]. Singiresu S. Rao, "Mechanical Vibrations", 4th Edition, Pearson Education.

[19]. Douglas Thorby, "Structural Dynamics and Vibration in Practice", Elsevier Ltd., 2008.

[20]. Smith, G. W., Birchak, J. R., "Effect of Internal Stress Distribution of Magnetomechanical Damping", Journal of Applied Physics 39, 2311-2316, 1968.

[21]. Smith, G. W., Birchak, J. R., "Internal Stress Distribution Theory of Magnetomechanical Hysteresis-An Extension to Include Effect of Magnetic Field and Applied Stress", Journal of Applied Physics 40, 25174-5178, 1969.